THE INFLUENCE OF MACHINE MODEL AND OPTIMIZATION PARAMETERS ON THE GENERATION OF NARROW SEGMENTS IN STEP AND SHOOT INTENSITY MODULATED RADIOTHERAPY PLANS FOR SIMPLIFIED GEOMETRIES

Author: Maryam Motmaen Dadgar, M.Sc. Physics

A Thesis Submitted to the School of Graduate

Studies in partial fulfillment of

the requirements for the degree:

Master of Science

McMaster University

September, 2011

Master of Science (2011) **McMaster University**

(Medical Physics)

TITLE: THE INFLUENCE OF MACHINE MODEL AND OPTIMIZATION PARAMETERS ON THE GENERATION OF NARROW SEGMENTS IN STEP AND SHOOT INTENSITY MODULATED RADIOTHERAPY PLANS FOR SIMPLIFIED GEOMETRIES

AUTHOR: MOTMAEN DADGAR, MARYAM

SUPERVISOR: DR. OREST OSTAPIAK

CO-SUPERVISOR: DR. KEVIN DIAMOND

NUMBER OF PAGES: x, 87

Abstract

Generation of narrow segments is a matter of concern in step-and-shoot intensity modulated radiotherapy for several reasons. The measurement, calculation and delivery of dose from narrow segments may be complicated due to: the dosimetric properties of the detector; the effect of beam penumbra and heterogeneities within the patient; and the requirement for high geometric delivery precision respectively. The main purpose of this thesis was to investigate the parameters affecting the generation of narrow beam segments in IMRT optimization. Parameters such as effective source size, Gaussian height and width, density of the target volume, and gap between the tumor and normal tissue were varied to determine their influence on the number of narrow leaf pair separations. The gradient and penumbra were also examined. Two simple geometric models (thick model and thin model) with different dimensions were used. In the thick model, two 6-MV photon beams were incident on the target at right angles. A rectangular target was centered in a phantom with dimensions 20.25 cm×5.25 cm×20.25 cm. In the thin model, one 6-MV photon beam was normally incident on a 20.25 cm×1.25 cm×20.25 cm slab phantom. The relationship between the penumbra and number of narrow separated leaf pairs were examined for the thick model. The results did not show a consistent pattern. For the thin model, creating a gap between the target and the OAR decreased the total number of narrowly separated leaf pairs along the interface but increased the average dose delivered to the OAR. By varying the OAR max dose or the gap between the target and OAR, a peak was created in the dose profiles to compensate the penumbra. As gradient increased the peak height increased to compensate the dose fall-off. The width of the peak at half maximum changed with gradient but not in a predictable fashion.

Acknowledgement

I would like to express my sincerest gratitude to my supervisor, Dr. Orest Ostapiak, who has supported me throughout my thesis with his patience, knowledge and guidance. His invaluable and knowledgeable comments on my work enabled me to develop my understanding of the subject. Without his effort and help, this thesis would not have been completed or written.

Also I am extremely grateful for the assistance, the good advice and support of my second supervisor, Dr. Kevin Diamond, who was very helpful in the progress of my thesis.

I would also like to thank Dr. Tom Farrell, for his valuable advice and assistance both in academic and personal level. He encouraged me during my Master's study as a helpful, kind and caring professor.

Also, I would like to give special thanks to my parents, for their unequivocal support and patience as always.

Contents

List of figures

List of tables

Chapter 1: INTRODUCTION

1.1 Intensity Modulated Radiation Therapy (IMRT)

Intensity-modulated radiation therapy is a radiation treatment technique which forms the desired dose distribution in the target volume and surrounding normal tissues by applying non-uniform intensities of radiation beams incident on the patient (Bentzen, 2005 & Bortfeld, 2006). Such beams superimpose from different directions. In IMRT the intensity of the beams incident on the tumor is increased while the intensity of the beams incident on the critical normal structures is decreased (Bortfeld, 2006). Multi leaf collimators (MLCs) are used to deliver the intensity modulated beams precisely (Xia *et al.*, 1998). MLCs consist of 20-80 absorbing tungsten leaf pairs that move against each other to shape fields (figure 1.1) (Bortfeld, 2006).

Figure 1.1: A multi leaf collimator (MLC) producing an intensity-modulated field with moving the leaves when the beam is on and perpendicular to this page (Bortfeld, 2006).

1.1.1 Step-and-shoot IMRT leaf sequencing

In step-and-shoot treatment mode the beam is off while the leaves move into position, while in dynamic treatment technique the leaves move while the beam is on (Bortfeld, 2006). Delivery efficiency is the advantage of using dynamic mode of MLC but an accurate control of the speed of each leaf is required. Step-and-shoot or segmental IMRT is a treatment technique

that employs the static mode of MLC. In this mode the MLC leaves remain fixed while the beam is on to form static subfields named segments (Luan *et al.*, 2004 and Kuperman *et al.*, 2006). Intensity modulated beams are the outcome of superimposing these static segments. In addition to availability and easy verification of planning with this technique, dose can be delivered accurately; however, treatment time may be increased (Xia *et al.*, 1998). Step and shoot IMRT applies the static mode of MLC to deliver the dose to the target by different shapes of subfields. Optimization of subfields can decrease the number of required intensity levels so that obtaining acceptable treatment times with the step and shoot technique is possible (Keller-Reichenbecher *et al.*, 1999).

1.2 Gradient

In treatment planning, lateral transport of radiation causes the dose to fall off near the boundaries leading to reduced dose inside the target region and increased dose outside. Adding margins to the target volume can counteract this problem. But the main goal, which is delivery of homogenous dose to the target while sparing of the normal tissue should be considered. Therefore the magnitude of the margin added to the PTV is important. Usually it is specified as the distance between the 50% off-centre-ratio (OCR) and 95% OCR. Another way to compensate the under-dose inside the target near the boundary is to escalate the fluence at points in the fall off area. Obtaining high gradients at the interface between the organ at risk and target is essential in order to produce sharp dose decline. One way to achieve this sharp gradient adjacent to the interface is to boost the fluence inside the target and diminish it inside the critical normal structure (Mohan *et al.*, 1996).

Mohan *et al.* showed that appropriate changes of fluence near the boundary can decrease the width of penumbra and increase the gradient. Extending the margin too much increases the

adjacent normal tissue exposure while intensifying the dose at the interface on the target side to a large amount may generate hot spots and excessive skin doses in the surrounding area. Thus escalation of dose inside the target alone or increasing the margin alone would not give a perfect result. An appropriate combination of both should be considered (Mohan *et al.*, 1996). In order to spare more normal tissue and control the local disease, margins should be minimized. For this purpose there are studies that try to decrease the margins while not increasing target dose uncertainty (Sharpe *et al.*, 2000). Uncertainties in the process of treatment planning abate the accuracy of dose delivery (Jaffrey *et al.*, 1999).

1.2.1 Beam Penumbra

There are two sources of penumbra. The particular geometric structure of a radiation source causes a certain photon fluence distribution that leads to *geometric penumbra*. When photons with high energies interact with the medium, the resulting secondary electrons transport laterally and produce *radiological penumbra* (Dawson *et al.*, 1984). Jaffray *et al.* (1993) suggested that the X-ray source can be considered as two parts: a focal component that refers to the area of high intensity radiation and an extra-focal component that is due to scattering from the accelerator head, collimators and flattening filter. The intensity of extra-focal area is low. Sharpe *et al.* (1995) created a model with two X-ray source components. In their model they observe an increment in the geometric beam penumbra as the field size expands. The reason for this phenomenon is that the collimators can partially veil the extra-focal source. When the field size enlarges, more of extra-focal source can be seen from the region outside the field edge; therefore geometric beam penumbra widens (Sharpe *et al.*, 1995).

A normal beam profile results when the beam enters unit density medium or water. Decrease of the density of material leads to increasing the lateral range of secondary electrons

and therefore reducing the gradient of beam profile. If the field is small enough, the dose on the beam axis will diminish with increasing lateral spread of electrons (Kornelsen *et al.*, 1982 and Hunt *et al.*, 1997). Hunt *et al.* reported that when lung (low density tissue) is located laterally adjacent to the target, the under-dosed area (penumbra) widens as the beam energy increases. Thus, as the beam energy increases and the target lies next to a low density organ at risk such as lung, wider margins are needed (Sharpe *et al.*, 2000). Also Ekstrand *et al.* studied the effect of beam energy on the penumbra for small fields. They indicated that as the X-ray energy increases, the beam penumbra increases and the dose on the central axis decreases. As a result, under-dosing of target and overdosing of organ at risk may occur.

There are several studies that examine possible ways to maximize the dose gradient at the edge of a photon beam. It is reported that increasing the field size by the amount of 1.0-1.5 standard deviations of patient alignment uncertainty may be the best for optimizing the treatment plan but at the same time augmenting the prescribed dose is needed relative to the case without patient position uncertainty consideration, to reduce the rounded shape of dose distribution shoulders (Lind *et al.*, 1993). According to Mohan *et al.*, one of the predominant factors affecting 50%-95% width of penumbra is phantom scattering. Increasing the beam intensity near the edges increases the homogeneity of dose distribution in the PTV and decreases the normal tissue irradiation. When multiple fields are applied in a treatment plan, the penumbra of co-planar fields overlaps at the superior and inferior boundaries so that an increment of the intensity near these boundaries is required. Dirkx *et al.* reported a method to reduce 50%-95% penumbra width by increasing the intensity of the beam near the superior and inferior boundaries of the field for prostate cancer patients. Narrow segments with low weight overlap on the superior and inferior edges of the field. They obtained a mean decline of 0.66±0.25 cm in penumbra width.

Brugmans *et al.* found that for beam energies of 8-MV and 18-MV, 2.0 cm and 2.5 cm margins between the beam edge and edge of the target respectively are necessary to deliver at least 95% of isocentre dose to a tumor located adjacent to the low density lung. To spare more lung tissue it is important to reduce the field sizes to the smallest possible value. They suggested that beams with energies beyond 10-MV are undesirable for treating these tumors. For smaller fields, intensity modulated beams can be applied to compensate the dose fall-off at the boundaries (Brugmans *et al.*, 1999).

Consequently, penumbra is one of the parameters that affect the dose gradient at the field edges. Compensating the penumbra can lead to a reduction in critical normal structure irradiation (Sharpe *et al.*, 2000[1]). Sharpe *et al.* employed compensating rinds for this purpose and then established the intensity and width of the rinds that result in an improved clinical treatment. 1 mm thick lead sheets were used to abate the in-field beam intensity by roughly 10%. Compensating rinds were obtained by cutting the lead sheets around the field edge to produce un-attenuated intensity. There are also studies that produce these rinds by dynamic MLC sequencing. Whereby a computer program yields the number of control points that determine the position of MLC leaves (Yu *et al.*, 1995). Dynamic MLC are used to produce compensating rinds. Head scatter distribution is calculated. With the help of a computational model they investigated the effects of beam energy, target density, intensity and width of compensating rind on the penumbra and margin reduction (Sharpe *et al.*, 2000[1]). The distance from the 95% dose level to the geometric field edge corresponding to the 50% dose level is often defined as penumbra. Also, the distance between the 50% dose level and the 5% dose level is used to evaluate the dose profiles outside the field boundary. For a 6-MV beam energy, a 10 mm wide rind offsets the 95% dose level toward the beam edge when the intensity is increased by 10%. No

significant increase is observed for dose spread beyond the beam edge. Greater increments in the rind intensity do not result in a substantial effect on the penumbra. Therefore, they concluded that there is a “saturated limit” for dose gradient. The same results were seen for a 3 mm rind width but the profiles were less sensitive to the rind intensity enlargement. Their model determines that a margin reduction of 6 mm can be achieved for 6-MV energy beam in water to reach the "saturated limit" of 2 mm dose gradient. With a 15%-20% increment of intensity in the 5-10 mm wide compensating rind, a 5-6 mm reduction of margin can be achieved. In lung, an 11 mm open field penumbra reaches the saturated limit of 3 mm with a greater intensity increment. For an 18-MV beam energy, the intensity of the rind should increase even more to increase the dose gradient at the field edge, because of the longer electron range. In lung, 30% augmentation of 15-20 mm wide rind intensity leads to a penumbra reduction from 15 mm to 5 mm (Sharpe *et al.*, 2000[1]).

According to Jackson 1971, electron range surface (ERS) refers to the dose build-up region that is due to the secondary electrons arising from interactions of the x-ray beam normally incident on the medium. In water, the half width of the ERS is approximately 3 mm for a 6-MV energy beam and 7 mm for an18-MV energy beam. In lung these values are 11 mm for 6-MV and 25 mm for 18-MV energy beams. On the other hand, secondary electrons deposit dose in water at the average lateral range of roughly 2 mm and 5 mm for 6MV and 18MV beam energies respectively. The ERS model predicts a greater electron lateral range because this model is simplified since the secondary electrons resulting from Compton scattering are considered to slow down continuously. The energy spreading out and multiple scattering of the secondary electrons are not considered in this model. The values for "Mean lateral range of dose

deposition" obtained from dose spread kernels are smaller than the ERS values (Sharpe *et al.*, 2000[1]).

Considering these two approximations (ERS and mean lateral range of dose deposition), they predicted that the mean lateral range of electrons should be doubled to obtain the minimum size for the rind width that gives optimal penumbra compensation. Thus, penumbra compensation is a reasonable way to reduce the margin and lower the dose to critical structures (Sharpe *et al.*, 2000[1]).

Some time before Sharpe *et al.*, Cadman and Sidhu, 2000 reported another work in which compensating filters are used to sharpen the penumbra. They tried to decrease the intensity towards the center of the beam profile by filters to decrease the dose fall-off at the edges. They shaped the fields with shielding blocks. The filters are thin lead shields that lie throughout the field and left a gap between the edge of the filter and the shielding blocks. The generated rind along the periphery of the beam causes dose increment at the dose fall-off region. This method manages to lower the penumbra in their prostate treatments nevertheless it relies on experiential estimation of penumbra compensation. The more compelling pursuit for penumbra sharpening would be achieved if the precise dose calculations are considered in the design of customs and filters. They suggested that the precise dosimetry of penumbra compensation filters can be useful (Cadman and Sidhu, 2000).

1.3 Dosimetric accuracy

According to ICRU report 50, the prescribed dose to the patient must be achieved within 5% accuracy. Because the process of delivering the dose contains multiple steps, each step should meet the accuracy well within 5% to satisfy the ICRU recommendation. Spatial uncertainties must be within ±5 mm (Sharpe *et al.*, 2000[2]). Planning target volume (PTV) is the

volume assumed for the target considering all possible errors and deviations. Minimum dose delivered to the PTV should be 95% of prescription dose (ICRU report 50, 1994).

There are several factors that cause uncertainties and errors during various phases of IMRT, namely calculation algorithms, mechanical characteristics of the MLC or LINAC or the beam sequencer (Bucciolini *et al.*, 2004). For instance in step and shoot IMRT, when desired segment shape is achieved by the MLC leaves, the MLC controller commences beam on. While the beam is on, the delivered MU data are transferred to the MLC controller every 50ms. This delay causes a discrepancy between planned and delivered MUs. Once the required amount of MUs is delivered, the LINAC controller ends the radiation. Therefore there are dosimetric inaccuracies (Boyer, 2003).

1.3.1 Short irradiation time

As discussed above, step-and-shoot IMRT delivers intensity modulated beams to the target. These uniform segments superimpose to create a non-uniform dose distribution in the target volume. By this method, the beam is on only when the MLC is not moving. Sometimes step-and shoot IMRT treatment plans consist of segments which have very little beam-on time. The segments with short exposure time or few MUs decrease the accuracy of dose delivery (Sharpe *et al.*, 2000[2]). Sharpe *et al.*, 2000[2] used the dose rate of 400MU/min to deliver the dose. For exposures greater than 4 MU, dose per MU delivered within ±2% relative to a 100 MU.

1.3.2 Small field sizes

Step-and shoot IMRT may include segments with small area that affect the dosimetric accuracy. Frequently, field sizes greater than 3×3 cm^2 are prescribed for radiotherapy treatments. Narrow segments delivered to the patient, may superimpose and cause a substantial reduction in precision of dose delivery (Sharpe *et al.*, 2000[2]).

Sharpe *et al.*, 2000[2] commissioned a system to calculate the dose for small field sizes (on the order of 1×1 cm^2) taking account of head scatter modifications. A 1% difference between measured and calculated values of dose per MU is obtained in water phantom. A 1 mm and 2 mm deviation from the initial field size causes 8% and 16% difference in the measured value respectively.

Bjarngard *et al.,* examined whether factors such as secondary electrons produced in the narrow beams and geometric penumbra affect the central axis dose for these narrow beams. They found that the lateral electronic equilibrium for 6-MV beam energy is achieved at a 1.0 cm beam radius. Reduction of dose on the central axis for narrower beams appears due to secondary electron scattering. In their study, the beam fluence that passes the collimator leaf gaps is not affected by beam diameter and scattered photons from the collimator do not exhibit particular influence on measured dose. Thus the effect of geometric penumbra is negligible (Bjarngard *et al.,* 1990).

In IMRT treatment planning, dose distributions are delivered to the target by multi leaf collimator shaped segments. Regularly, narrow segments with a size of less than 2 cm in one dimension are needed. Also, in step and shoot techniques, the calculated penumbra for segments determines the absolute MLC position. Hot and cold spots can be generated between two contiguous segments if penumbra calculation is imprecise. Thus, high resolution dosimetry is required to achieve high accuracy in absolute dose calculations (Laub *et al.,* 2003).

Scattered photons and electrons created inside small fields, whose width is smaller than the range of electrons, can possibly escape. Further reduction in field size leads to smaller scattering angles required for photons and electrons to depart from the field without replacement.

When the density of the medium is low, an energy increment leads to a decline in photon scattering angle. Then the number of interacted photons and the rebound angle of electrons diminish while the range of electrons enhance. Consequently when small fields are generated in low density tissues, increasing the energy can result in more electrons departing from the field to a distance farther away where they deposit their dose distal to the field. Correspondingly less dose is deposited on the central axis of the small field in a low density medium (Jones *et al.*, 2003).

The increased range of electrons due to beam energy enhancement causes beam penumbra widening so that the entire profile for small fields may be considered penumbra (Sixel and Podgorsak 1993). Sixel and Podgorsak found that the depth of maximum dose for small field sizes decrease as size of the field decreases. Although for large field sizes, as the field size increases the depth of maximum dose decreases as well.

Lydon, 2005 reported that the accuracy of Pinnacle^3 version 6.2b for narrow fields is within 2%. Because of the limited dose grid resolution, Pinnacle^3 cannot calculate the dose for segments narrower than 1 cm precisely. They suggest not applying segments with the width of smaller than 1 cm for IMRT.

1.3.3 Ionization chamber (detector)

Ionization chambers are used to steer the beam and to turn it off when the prescribed dose is delivered. It is worth considering that it takes time to balance these circuits and that beam features can change as time passes. Transient beams that exist at any moment add together over the total exposure. Hence, any change in the symmetry or flatness can lead to an uncertainty in overall exposure (Barish *et al.*, 1987).

Lateral electron equilibrium is not achieved for small beams. Fields with an effective diameter less than 30 mm lead to two difficulties in dose measurement:

a. Presence of lateral electronic disequilibrium can affect the dose measurement on the central axis, because of partial volume effects within the detector due to the rapid decline in the dose toward the edge of the detector.
b. To measure the dose away from the central axis, high dose gradients may complicate the measurement (Rice *et al.,* 1987).

In order to achieve an appropriate model in IMRT it is important to measure the penumbra region accurately. The ionization chamber volume affects the accuracy of penumbra measurement. As the size of the chamber increases, an artificial increment in the measured penumbra width occurs. These inaccuracies in the penumbra measurement influence the accuracy of dose calculation for small fields (Arnfield *et al.,* 2005). Arnfield *et al.* tried to use high resolution film dosimetry to modify these uncertainties in the measurement of penumbra. The results show that film dosimetry can improve the accuracy of measured penumbra in the sharp gradient region. Therefore, they can modify the dose distribution to some extent.

1.3.4 MLC leaf positional accuracy

Uncertainty in MLC leaf position influences the dose delivered to the target volume and critical normal tissues in IMRT. Therefore, quality assurance becomes an important factor in IMRT practice. Factors such as mechanical design and computer control of MLC can lead to errors in the position of leaves. According to Klein *et al.,* accuracy for leaf position in MLC should be better than 1 mm (Mu *et al.,* 2008). For static MLC Bayouth *et al.* employed a technique to measure exact positions of MLC leaves pertaining to dosimetric data over 3 months.

In this study they use the Siemens medical system with 29 leaf pair MLC for exposure. During calibration, rotational error leads to a maximum value of 1.5 mm for absolute leaf position error.

1.3.5 Non uniformity in the target

Factors such as beam energy and existence of non-uniformities affect the homogeneity of dose distribution in the target volume. Bone and air cavities are examples of non uniformities that cause electronic disequilibrium when they are located adjacent to the target (Rustgi *et al.*, 1997). Rustgi *et al.* examined how beam profiles of small fields with the diameter of less than or equal to 40 mm are affected by air inhomogeneities abutting the target. The air cavities cause a substantial dose perturbation on the central axis and close to the beam boundaries because of electronic disequilibrium at the air gap. They found that the target would receive a dose less than that prescribed and the normal tissues beside the target would receive a dose more than that expected when the target is located next to an in-homogeneity with low density. Dose augmentation outside of the field boundary is greater for larger incident beam energies because electrons migrate longer distances after passing through the air gap. The penumbra (10%-90% dose level distance) increases with increasing depth of air cavity and field size (Rustgi *et al.*, 1997).

1.3.6 Targeting uncertainties

There are various reasons for radiotherapy errors, namely, targeting uncertainties that can be divided into two categories:

1. *Setup error:* refers to the change in the patient's position relative to the beam.
2. *Organ motion:* refers to the change in the target's position inside the patient (Jaffrey *et al.*, 1999).

To apply as small as possible margin to the plan it is important to minimize these errors. There are several approaches to lower setup errors and organ motion uncertainties, namely, depreciating the amount of change in position with the aid of devices; and correcting the variance by repositioning the target/organ at the time of treatment (Jaffray *et al.*, 1999).

Hanley *et al.*, 1997 used a body cast to stabilize 50 prostate cancer patients. When setup errors of more than 2 mm are observed, position corrections are carried out for the next fraction. Standard deviation for random errors is found to be around 2 mm while this value for systematic errors is less than 2 mm. Considering systematic and random uncertainties together, they determined standard deviations between 2.2 mm and 2.7 mm for the total setup errors. 10 of 50 patients show the total dislocation of 2 to 7 mm over the treatment time. Fluctuations in the patient setup errors are found to be within ±2 mm when the translation is considered as a function of time. In another prostate study standard deviation for random setup errors are found to be 1.3, 1.7 and 2.2 mm in the LR, AP and SI directions respectively. After position corrections, margins could be decreased in LR, AP and SI directions from 2.3 to 1.8 mm, 3 to 2.1 mm and 3.7 to 1.8 mm respectively. They found that the minimum margin of 2 mm is needed after one or two position corrections (Graf *et al.*, 2010).

Some instruments made to reduce random errors can decrease systematic errors as well. For instance, when a silk tape is used to prevent a patient's chin from moving and make it more stable the random error is decreased. This situation helps to reduce instability by creating a particular position (Jaffrey *et al.*, 1999). Jaffrey *et al.* rearranged the position of fields shaped by MLC to adjust setup errors for 20 patients. Systematic error varies from 2 mm to 7 mm with an average of 4 mm before MLC adaptation. After adaptation the average declines to 0.5 mm.

Intra-fraction motion of the patient is another factor that causes uncertainties in the delivery of the dose to the patient. If an organ within the patient moves due to respiration during dose delivery, then dose may not correctly sum up with the doses from other segments. Clearly, narrow beam result in greater errors due to intra-fraction movements (Bortfeld *et al.*, 2002). To deliver the dose to the patient accurately, the treatment setup requires devices to immobilize the patient (Kutcher *et al.*, 1994). Because of intra-fraction organ motion and setup errors, a margin between the planning target volume and treated volume is considered. Blurring of dose distribution is the result of organ motion. With no margins, blurring would cause cold areas near the edges of target volume. With IMRT those cold areas are reduced either by adding a margin or by increasing the intensity near the edges (Bortfeld, 2006).

Also Pérez-Romasanta *et al.*, 2009 estimated setup errors and organ motion uncertainties for a number of prostate cancer patients. In the directions of LR, AP and SI they observed standard deviations of 2.4, 4.2 and 3.1 mm for systematic organ motion respectively. They obtained smaller values for setup errors. Thus organ motion can have more influence on errors (Hanley *et al.* 1997).

1.4 Other works

In IMRT, each beam is divided into several beamlets. The intensity of beamlets is modulated and their weights are optimized to achieve optimization objectives. The separation between MLC leaf pairs regulates the width of the beamlets (Zhang *et al.*, 2005). Shepard *et al.* employed a simplified model to help them study optimization and delivery method. They used three 2-MeV pencil beams. They considered that the beams are coplanar with two of them parallel. Also, electron contamination was disregarded and single slice optimization was performed. A phantom with a diameter of 20 cm was used. Three different methods (uniform,

segmented, intensity modulated) are used to deliver the dose to the target. Only intensity modulated beams present both uniform dose delivery to the target and spare the normal tissue adjacent to the target volume from irradiation (Shepard *et al.*, 1999).

Other investigators managed to decrease objective function from 2.39 to 0.78 by diminishing the beamlet step-size from 10 mm to 1 mm respectively. The average dose delivered to surrounding normal tissue reduces by 10.3% when the beamlet step-size decreases from 10 mm to 1 mm. For the same reduction of beamlet step-size, a reduction of 13.2% is observed for the range of hotspots while dose gradients increase by 3.1%. However, while small beamlet sizes enhance conformal delivery of the dose, as discussed before, there are still some constraints to using such small beamlets in IMRT treatment planning (Zhang *et al.*, 2005).

The number of segments for each beam in IMRT planning has been discussed in studies. Jiang *et al.* assayed the relationship between the number of apertures and objective function for each beam. With the help of that, they could evaluate the quality of the plan. By increasing the number of segments for each beam above 9, they do not realize a significant gain in dosimetry. There are many cases (for instance in prostate treatments) where using small intensity modulated fields with 5 segments each leads to high plan quality. Lee *et al.* examined the same relationship for liver cancers. For a few cases, decreasing the number of segments worsens the conformity of the plan and delivers more dose to the organ at risk. For a large number of cases that include larger and more complicated tumor shapes, increasing the number of segments is not beneficial. In these cases, using a small number of segments leads to better quality and less complexity for the plan. Reducing the complexity of an IMRT plan can decrease errors. Therefore, diminishing the number of segments can decrease the negative influence of these errors. Also, dosimetric

accuracy of less complex plans is better than that of more complex IMRT plans. Application of smaller number of segments results in a reduction in treatment time (Lee *et al.*, 2010).

In IMRT planning, it is common to divide the two dimension open field into various beamlets with different intensities to achieve an optimum intensity map. Some investigators assume a matrix that determines the contributed dose to the patient by each beamlet. The relationship between segment positions and corresponding delivered dose to the target is assayed. Beams are divided into 0.25×0.5 cm^2 segments. The weights and shapes of MLC segments are optimized for 6-MV x-rays. The resulting depth dose curve shows that when there is an air cavity in the target, a dose decline occurs inside the air gap and another buildup region occurs at the interface between air and tissue resulting in an under-dose of the target. In this work, a single optimization method called direct aperture optimization is applied. The uncertainties due to MLC leaf movements and patient motion are considered. In this method, fewer apertures are required because the shapes and fluences of apertures are both optimized. Based on the intensity pattern used in the plan, the number of intensity levels for N segments can vary from N to 2^N-1. Consequently, with the help of this method, simple plans can be produced and aperture shapes can be simply provided (Bergman *et al.*, 2006).

As discussed before, in IMRT there are always dose gradients and penumbra regions at the edge of the beam, or at the interface between the tumor and organ at risk, or in an overlapping area. As a result, accurate measurement of penumbra is essential to place the dose gradient precisely during the optimization. A proper algorithm for dose calculation should consider the small beamlets that are located in the penumbra region (Jeleń *et al.*, 2005). Jeleń *et al.* made a simple model (i.e. the field size and SSD do not depend on the penumbra that is due to scattering from the phantom or the head of the accelerator) and used a pencil beam dose

calculation algorithm. The algorithm manages to generate the profiles of segments and output factors precisely. This model is successful in creating reasonable dose gradients at each stage of optimization and can remove the problem of substantial difference between the computed and optimized dose for the organ at risk.

1.5 Current work

A simple model consisting of tumor target and an organ at risk was set up. Pinnacle[3] Radiation Therapy Planning software was used to optimize a step and shoot IMRT plan. The main purpose of this thesis was to investigate the parameters affecting the generation of narrow beam segments in IMRT optimization. Parameters such as effective source size, Gaussian height and width, density of the target volume and a gap between the tumor and normal tissue were varied while the number of narrowly separated MLC leaf pairs, the gradient and penumbra were examined.

This thesis includes four chapters. The first chapter consists of the brief introduction of IMRT treatment planning, dose gradients produced at the beam edges, problems with small beam segments and other works related to this problem. Chapter 2 is the description of the Pinnacle model used in this thesis. Chapter 3 presents the analysis of results and chapter 4 presents a discussion and conclusions regarding the results.

Chapter 2:

PLAN SET UP AND OPTIMIZATION

2.1 Physics model of planning system

2.1.1 Pinnacle$^{3®}$ version 8.0

The software "Pinnacle$^{3®}$ Radiation Therapy Planning (RTP)" version 8.0 was used to optimize the model in this thesis.

2.1.2 MLC

2.1.2.1 Curved edge of leaves

The machine used in this work is a Varian, 21EX with Millennium 120 MLC. The rounded end of the leaf is the part of a circle that is broadened over the thickness of the leaf as shown in figure 2.1.

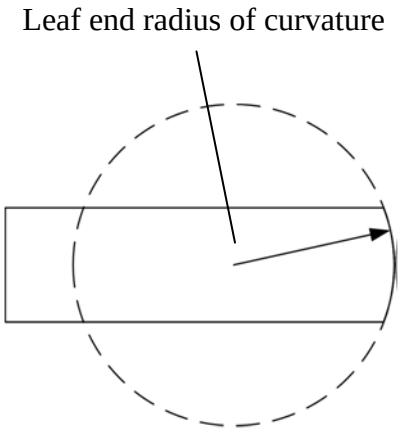

Figure 2.1: The curved edge of MLC leaf (Pnnacle^3 Physics)

As a default in Pinnacle^3 the radius of this circle for Varian MLC is 8 cm. Penumbra of the beam increases as the curvature radius diminishes. Beam penumbra reduces as the curvature

radius increases. The position of the leaf presented by Pinnacle[3] is the projection of the leaf apex to the isocentre plane (Pinnacle[3] Physics).

2.1.2.2 Tongue and groove

Figure 2.2 shows the side and the top view of MLC leaves and the positioning of the tongue and groove for each leaf. Existence of the tongue and groove causes a reduction in interleaf leakage. The tongue of one leaf lies inside the groove of the adjacent leaf. The width of tongue and groove can be changed from 0.005 to 0.200 cm in the Pinnacle model. Increasing the width causes the penumbra to expand and decreasing the width causes the penumbra to shrink (Pinnacle[3] Physics).

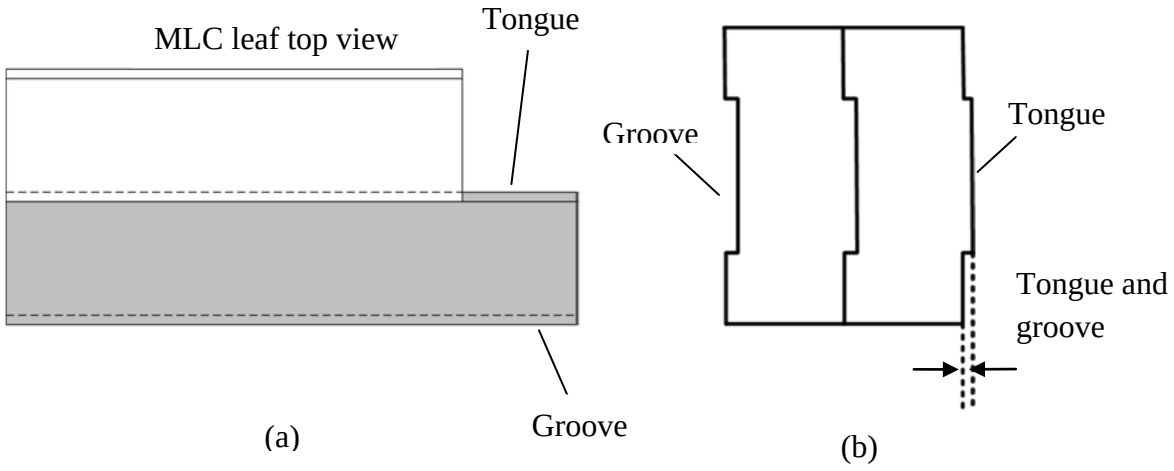

Figure 2.2: (a) View of MLC leaf from the top (b) view of MLC leaf from the side (Pinnacle[3] Physics)

We consider individual step and shoot segments shaped by the MLC. The separation between any opposing leaf pair is determined (figure 2.3). The numbers of opposing leaf pairs separated by a gap ranging between 5-8 mm or between 8-12 mm are counted.

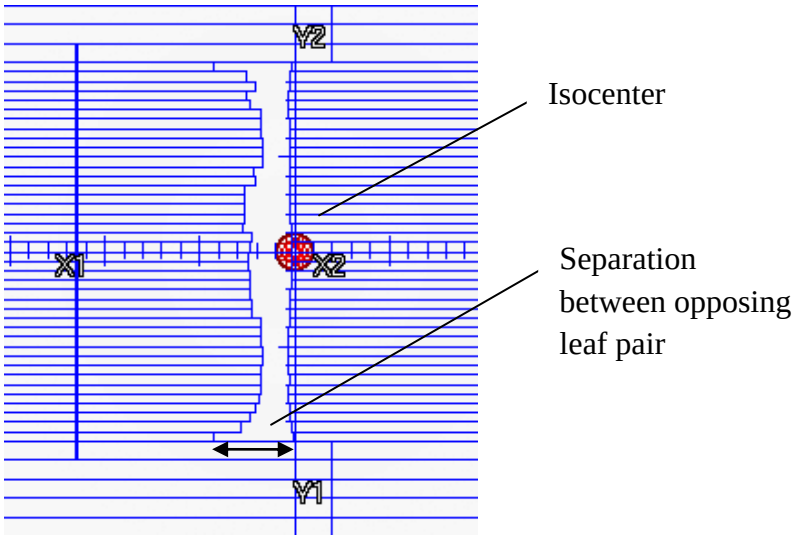

Figure 2.3: Beam's eye view of an optimized segment

Dose distributions are calculated using a convolution algorithm considering the effects of tissue inhomogeneities and patient surface (Pinnacle^3 Physics).

2.1.3 Photon beam modeling

In this thesis we use a 6-MV photon beam. Copies of the existing clinical machine are created in order to change parameters that would affect the penumbra width. To achieve the widest penumbra we create a large penumbra machine. To achieve the sharpest penumbrae, we create a machine with high electron contamination (High EC machine).

2.1.3.1 Out of field parameters

Using out of field parameters, profile tails and penumbra width can be changed. These parameters are grouped into three sections:

(a) *Effective source size* determines the geometric penumbra. The source size perpendicular to the gantry axis (X-direction) and that parallel to the gantry axis (Y-direction) can be adjusted

independently. The shoulders and tail of the profiles get more curved as the effective source size increases (figure 2.4) (Pinnacle[3] Physics).

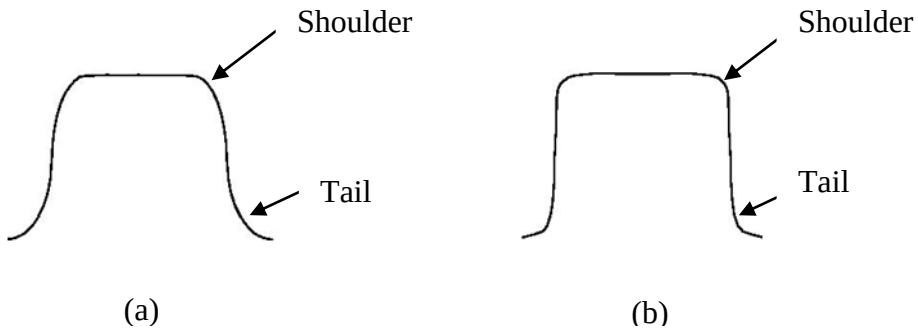

Figure 2.4: Illustration of shoulders and tails for (a) larger source size (b) smaller source size (Pinnacle3 Physics)

The source size is proportional to the geometric penumbra. This relationship can be proven using the law of similar triangles (figure 2.5).

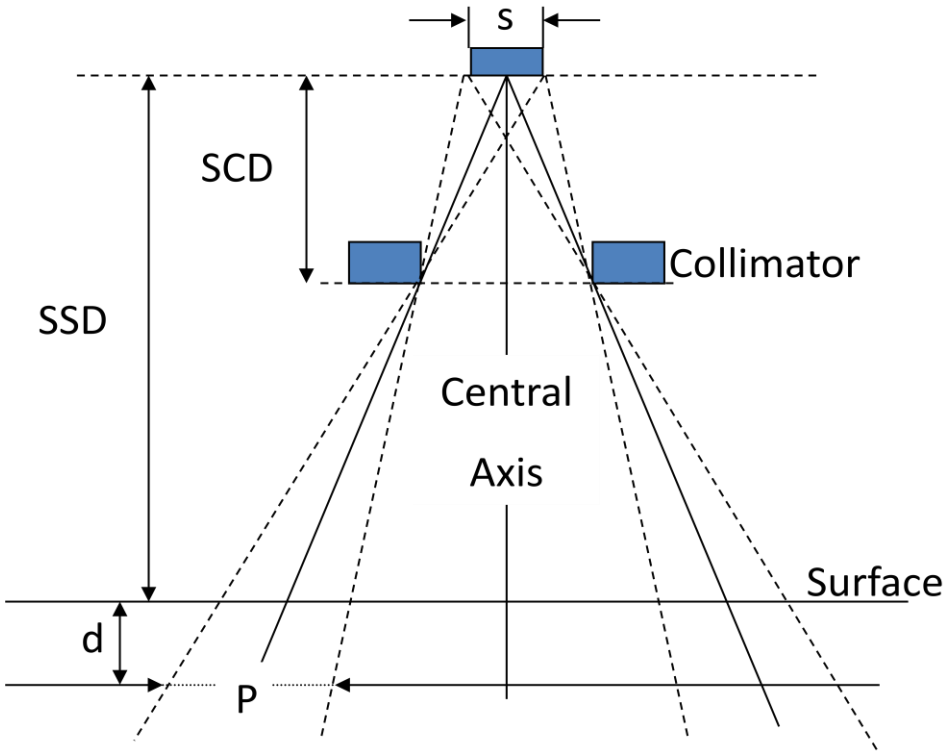

Figure 2.5: geometric illustration of penumbra region at the edges of the beam (Khan)

Following equation can be concluded from figure 2.5, using law of similar triangles:

$$\frac{P}{S} = \frac{SSD + d - SCD}{SCD} \Rightarrow P = \frac{S(SSD + d - SCD)}{SCD} \qquad (1)$$

P refers to the penumbra, S refers to the source size, SSD refers to the source to surface distance, SCD refers to the source to collimator distance and d refers to the surface to point of measurement depth. For our isocentric geometry, SSD + d = 100 cm while the MLC defines the field size at an SCD of 50 cm. Therefore the geometric component of penumbra for our mode is expected to match the source size: P = S.

(b) *Flattening filter scatter source* has an influence on the tails of the profile. This parameter consists of two parts, first the Gaussian height, which is the portion of energy fluence on the central axis that is due to scattering from flattening filter. The second part is the Gaussian width in centimeters. This Gaussian curve is applied for modeling the flattening filter scatter source (Pinnacle^3 Physics).

(c) *Transmission factors* consist of two parameters, jaw transmission factor which is the portion of the energy fluence that is due to jaw transmission and varies from 0.001 to 1.00 and the MLC transmission factor which is the portion of the energy fluence that is due to MLC leaf transmission and varies from 0.001 to 0.200 (Pinnacle^3 Physics).

Table 2.1 presents the out of field characteristics of machines we used in this study.

Machine	Effective Source Size		Flattening filter scatter source		Transmission factors	
	Perpendicular to gantry axis (cm)	Parallel to gantry axis (cm)	Gaussian Height	Gaussian Width	Jaw transmission	MLC transmission
Clinical	0.04	0.04	0.08	1.4	0.007	0.01500
Large Penumbra	2	2	0.3	5	0.007	0.01500
High EC	0.01	0.01	0	0	0	0.00001

Table 2.1: Out of field parameters for clinical machine and created machines

2.1.3.2 Electron contamination (EC)

Pinnacle has the option to add electron contamination dose to the photon dose. The relationship between the depth and electron dose is illustrated in figure 2.6. The initial part is linear. As the depth increases the electron dose decreases exponentially on the central axis.

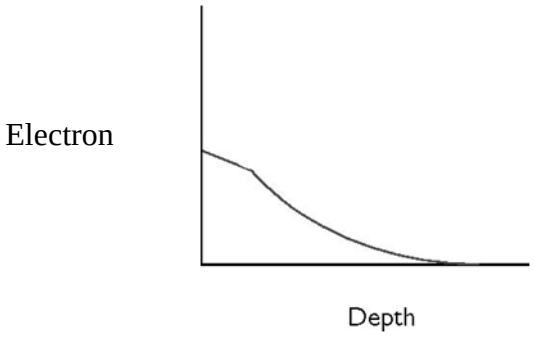

Figure 2.6: Electron dose modeling to account for the electron contamination in Pinnacle (Pinnacle3 Physics)

With the software one can control the trend of electron dose decline, the maximum depth that is affected by electron contamination and amount of electron contribution to the total dose

(Pinnacle^3 Physics). Table 2.2 shows the parameters we changed to achieve high electron contamination and hence, a small penumbra machine.

EC Parameters	Value
Max Depth (cm)	10
EC Surface Dose (D/Flu)	1
Depth Coefficient (1/cm)	0.0001
Depth Fraction	0
Scale Fraction	1
Off-axis Coefficient (1/rad^2)	0

Table 2.2: Electron contamination parameters for small penumbra machine

The Max Depth determines the maximum depth that is affected by the electron dose. EC Surface Dose refers to the amount of electron dose on the surface. The Depth coefficient determines the rate at which the electron dose declines as depth increases. The Depth Fraction refers to the depth where the linear part ends and the exponential region of the EC begins. The primary exponential curve of EC can be controlled by the Scale Fraction to achieve the origin of the linear part of the curve. The Off-axis Coefficient relates to the effects of the EC which reduce as the distance from the axis increases. This effect is modeled as a Gaussian curve. Zero value for Off-axis Coefficient results in uniform EC. The more this Coefficient increases, the more the EC decreases away from the axis (Pinnacle^3 Physics). Since EC falls abruptly to zero outside the field, the high EC machine model produces a very sharp penumbra.

2.2 IMRT

This thesis consists of two parts. Different models and optimization parameters are used in each part:

2.2.1 Thick model

2.2.1.1 System setup

In this model we consider a rectangular phantom with dimensions: 24.25 cm×9.25 cm×24.25 cm (Left-Right (LR) × Anterior-Posterior (AP) × Superior-Inferior (SI)) and density of 1 g/cm^3. We consider the LR as X, AP as Y and SI as Z directions. A rectangular target is centered in the phantom with (Left-Right (LR) × Anterior-Posterior (AP) × Superior-Inferior (SI)) dimensions: 20.25 cm×5.25 cm×20.25 cm. There is a 2 cm margin from the edge of the target to the outside edge of the phantom in each direction. The target is divided into equal two parts: ROI-1 is considered to be the tumor and ROI-2 is considered to be the organ at risk. Two 6-MV photon beams are incident on the target at right angles. The orientation of the beams and the positioning of the phantom, ROI-1 and ROI-2 are presented in figure 2.7.

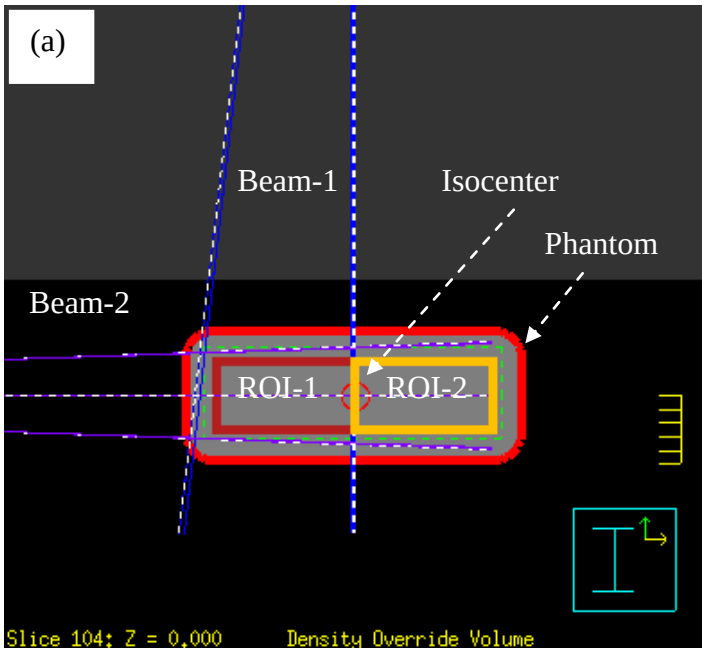

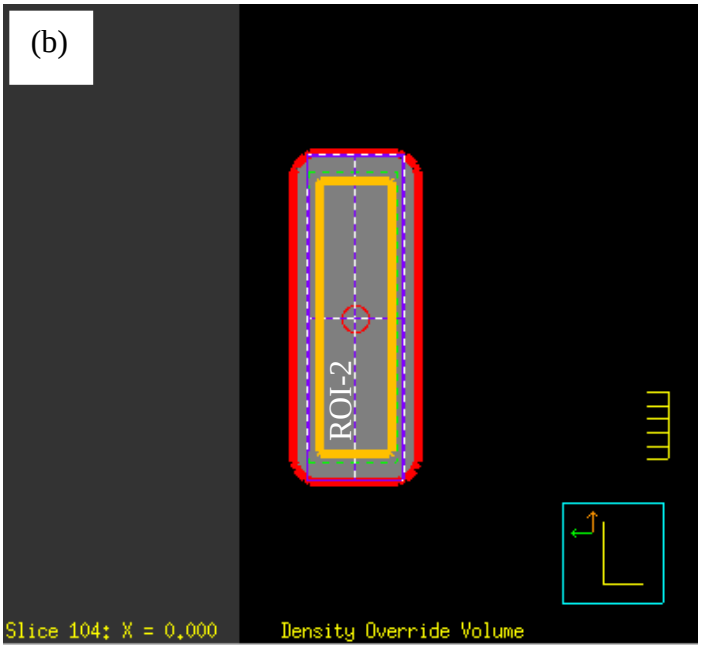
(b)
ROI-2
Slice 104: X = 0.000
Density Override Volume

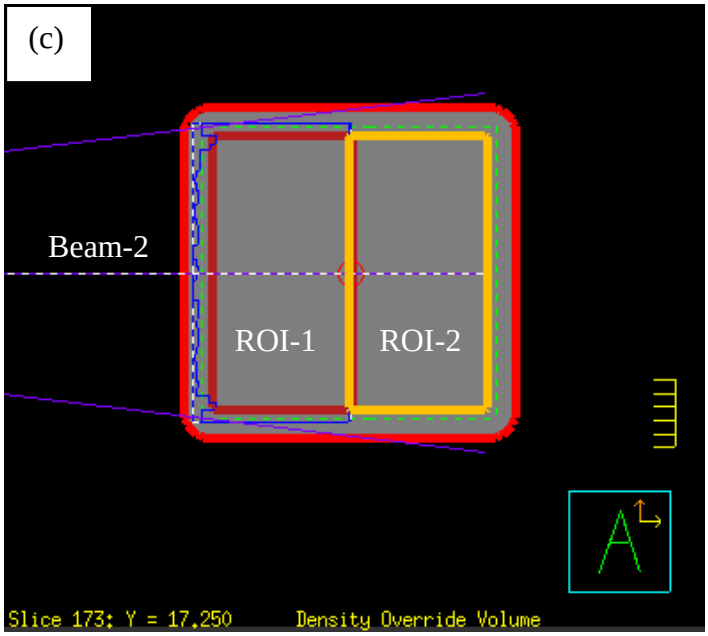
(c)
Beam-2
ROI-1
ROI-2
Slice 173: Y = 17.250
Density Override Volume

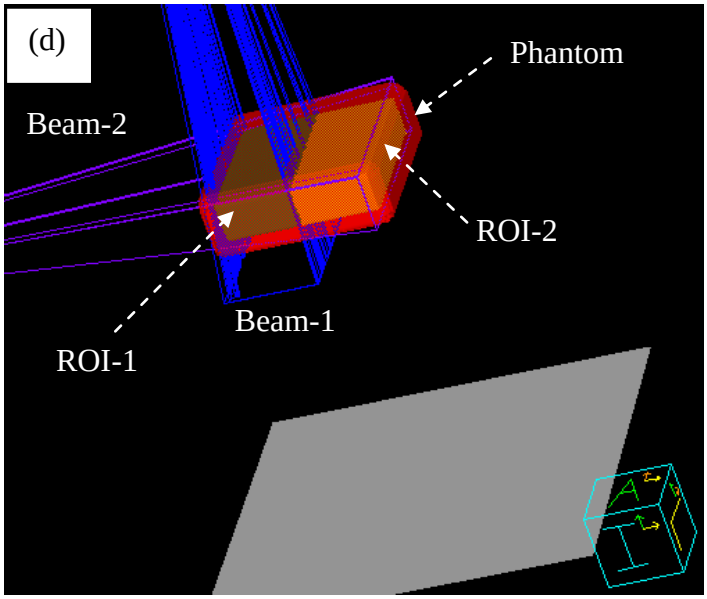

Figure 2.7: Two dimensional view of the thick model and orientation of the beams from (a) Sup-Inf (b) Lateral (c) Ant-Post; directions and (d) Three dimensional view of the model

This model has 208 slices in each SI, AP and LR directions. Isocentre is placed in the center of the phantom at the boundary between ROI-1 and ROI-2. The dose grid resolution is 0.254 cm, 0.250 cm and 0.250 cm in LR, AP and SI directions respectively. Table 2.3 presents the beams characteristics.

Beam Parameter	Beam-1	Beam-2
Energy/Modality	6-MV photons	6-MV photons
SAD (cm)	100.0	100.0
Couch Angle	0.0	0.0
Gantry Angle	0.0	270.0
Collimator Angle	0.0	0.0
SSD (cm)	95.40	87.90

Table 2.3: Beam setup and beam geometry data for the thick model

To set the IMRT parameters, first we defined the objectives for the regions of interest. The desired goal of IMRT is defined by the objectives. The software tries to provide an optimum

plan to achieve this goal. Weights are applied to convey the level of importance of each objective (P^3IMRT). Table 2.4 lists the types of objectives and corresponding weights defined for the ROIs.

The min dose objective means that the ROI should receive a dose greater than that specified and the max dose objective means that the ROI should receive a dose less than that specified in order to satisfy the objectives. When the uniform dose is specified, the software tries to deliver the defined uniform dose throughout the ROI (P^3IMRT).

ROI	Objective Type	Target (c Gy)	Weight
ROI-1	Min Dose	6900	90.00
ROI-1	Max Dose	7100	20.00
ROI-1	Uniform Dose	7000	20.00
ROI-2	Max Dose	2000	80.00

Table 2.4: Objective data for the thick model

Then we set the optimization parameters for Direct Machine Parameter Optimization (DMPO). With DMPO, the MLC settings are generated while the optimization is in progress. Thus conversion, weight optimization and filtering are not required after optimization completes. Optimization parameters were set as shown in table 2.5. Maximum iterations specify the maximum number of times that the software searches for solutions to improve the plan. Before the software starts to calculate the dose by convolution, it will complete the number of iterations specified by the convolution dose iteration. The stopping tolerance value refers to the change in the objective value between two successive iterations. If this change is less than the stopping tolerance, then the optimization is assumed satisfied and stops. If the leaf is to block the whole field, the distance that the leaf should extend under the opposite jaws is determined by the

Leaf/Field edge overlap. To treat a broad field, the jaws should overlap to split the beam. The minimum overlap distance for beam splitting refers to this overlapping distance (P^3IMRT).

Optimization parameters	Value
Maximum iterations	30
Convolution dose iteration	10
Stopping tolerance	1.00E-05
Maximum number of segments	20
Minimum segment area (sq cm)	2.00
Minimum segment MUs	5.00
Leaf/Field edge overlap (cm)	0.50
Minimum overlap distance for beam splitting (cm)	2.00

Table 2.5: Optimization and DMPO parameters for the thick model

At this stage we optimize the plan on three machines:

(a) *A copy of the clinical machine:* We vary out of field parameters for this machine. After each variation the optimization is carried out. The density of phantom is set to be $1g/cm^3$.

(b) *High EC machine:* This machine is used to investigate the relationship between very sharp penumbra and generation of narrow segments. The density of phantom is set to be $0.001g/cm^3$ to achieve the sharpest penumbra.

(c) *Large Penumbra machine:* This machine is used to investigate the relationship between very wide penumbra and the production of narrow segments. The density of phantom is set to be $0.001g/cm^3$ to compare with the results from the sharp penumbra machine.

For each optimization we count the number of leaf pairs separated by a narrow gap. After each variation in the machine the 95-50% penumbra width is determined to investigate the relationship between the number of narrow leaf pair gaps and beam penumbra. To determine the

penumbra width we consider the distance from the 50% isodose level to the 95% isodose level (Figure 2.8). Isodoses are normalized relative to a reference point. Since SAD is fixed in the treatment technique, then the isocentre is considered as the reference point. The dose at the reference point is considered to be 100%, thus the percent dose at any other isodose level can be determined (Gunilla C. Bentel).

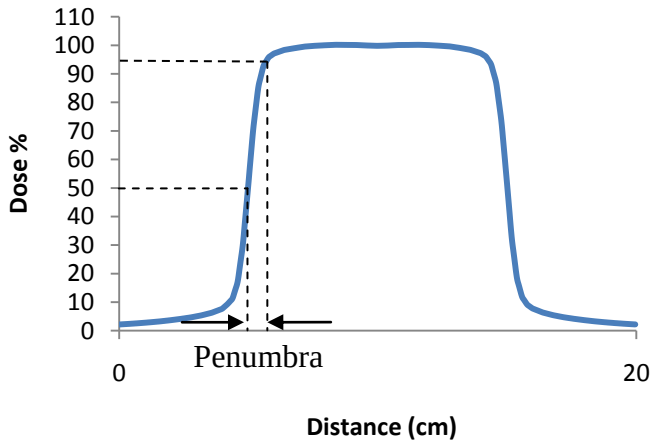

Figure 2.8: Illustration of dose profile and penumbra width

In the thick model we were trying to find out if there was a relationship between the penumbra and generation of narrow segments. We could not find any consistency in the results. Therefore we decided to vary other parameters such as organ at risk max dose objective, the gap between the target and OAR and %volume in the DVH study to see if they affect the narrow segments. In these studies beam-2 (lateral) does not participate in the generation of narrow segments along the interface. Thus we remove beam-2 and obtaine simpler model with a single beam. For this purpose we reduce the thickness to improve dose uniformity along the incident beam direction.

2.2.2 Thin model

2.2.2.1 System setup

Our aim is to simplify the previous model. For this purpose we change the dimensions of the target to make it thin along the ant-post direction. Therefore, there is no need to compensate for dose fall-off with depth, allowing the elimination of beam-2. The dimensions of the thin target are 20.25 cm×1.25 cm×20.25 cm (LR × AP × SI) and the density is set to 1 g/cm^3. The dimensions of the phantom remain the same as the thick model. There is a 2 cm margin from the edge of the target to the outside edge of the phantom in the LR and SI directions and 4 cm margin in the AP direction. The target is divided into two equal parts: ROI-1 is considered to be the target and ROI-2 is considered to be the organ at risk. One 6-MV photon beam is normally incident on the target. The orientation of the beam and positioning of the phantom, ROI-1 and ROI-2 are illustrated in figure 2.9.

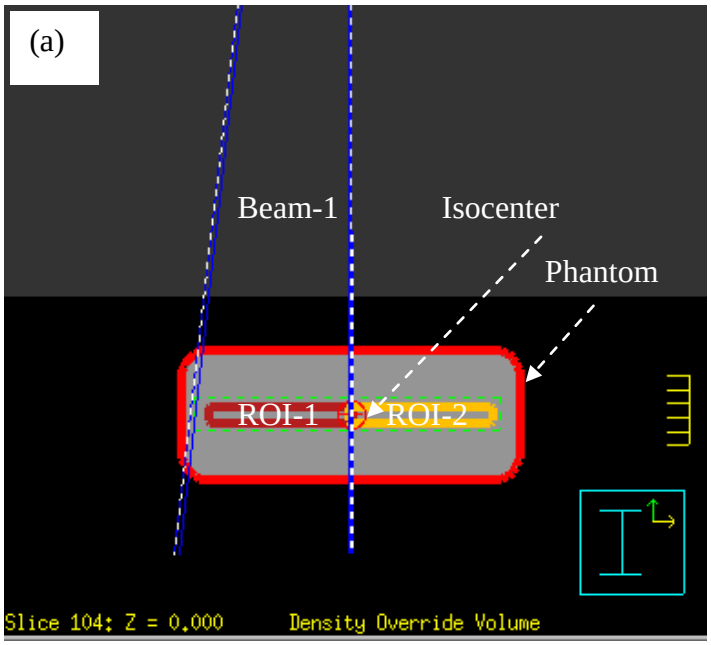

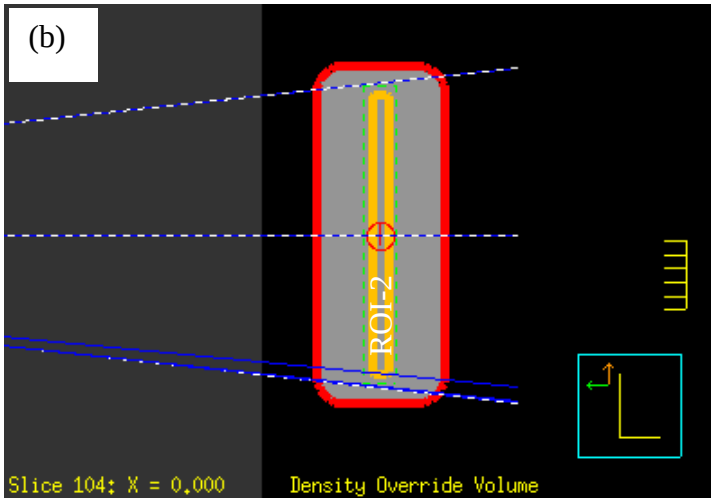
(b)
ROI-2
Slice 104: X = 0.000
Density Override Volume

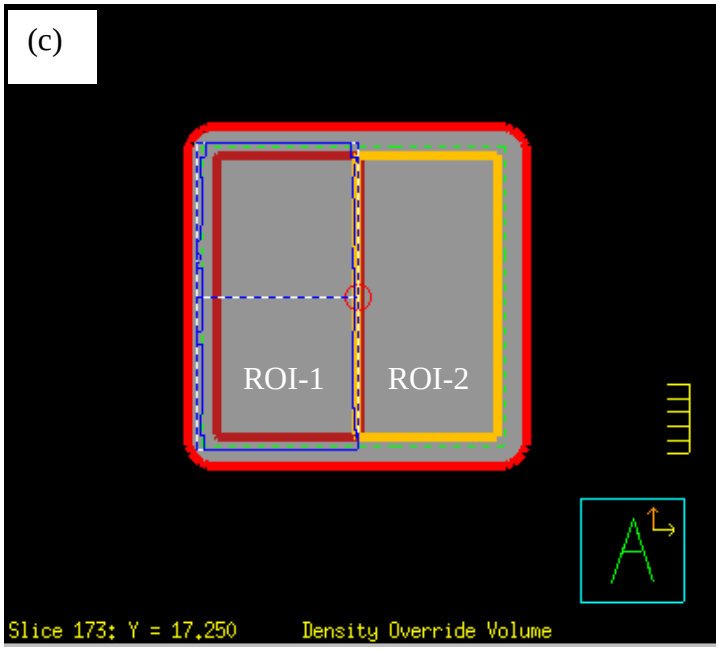
(c)
ROI-1
ROI-2
Slice 173: Y = 17.250
Density Override Volume

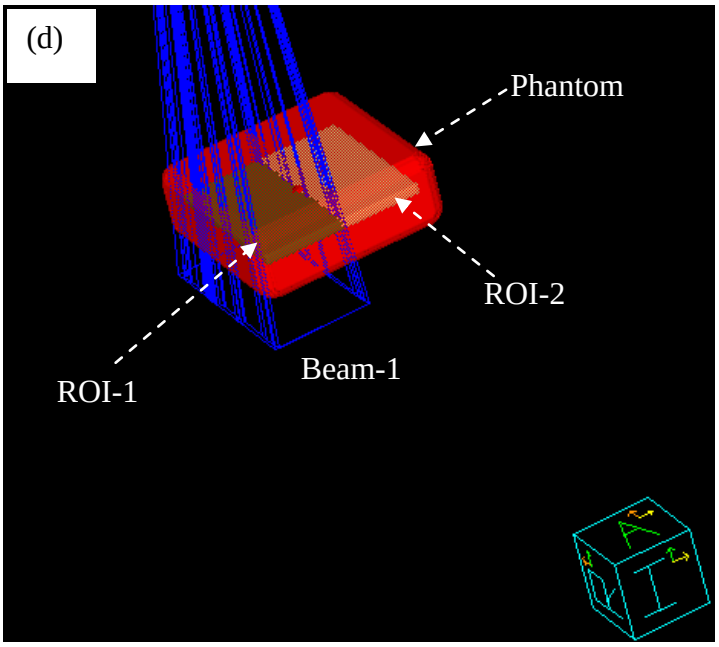

Figure 2.9: Two dimensional view of the thin model and orientation of the beams from (a) Sup-Inf (b) Lateral (c) Ant-Post; directions and (d) Three dimensional view of the model

This model has 208 slices in each LR, AP and SI direction. The isocentre is placed in the center of the target. The dose grid resolution is 0.254 cm, 0.250 cm and 0.250 cm in LR, AP and SI directions respectively. Table 2.6 presents the beams characteristics.

Beam Parameters	Beam-1
Energy/Modality	6-MV photons
SAD (cm)	100.0
Couch Angle	0.0
Gantry Angle	0.0
Collimator Angle	0.0
SSD (cm)	95.26

Table 2.6: Beam setup and beam geometry data for the thin model

The optimization type was set to DMPO. Table 2.7 lists the optimization parameters used for this model.

Optimization parameters	Value
Maximum iterations	20
Convolution dose iteration	8
Stopping tolerance	1.00E-05
Maximum number of segments	6
Minimum segment area (sq cm)	2.00
Minimum segment MUs	5.00
Leaf/Field edge overlap (cm)	0.50
Minimum overlap distance for beam splitting (cm)	2.00

Table 2.7: Optimization and DMPO parameters for the thin model

Table 2.8 presents the types of objectives and corresponding weight used for each ROI.

ROI	Objective Type	Target (c Gy)	Weight
ROI-1	Min Dose	7000	100.00
ROI-2	Max Dose	variable	5.00

Table 2.8: Objective data for the thin model

With this model we perform three series of optimizations:

(a) The Maximum dose to ROI-2 is varied to examine if the dose difference between the two regions of interest affects the generation of narrow segments along the interface between the two regions.

(b) We fix the maximum dose to 10 Gy for ROI-2 and create a gap between the tumor and the organ at risk. Then the influence of gap width on the production of narrow segments is evaluated. A negative gap width (indicating that the target and the critical structure overlapped) is also considered.

(c) The objective type is changed to maximum dose volume histogram (DVH) for ROI-2. The target dose is set to be 10 Gy. We vary the percent volume of ROI-2 that can receive more than 10 Gy. The effect of this variation on the generation of narrow gaps between leaf pairs is examined.

Chapter 3:
RESULTS AND ANALYSIS

As discussed in chapter 2, we set up two geometrical models. In this chapter we will analyze the results we obtained with each of these models.

3.1 Thick model

For the thick model we vary out-of-field parameters for a copy of clinical machine and optimize the plan. For each variation the numbers of narrow leaf pair separations are counted. We divide segments into five categories: 0-3 mm, 3-5 mm, 5-8 mm, 8-12 mm and larger than 12 mm wide segments. We consider the segments smaller than 12 mm in width as narrow segments. The beam penumbra is determined as the distance from 50% to 95% dose level in LR (X) direction through the isocentre. The relationship between the number of narrow leaf pair separations and beam penumbra for each variation are investigated.

3.1.1 Effective source size

Effective source size parameter includes two components: perpendicular to gantry axis (X direction) and parallel to gantry axis (Y direction). We vary the source size both equally in X and Y directions and unequally by holding X fixed and varying Y and vice versa to investigate the effect of the change on the production of narrow segments.

3.1.1.1 Changing the source size with equal X and Y dimensions

The X and Y component of the source size are changed equally from 0.04 cm to 2 cm. The relationship between the penumbra and related source size is presented in figure 3.1. As source size increases penumbra increases.

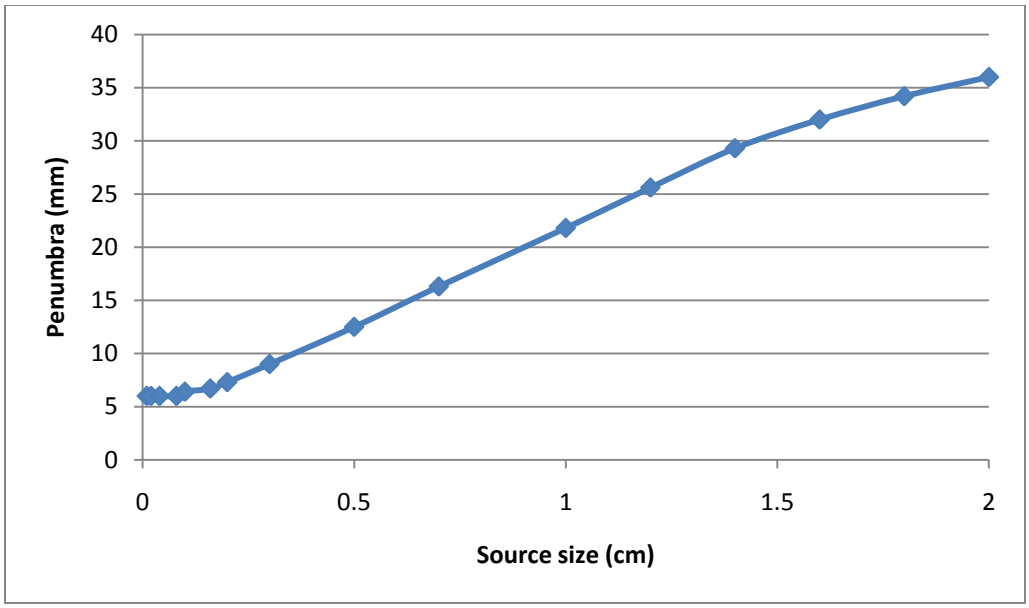

Figure 3.1: Effect of symmetric change in source size on the beam penumbra

The influence of penumbra and source size on the generation of narrow segments is shown in figure 3.2 and 3.3 respectively.

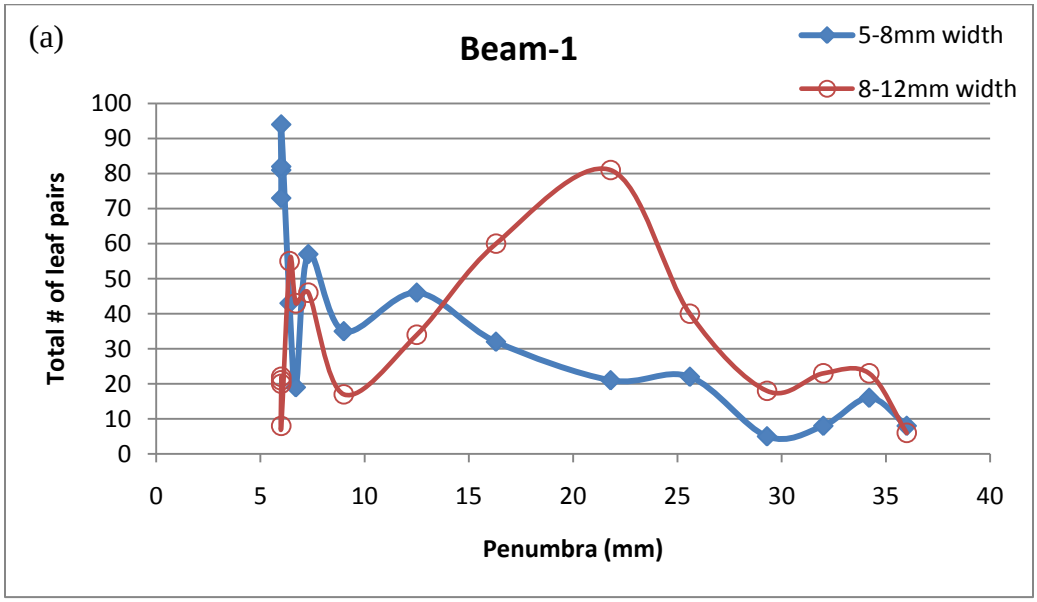

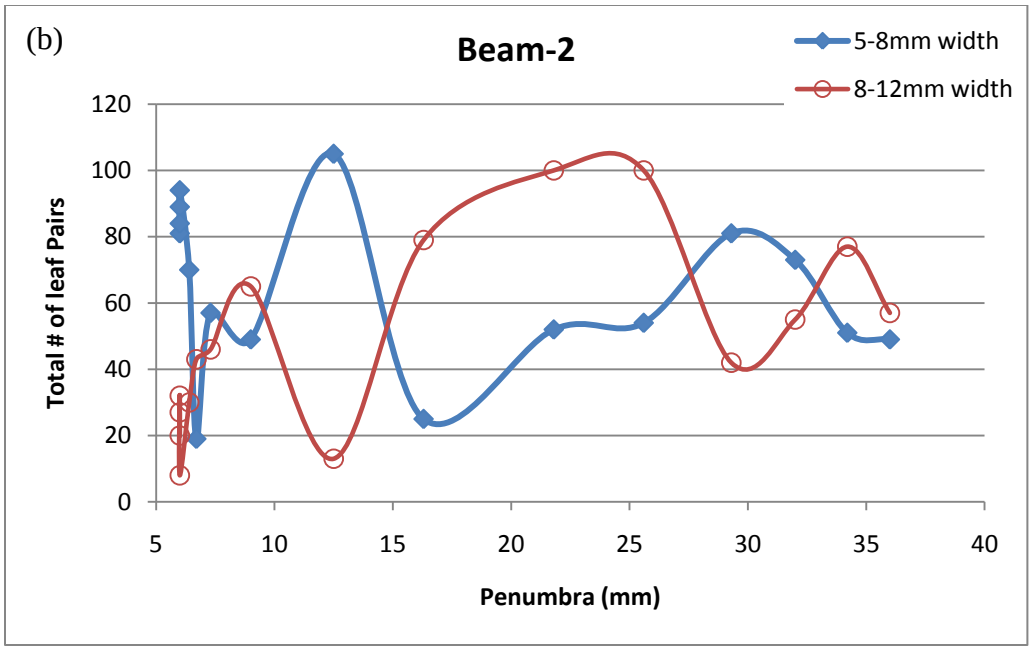

Figure 3.2: Total number of leaf pairs versus beam penumbra when source size changed for (a) beam-1 (b) beam-2

The change in total number of narrow leaf pairs is the same when it is plotted against the source size since the source size is proportional to the penumbra. In beam-1 there is an overall decrease in the number of leaf pairs with 5-8 mm gap. The number of leaf pairs with an 8-12 mm gap is maximized at a source size of 1 cm and a penumbra of 21.8 mm.

Now we consider focusing on the small source sizes. Therefore we vary the source size from 0.01 cm to 0.2 cm. Figure 3.3 presents the change in the total number of narrow leaf pairs with change in the penumbra for beam-1 and beam-2.

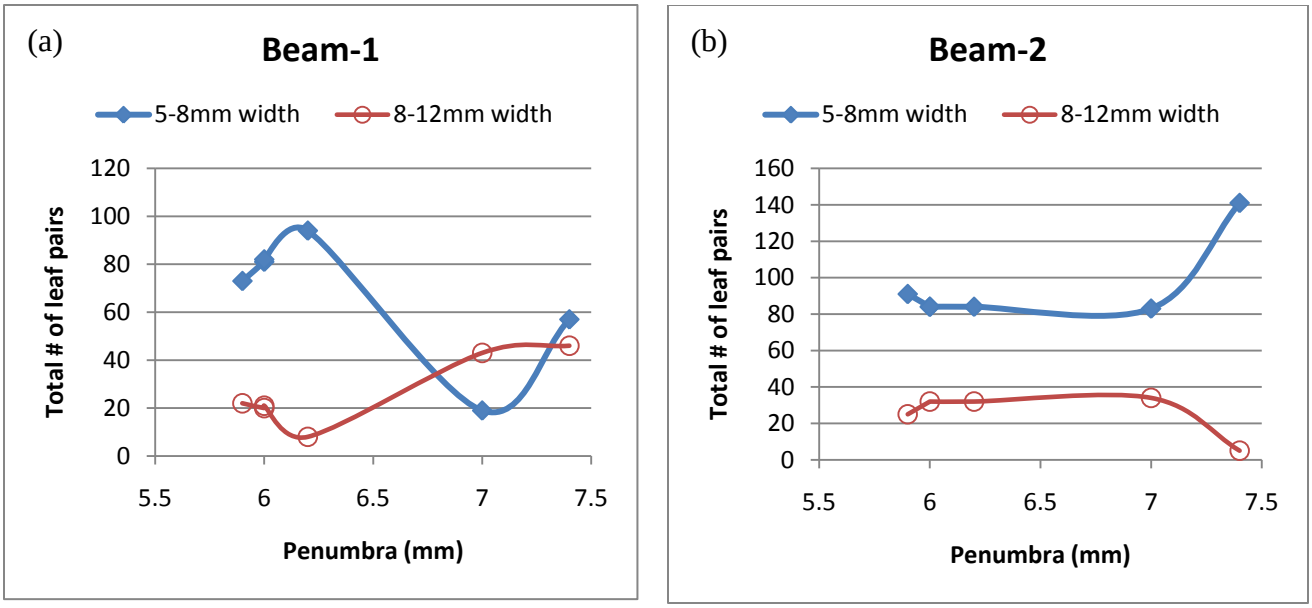

Figure 3.3: Change in total number of narrow leaf pairs with penumbra when source size changed from 0.01 to 0.2 cm equally in X and Y directions; for (a) beam-1 (b) beam-2

The penumbra increases as the source size increases. The change in total number of 5-8 mm leaf pairs in figure 3.3 shows an opposite trend relative to 8-12 mm leaf pairs for both beam-1 and beam-2. A maximum of 94 5-8 mm leaf pairs corresponds to a 6.2 mm penumbra with x and y source dimensions of 0.08 cm for beam-1. At the same point there is a minimum of 8 for 8-12 mm leaf pairs. Also beam-2 indicates a maximum of 141 5-8 mm leaf pairs for 7.4 mm wide penumbra and 0.2×0.2 cm^2 source size. 8-12 mm leaf pairs have the minimum value of 5 at the same point. Also total number of narrowly separated leaf pairs in beam-2, does not present a significant dependence on the penumbra for penumbra value of less than 7.0 mm.

3.1.1.2 Changing the source size with unequal X and Y dimensions

(i) *Perpendicular to gantry axis change*

In this section we vary the perpendicular to gantry axis (X) component of the source and left the parallel to gantry axis (Y) component, constant at value of 0.04 cm. This experiment is carried out for small source sizes to examine the effect of each component of source size on the

generation of narrow segments. The change in total number of narrow leaf pairs relative to penumbra shows almost the same results as the case when the source size is changed in both X and Y directions equally (figure 3.4).

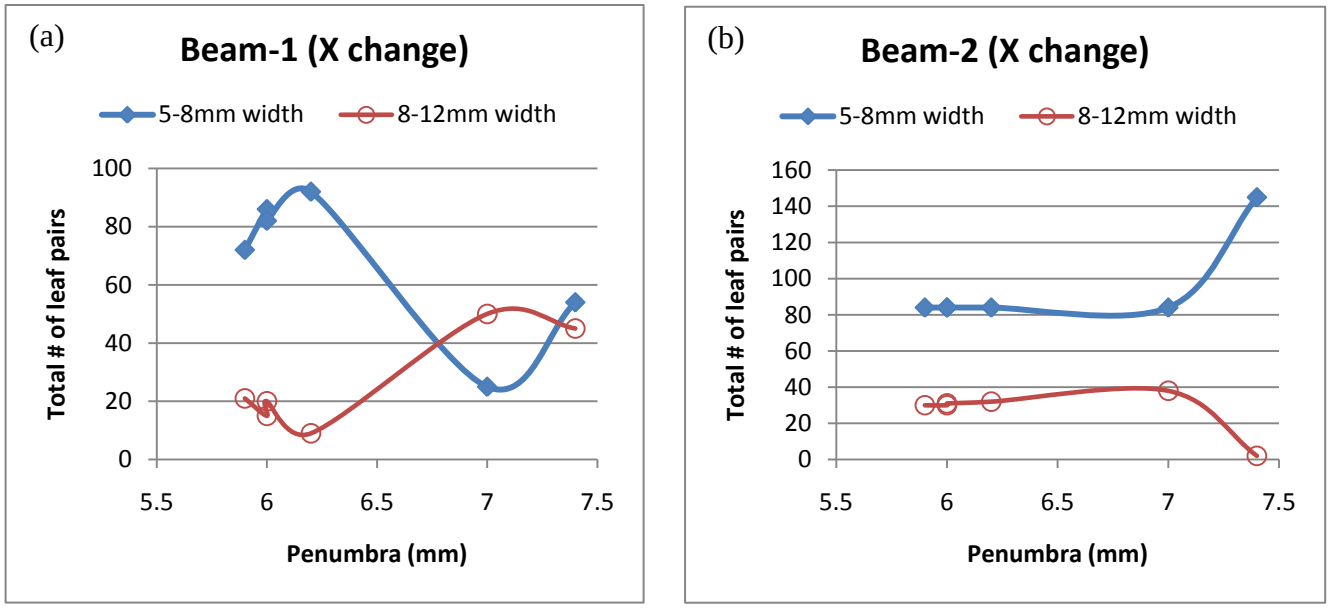

Figure 3.4: Change in total number of narrow leaf pairs with penumbra when source size changed from 0.01 to 0.2 cm only in X direction; for (a) beam-1 (b) beam-2

(ii) *Parallel to gantry axis change*

The change in the parallel to gantry axis component of source size (Y) while X component remains constant at 0.04 cm does not result in significant change in penumbra in LR (X) direction of the geometrical model and in the total number of narrow leaf pairs (figure 3.5). The penumbra in this case is determined to be 6.0 mm.

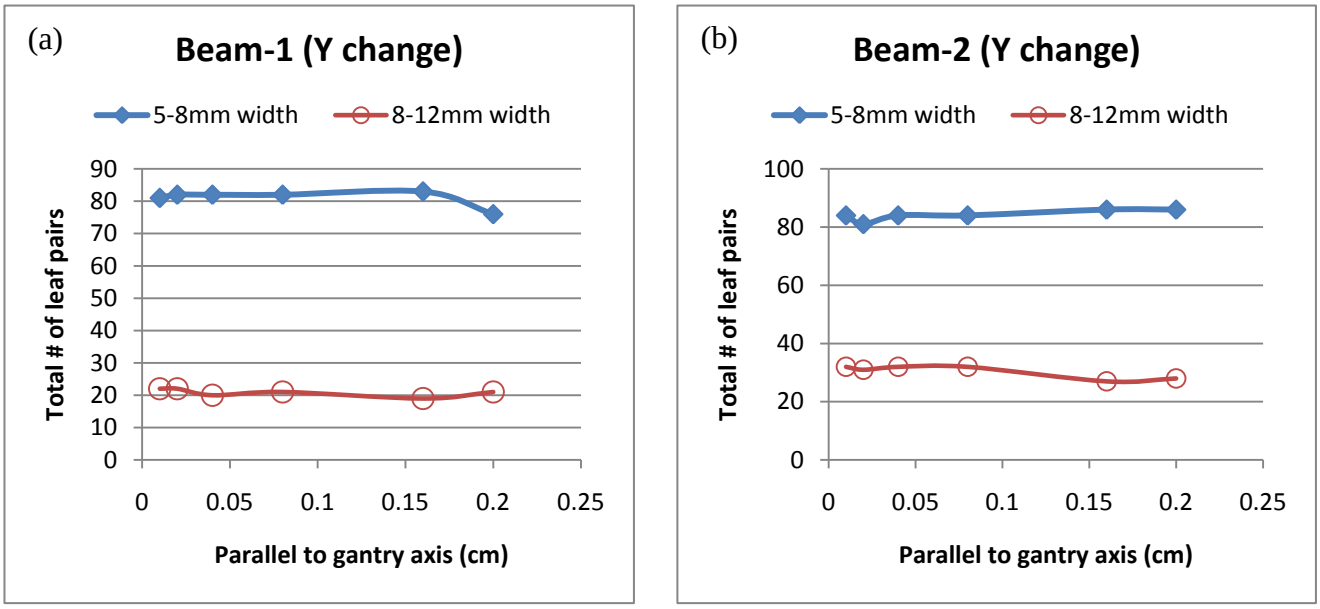

Figure 3.5: Effect of change in Y component of the source size on the total number of narrow leaf pairs for (a) beam-1 and (b) beam-2

3.1.2 Gaussian height

Gaussian height is varied from 0 to 0.3 while other out of field parameters remain the same as for clinical machine. The results are shown in figures 3.6 and 3.7.

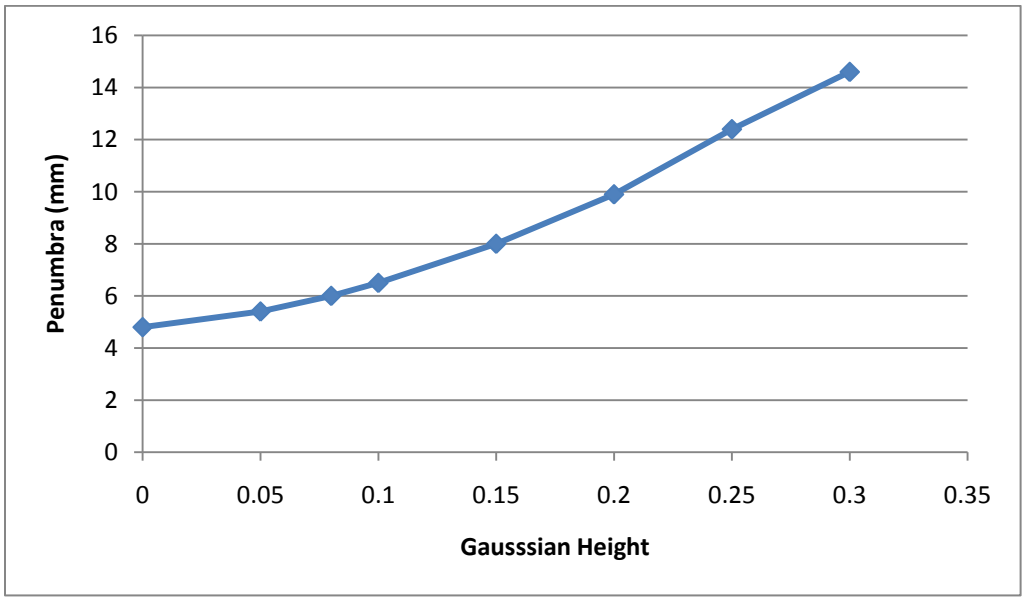

Figure 3.6: Determined penumbra versus Gaussian height

Penumbra increases as Gaussian height increases.

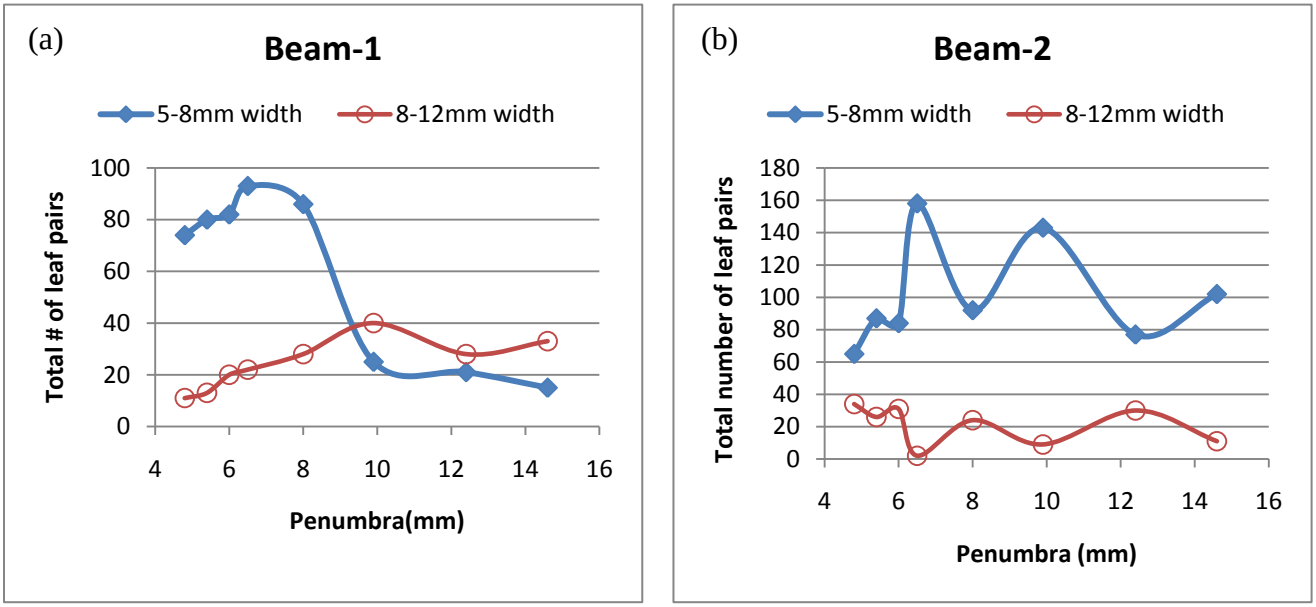

Figure 3.7: Relationship between total number of narrow leaf pairs and penumbra as Gaussian height varied; for (a) beam-1 and (b) beam-2. Because the penumbra and Gaussian height vary proportionally, the plot of total number of leaf pairs against Gaussian height would present the same results.

It can be seen from the graphs that beam-1 does not present any specific trend for 5-8 mm leaf pairs as penumbra increases up to 9.9 mm. It remains almost constant for penumbras larger than 9.9 mm. 8-12 mm leaf pairs behave the same for larger penumbras but they show an increase as penumbra increases up to 9.9 mm. Beam-2 demonstrates the opposite behavior of 5-8 mm and 8-12 mm leaf pairs. As a whole total number of leaf pairs exhibit a much higher value for 5-8 mm width relative to 8-12 mm width for any penumbra.

3.1.3 Gaussian width

Gaussian width is changed from 0 to 5 cm. As Gaussian width increases, penumbra increases to a maximum value of 6.0 mm which refers to clinical machine. There is a reduction

in penumbra for the Gaussian height above 1.4 cm. The smallest penumbra (4.8 mm) refers to Gaussian width of 0 cm. Overall change in the penumbra is 1.2 mm (figure 3.8).

Figure 3.8: Change in penumbra as Gaussian height increases

Beam-1 shows a minimum in the number of 5-8 mm leaf pairs (38 leaf pairs) at 5.6 mm penumbra width which refers to 2 cm Gaussian width. A very low variation in the number of 8-12 mm leaf pairs occurs. Again total number of 5-8 mm leaf pairs presents a significantly higher amount relative to 8-12 mm leaf pairs (figure 3.9).

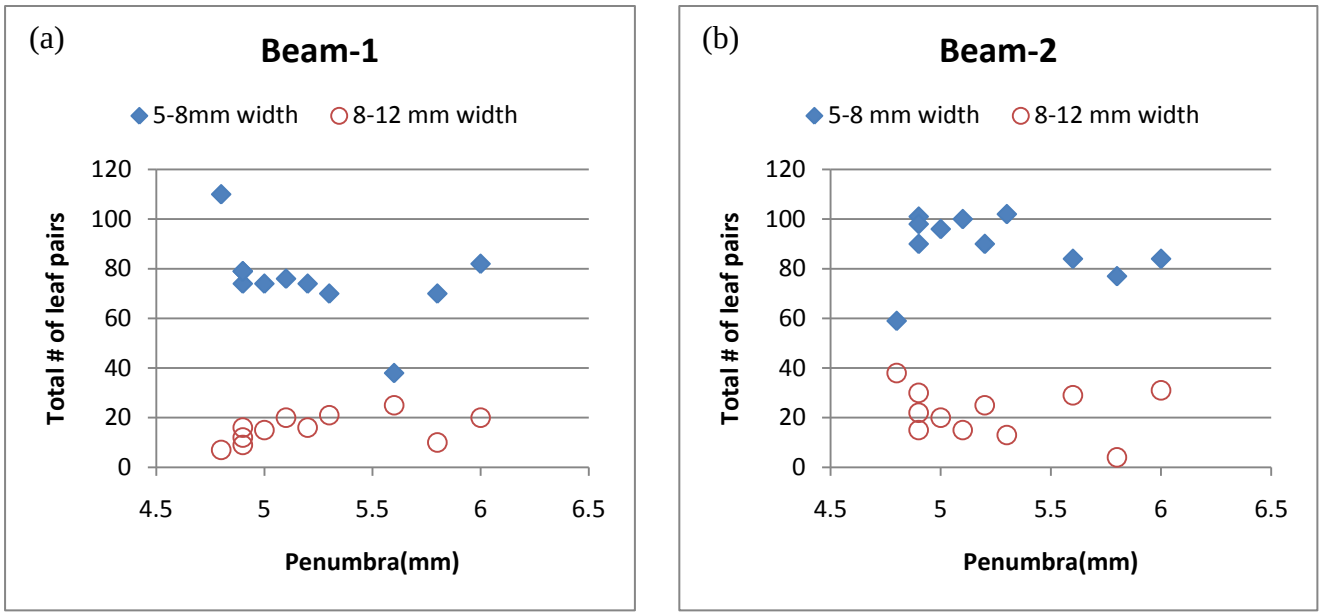

Figure 3.9: Change in total number of narrow leaf pairs as Gaussian width and therefore penumbra changes; for (a) beam-1 and (b) beam-2

Jaw transmission and MLC transmission variation does not influence the beam penumbra and generation of narrow segments.

3.1.4 Small, large and clinical penumbra

As discussed in chapter 2, a machine with high electron contamination is created. Using this machine with a very low density (0.001g/cm^3) phantom, results in the smallest possible penumbra (1.1 mm). Another machine is created with no electron contamination and used with the same phantom density to obtain a very large penumbra (25.2 mm). The clinical machine is used as a medium penumbra (6.0 mm) machine. We perform three series of optimizations using these three machines to investigate the effect of penumbra on the generation of narrow segments. A change in the organ at risk max dose objective (50 Gy, 20 Gy and 5 Gy) while the tumor objectives remain constant (Min dose 69 Gy, Max dose 71 Gy and uniform dose 70 Gy), affects the total number of narrow leaf pairs (figure 3.10). 8-12 mm leaf pairs for beam-2 show the same trend in figure 3.10 (b), (d) and (f). There are no 5-8 mm leaf pairs when the ROI-2 max

dose objective is 50 Gy. The number of 5-8 mm leaf pairs increase as the ROI-2 max dose objective decreases. With an ROI-2 max dose objective of 5 Gy, the overall number of leaf pairs is higher than with an ROI-2 max dose objective of 20 Gy.

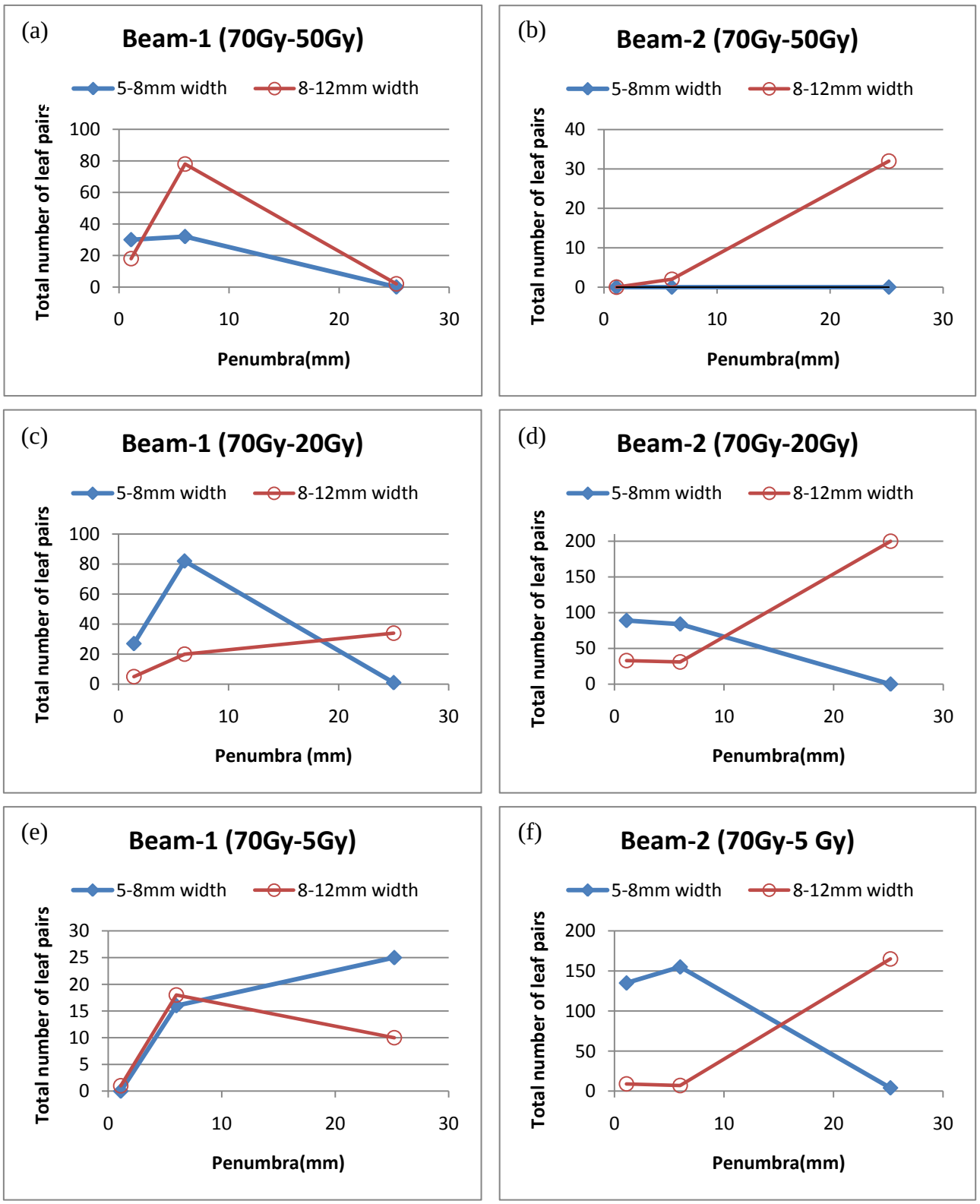

Figure 3.10: Total number of narrow leaf pairs for small, medium and large penumbra; for (a) and (b) beam-1 and beam-2, ROI-2 max dose objective 50 Gy (c) and (d) beam-1 and beam-2, ROI-2 max dose objective 20 Gy (e) and (f) beam-1 and beam-2, ROI-2 max dose objective 5 Gy

3.1.5 Phantom density change

We set the plan for OAR max dose objective of 20 Gy again and use the clinical machine, while changing the density of phantom to examine its effect on penumbra and number of narrow leaf pairs (figures 3.11 and 3.12).

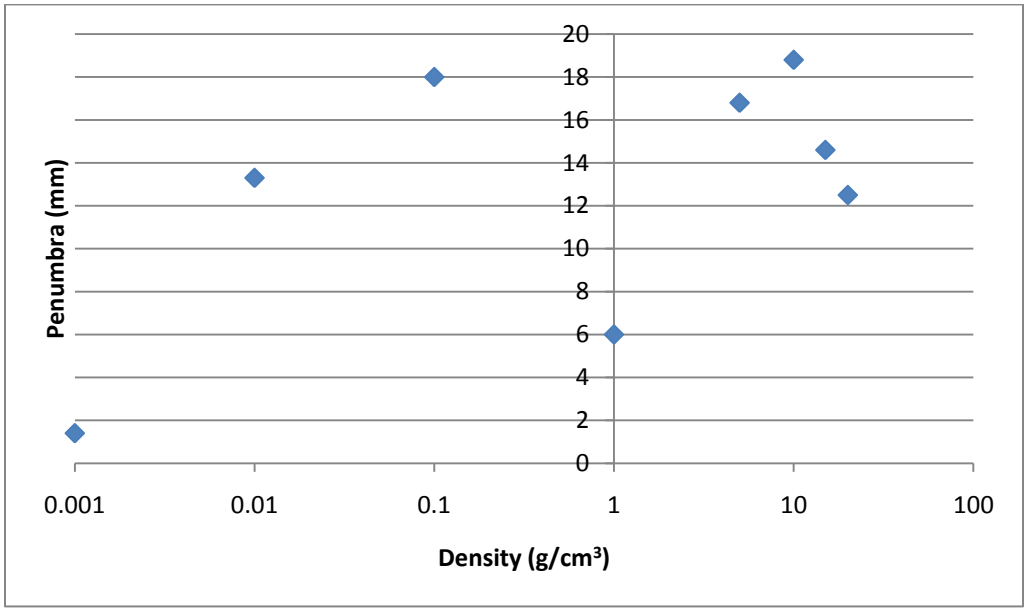

Figure 3.11: Change in penumbra with phantom density variation

According to figure 3.12, total number of 5-8 mm leaf pairs exhibit higher values relative to 8-12 mm leaf pairs. For beam-1 8-12 mm leaf pairs do not show a significant variation as density and penumbra varies, and they stay below 20 leaf pairs. For beam-1 there is maximum of 80 for 5-8 mm leaf pairs at unit density and penumbra of 6.0 mm. We can demonstrate that there is an overall decrease in the total number of 5-8 mm leaf pairs as penumbra increases.

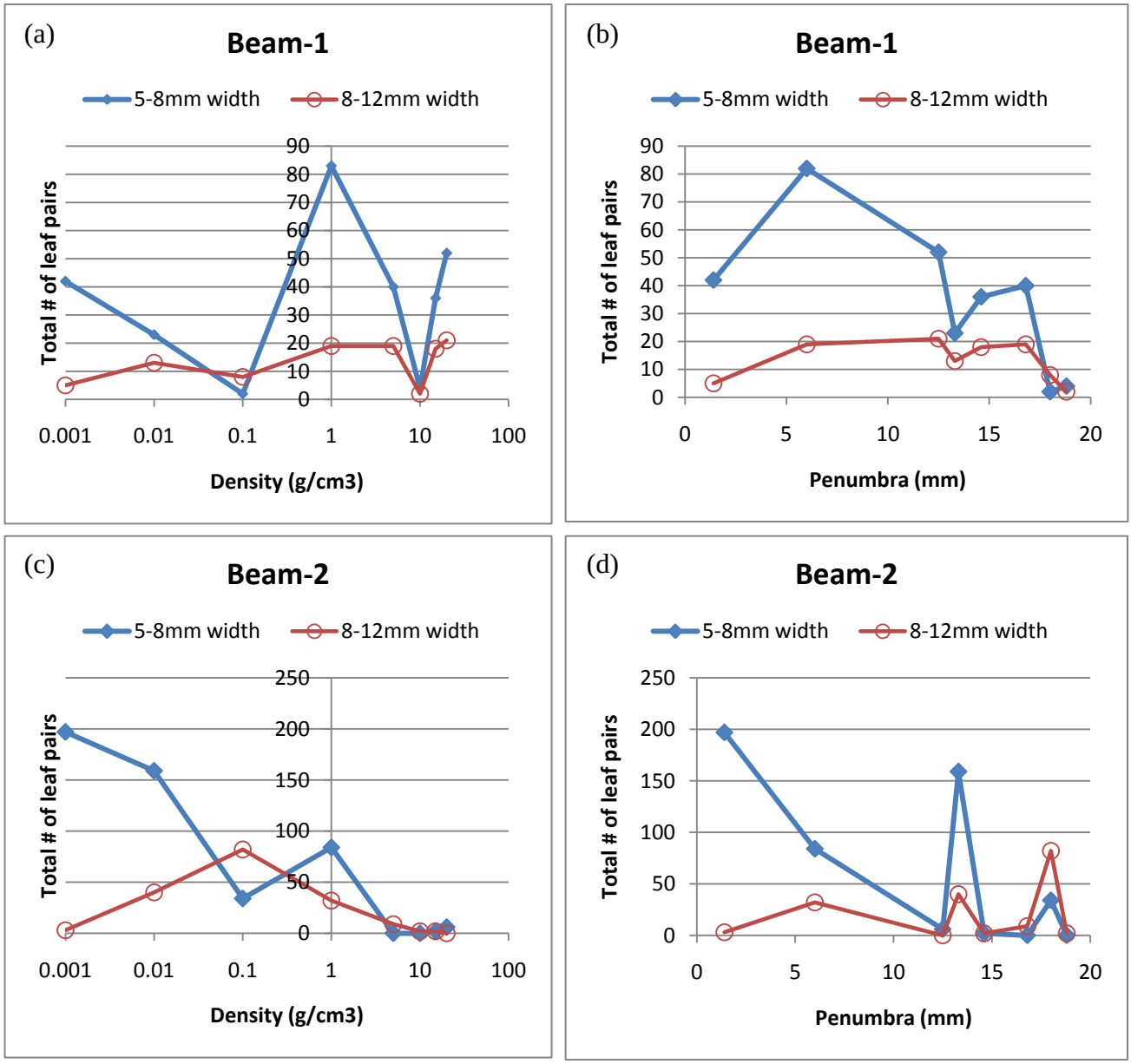

Figure 3.12: The change in total number of narrow leaf pairs for the beams, (a) and (c) as density of the phantom changes, (b) and (d) as the penumbra of the beams changes

3.2 Thin model

In the thick model we examine the relationship between the beam penumbra and the generation of narrow segments. Because the results are inconsistent, we decided to investigate which factors affect the generation of narrow segments other than the beam penumbra. For this purpose we simplify the model by decreasing the thickness of the target. Therefore beam-2 is

removed and optimization is carried out with beam-1 only. The clinical machine is used with a unit density phantom.

In this part of the study some of the beam profiles show a peak near the interface. The existence of the peaks serves to compensate the penumbra. Therefore parameters such as peak height, peak width, gradient near the interface, maximum gradient, and average dose over 2 cm outside the target are determined to find their dependence on optimization parameters. Figure 3.13 illustrates one of these profiles we obtain when the OAR max dose objective is set to 30 Gy. The interface is located at the distance of 10 cm from the origin. Peak width is determined at the height of H (figure 3.13). H is determined as follows:

$$H = \left(\frac{Peak\ height(Gy) - Dose\ at\ 5cm\ inside\ the\ target(Gy)}{2}\right) + Dose\ at\ 5cm\ inside\ the\ target(Gy)$$

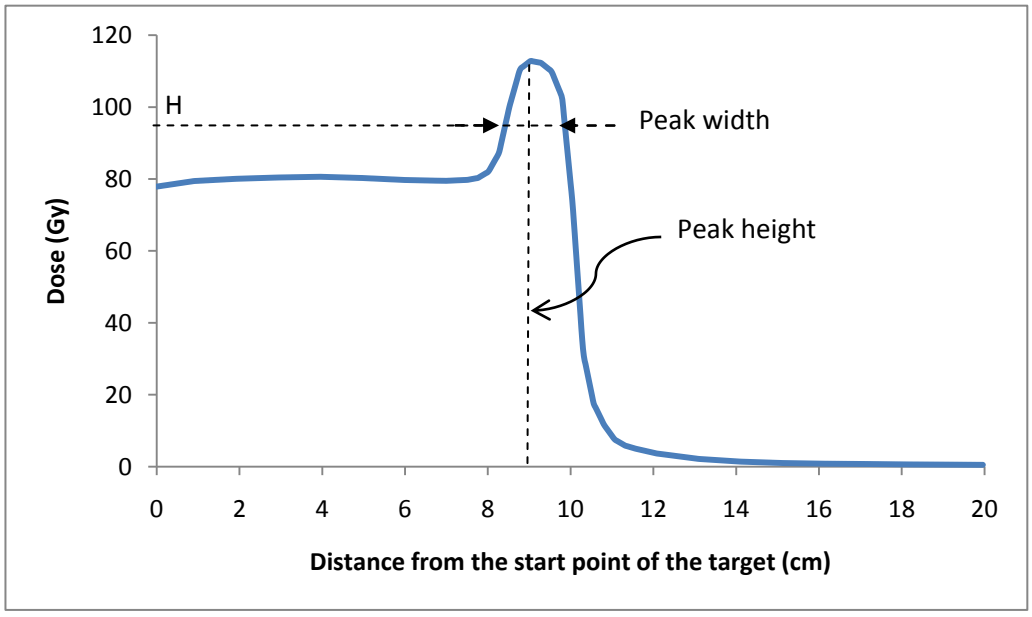

Figure 3.13: Illustration of a profile with a peak near the interface

3.2.1 Organ at risk (OAR) max dose objective change

Previously, the OAR max dose objective was set to 20 Gy. At this stage it is varied from 1 Gy to 70 Gy to find out if it has an influence on the number of narrow leaf pairs. Figure 3.14 shows the number of leaf pairs plotted against the OAR max dose objective. Leaf pairs with 5-8 mm gap do not appear. The number of leaf pairs with 8-12 mm gap varies as the OAR max dose objective increases but not in a monotonic fashion. When the OAR max dose objective is more than 55 Gy or the OAR max dose objective is less than 10 Gy, leaf pairs with 8-12 mm gap do not appear.

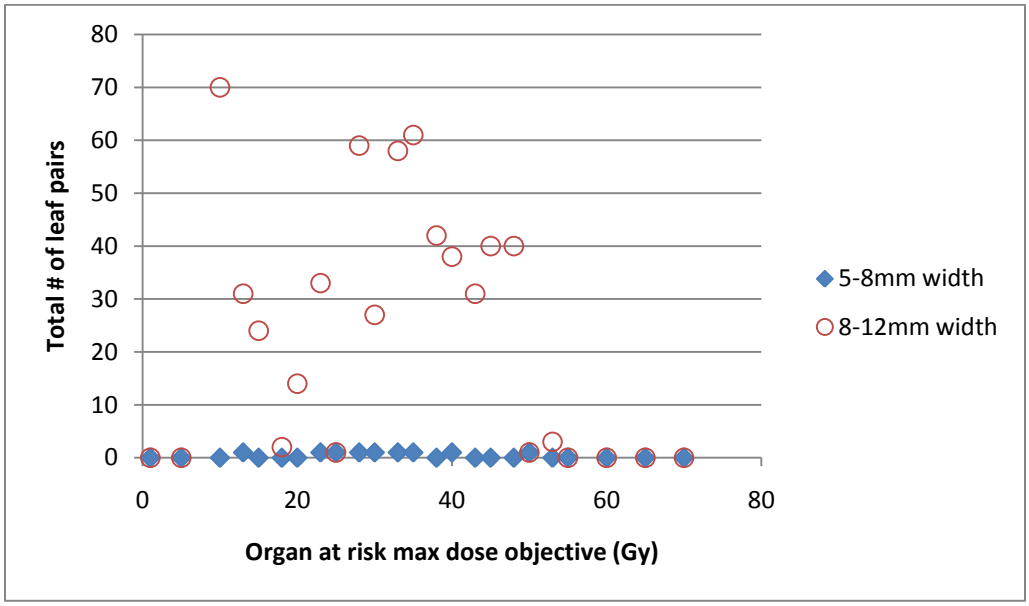

Figure 3.14: Change in the total number of 5-8 mm and 8-12 mm wide leaf pairs with the increase in the OAR max dose objective

Average dose delivered from 10 cm distance (interface) to 12 cm distance is determined and plotted against the OAR max dose objective. Also point doses at 0.5 cm inside the target, interface and 0.5 cm outside the target are determined (figure 3.15).

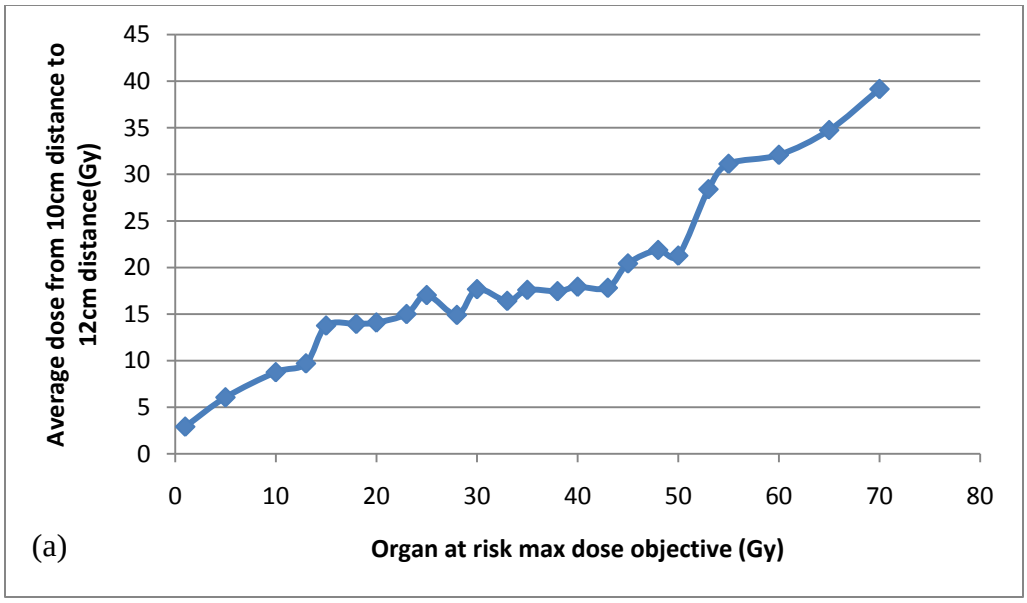

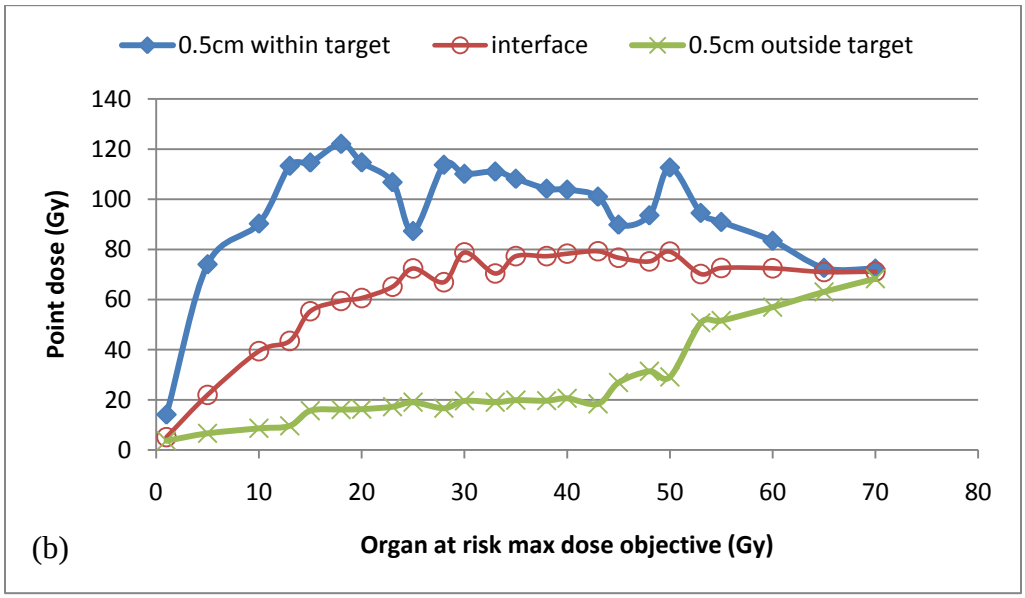

Figure 3.15: (a) Average dose over 2 cm outside the target and (b) doses at three different points, variations as OAR max dose objective increases

Increasing the OAR maximum dose objective allows the system to deliver more dose to the OAR. Thus the average dose delivered over 2 cm outside the target increases as well. For OAR max dose objectives less than 15 Gy, the OAR receives an average dose of almost the same as OAR max dose objective but for OAR max dose objectives larger than 15 Gy this value is almost half of OAR max dose objective. When there is a small or no difference between the

OAR max dose objective and target min dose objective, then the delivered dose in both regions would be nearly the same. Figure 3.15 (b) shows that an OAR max dose objective less than 5 Gy outside the target cannot be satisfied. There is a dramatic increase in the dose outside the target when OAR max dose objective is larger than 45 Gy. But for an OAR max dose objective less than 45 Gy the dose outside the target remains below 20 Gy.

The maximum gradient and its position were determined to investigate if it was influenced by the OAR max dose objective (figure 3.16). Maximum gradient exhibits a maximum value of 217.4 Gy/cm at the OAR max dose objective of 18 Gy. There is a shift in the position of maximum gradient almost at every 25 Gy change in the OAR max dose objective. It means that as the OAR max dose objective increases, the maximum gradient occurs closer to the OAR. For the OAR max dose objective larger than 35 Gy it occurs outside the target.

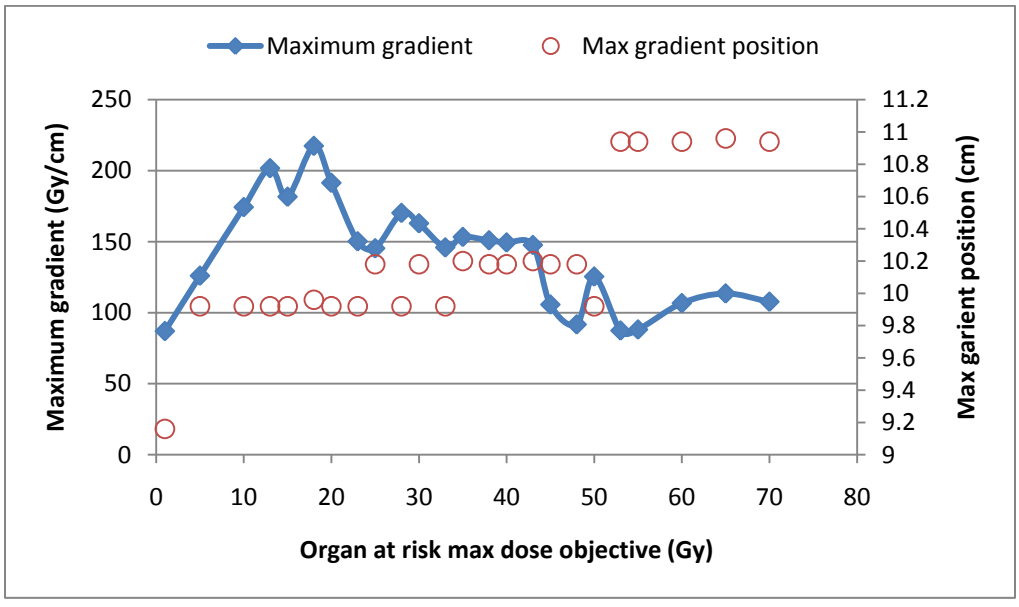

Figure 3.16: Maximum gradient and its position that measured at any change in the OAR max dose objective

The gradients over 1 cm (from 9.52 cm distance to 10.52 cm distance) and over 2 cm (from 9 cm distance and 11 cm distance) are determined. The maximum value of these gradients corresponds to an OAR max dose objective of 18 Gy, similar to the maximum gradient. Increasing the OAR max dose objective above 50 Gy results in a large reduction in the gradient (figure 3.17).

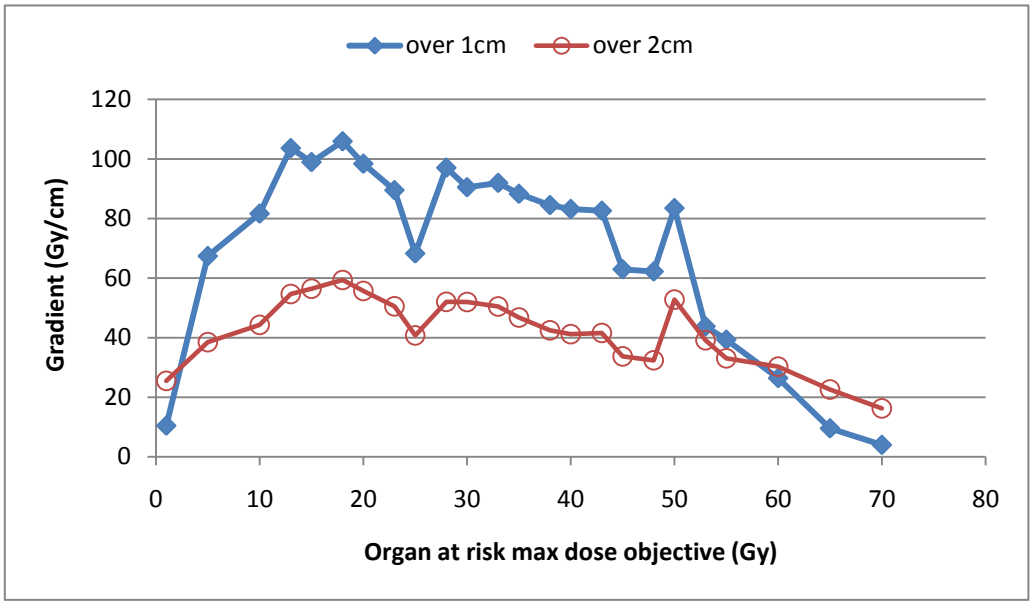

Figure 3.17: Change in the gradient averaged over 1 cm and 2 cm as OAR max dose objective increases

If the profile is linear from 9 cm distance to the 11 cm distance, then it is expected that the gradients over 1 cm and 2 cm are equal to the maximum gradient. But it does not seem to be true from the graphs. Therefore gradients over 1 cm and 2 cm are plotted against the maximum gradient to find out if it is a straight line (figure 3.18). The results are not exactly a straight line, thus gradients averaged over different areas do not necessarily correspond. However the gradient seems to be proportional for the max gradient values larger than 125 Gy/cm.

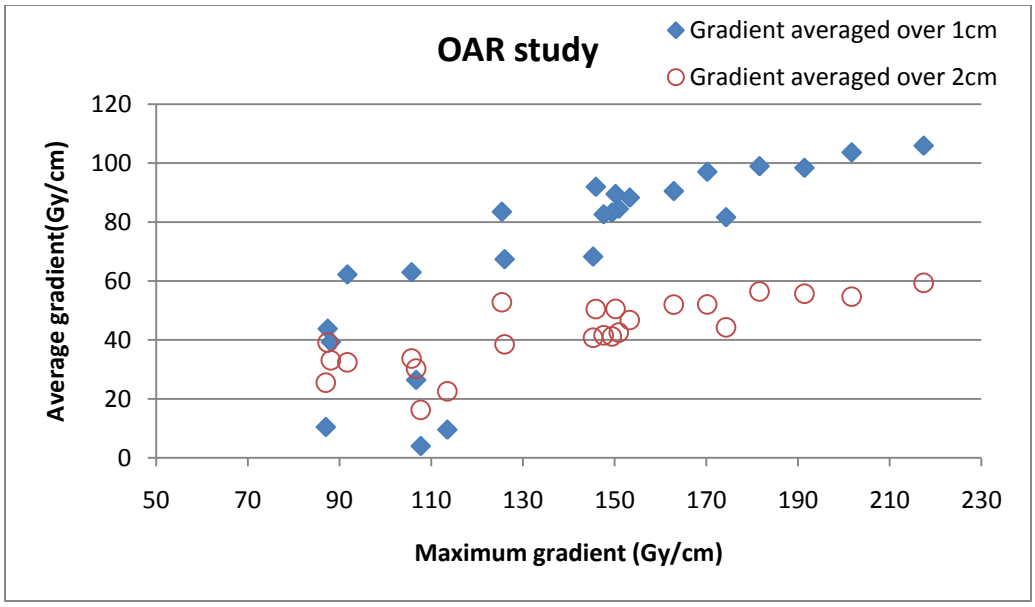

Figure 3.18: Gradients averaged over 1 cm and 2 cm versus maximum gradient for OAR study

The peak height and peak width and peak ratio ($\frac{Peak\ height}{peak\ width}$) plotted against the OAR max dose objective is shown in figure 3.19. Peak height and peak width of zero is assigned to the profiles with no peaks.

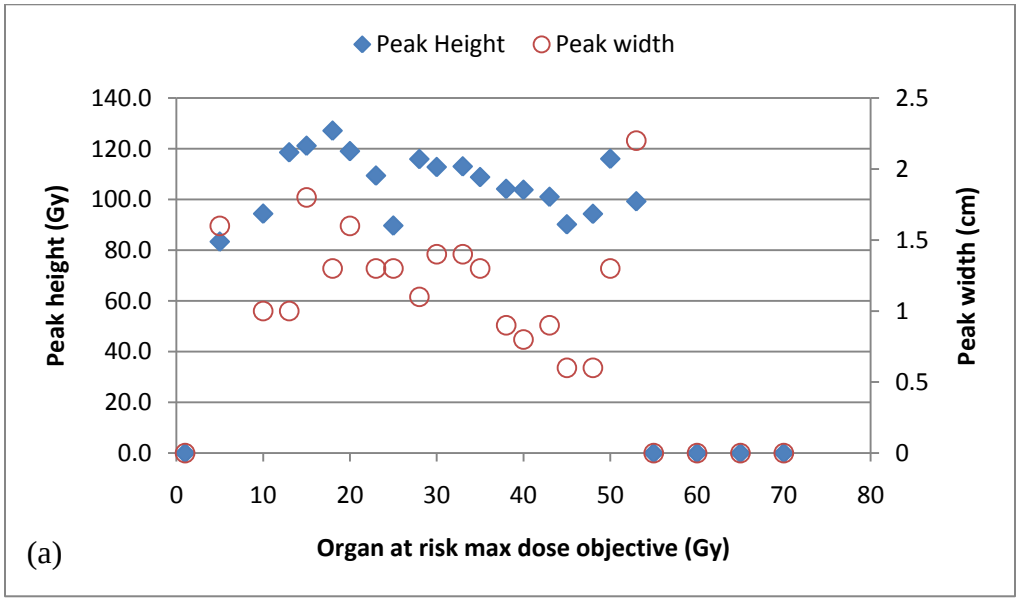

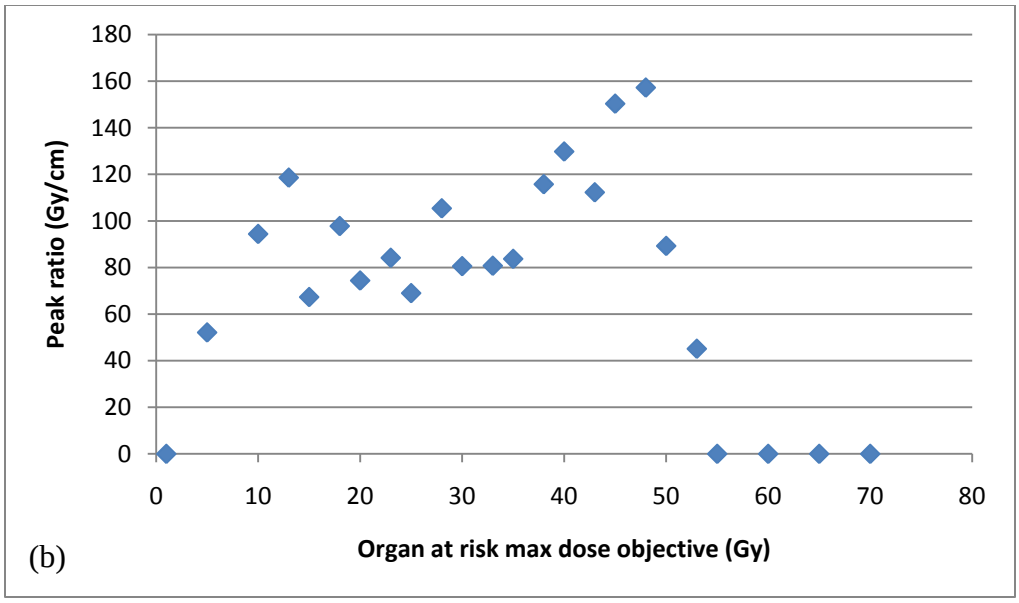

Figure 3.19: (a) Height and width of the created peaks (b) peak ratio; plotted against OAR max dose objective change

Peak height decreases slightly (from 116 Gy to 94.3 Gy) as OAR max dose objective increases up to 50 Gy. There is an overall decrease in the peak width in this range. Peak ratio shows scattered data against the OAR max dose objective range.

3.2.2 Gap change

This section consists of three series of optimizations:

3.2.2.1 Gap creation

A gap between the target and organ at risk was created in the LR direction (as defined in chapter 2). The width of the gap is varied from -10 mm to 10 mm (where a negative gap indicates overlap) to examine if it affects the generation of narrow segments. Since, in the OAR study, the maximum number of leaf pairs with 8-12 mm separation resulted with an OAR max dose of 10 Gy, we set the OAR max dose objective to 10 Gy and change the gap to find out if it affects the number of narrowly separated leaf pairs.

3.2.2.2 DVH study

In this study the objective type for organ at risk was changed to max DVH. The gap between the target and OAR was reset to zero. Percent volume of the organ at risk which could receive more than 10 Gy was varied from 0% to 50%. However values greater than 10% have no effect on the optimization and are therefore excluded. Percent volume in the DVH study can be related to an effective gap between the target and organ at risk. If a volume of A% is considered, it means that A% of the volume receives more than 10 Gy. When an equivalent gap of G mm is considered, it means that the volume of GYZ could receive more than 10 Gy. Therefore we relate the percent volume in the DVH study to the equivalent gap as follows:

$$\left(\frac{A}{100}\right) \times XYZ = GYZ \Rightarrow \left(\frac{A}{100}\right) \times X = G$$

X, Y and Z are the organ at risk dimensions. X for the OAR was 100 mm, thus G = A mm.

3.2.2.3 DVH study with 2.5 mm gap between the target and OAR

The DVH study was repeated with a 2.5 mm gap between the target and OAR. Consequently the equivalent gap would be: G = A+2.5 mm.

Figures 3.20 to 3.24 present the total number of leaf pairs and other profile parameters plotted against gap, for these three studies. The gap study shows that the existence of a gap between the target and OAR eliminates the narrow segments. When they overlap, narrow segments arise (with the exception of 7.5 mm overlap). The DVH study shows a small number of leaf pairs with 5-8 mm separation and DVH study with 2.5 mm gap shows even fewer at 4 mm gap (4% of the OAR volume receiving a dose of more than 10 Gy). Figure 3.20 (b), illustrates the elimination of leaf pairs with 8-12 mm separation once a 2.5 mm gap is introduced. The largest number of 8-12 mm wide leaf pairs happens at a zero gap. Even when the target and OAR

overlap, the number of 8-12 mm wide leaf pairs is small except for a large overlap (10 mm overlap). Data for DVH study fluctuate. However there is no narrow leaf pair for the gaps larger than 6 mm. The DVH study with an initial 2.5 mm gap shows fewer narrowly separated leaf pairs and none for equivalent gaps larger than 4 mm.

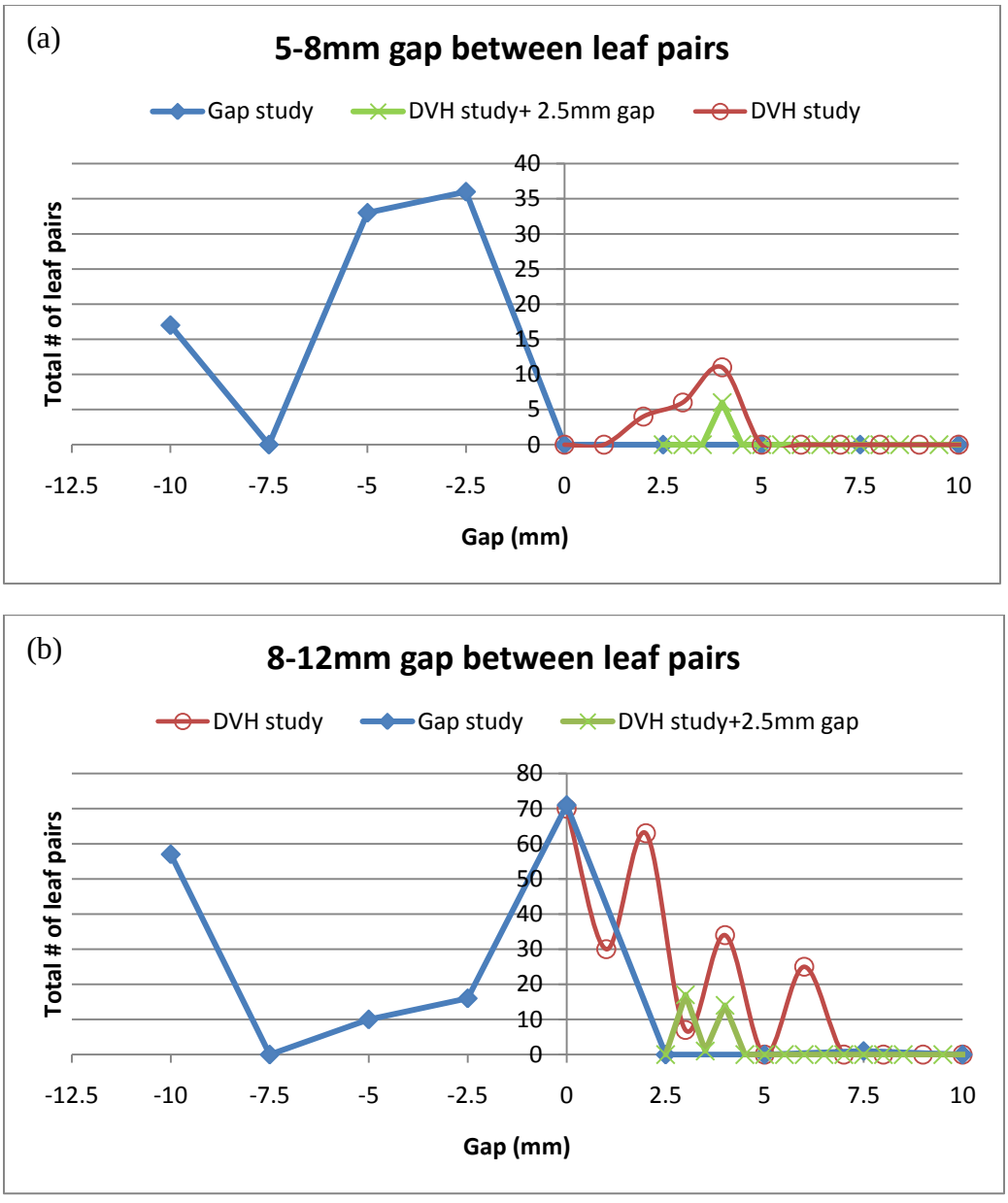

Figure 3.20: Total number of leaf pairs with (a) 5-8 mm separation and (b) 8-12 mm separation versus gap for gap study, DVH study and DVH study with a 2.5 mm gap

Figure 3.21 presents the average dose over 2 cm outside the target and point doses, as gap between the two regions of interest is varied.

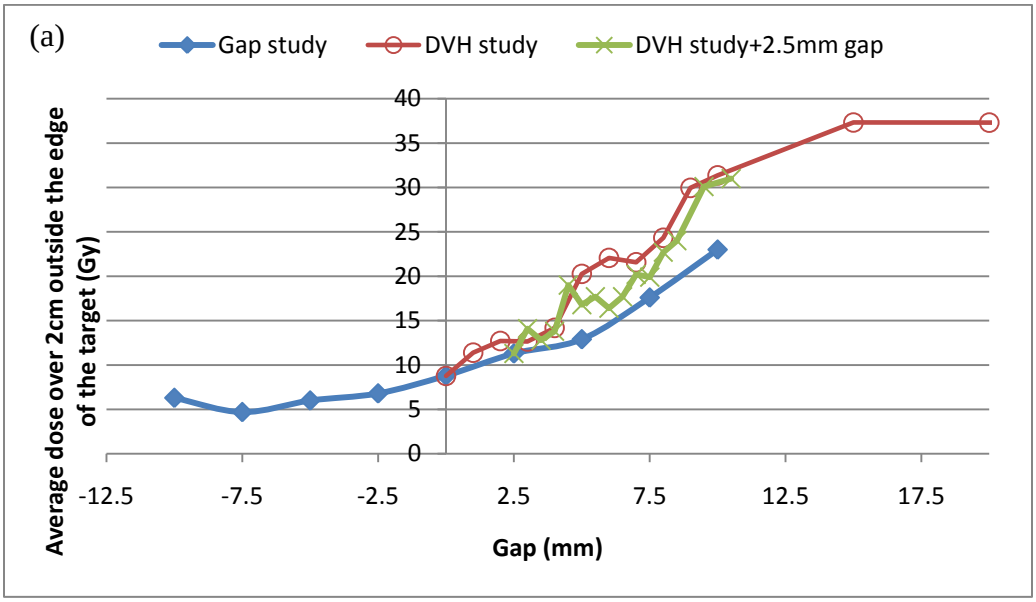

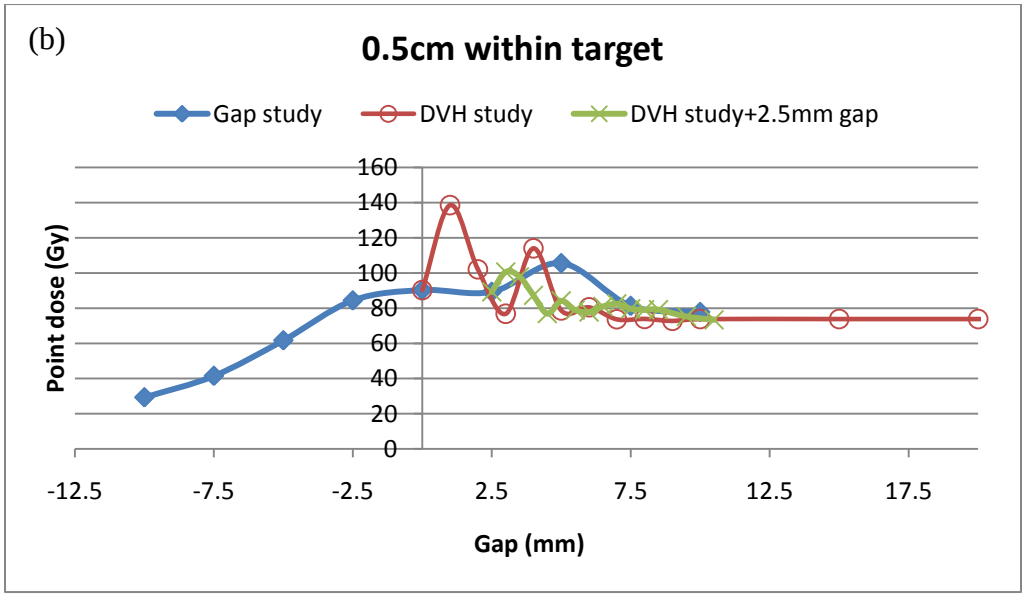

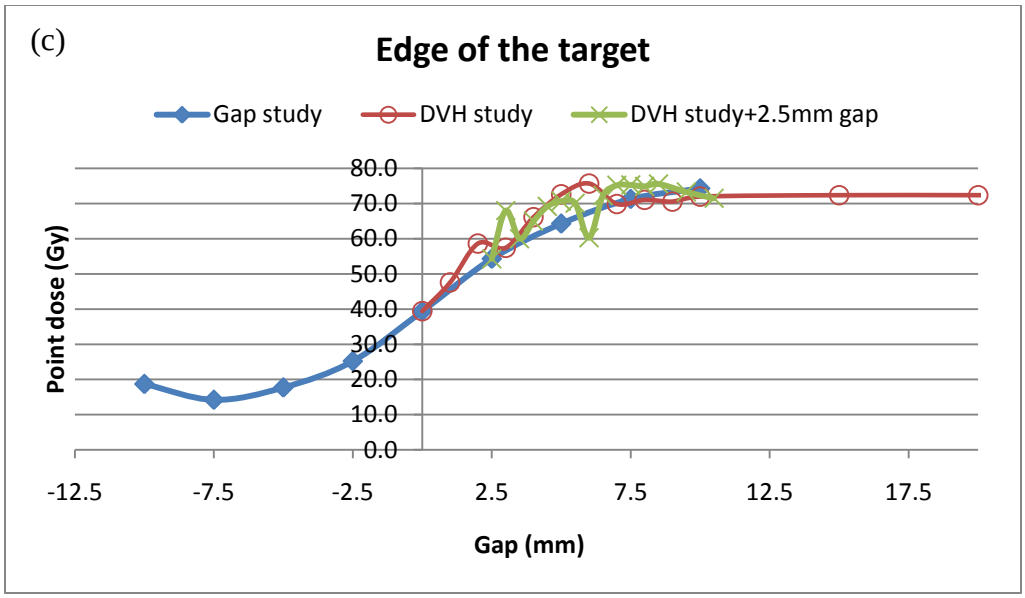

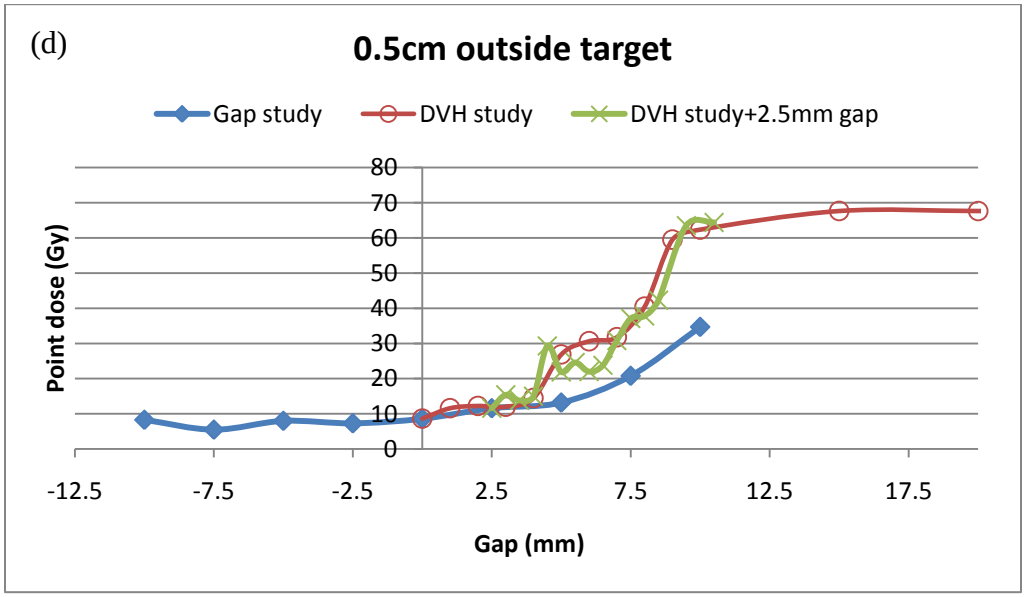

Figure 3.21: (a) Average dose over 2 cm outside the target, (b) The dose at 0.5 cm inside the target, (c) The dose at edge of the target and (d) Dose at 0.5 cm outside the target; plotted against the gap

Different studies show consistent results. Average dose over 2 cm outside the target and point dose at 0.5 cm outside the target both increase with gap for the three studies. It means that creating a gap between the target and OAR can lead to an increased dose outside the target. For a zero gap and for the cases when the target and OAR overlap, the OAR receives less than 10 Gy as specified. When the gap is between zero and 5 mm, the point 0.5 cm outside the target occurs

within the OAR and receives a dose larger than 10 Gy which does not satisfy the maximum dose objective for the OAR. It appears that creating a gap between the target and OAR might not be good for sparing the OAR (figure 3.21 (d)). However, creating a gap increases the dose at the edge of the target (figure 3.21 (c)). 0.5 cm within the target presents an increase when the overlapping area decreases and creating a gap between the target and the OAR allows delivery of the prescribed dose to the target (figure 3.21 (b)) without the associated creation of the narrowest segments (figure 3.20(a)).

In figure 3.22 (a), the gap study shows that there is an increase in the maximum gradient as the overlapping width decreases (except for 7.5 mm overlap) and reaches the highest value of 174.3 Gy/cm at zero gap. As the gap between the target and the OAR increases the maximum gradient drops below 150 Gy/cm. The DVH study with zero gap does not demonstrate a significant change in the maximum gradient value for gaps larger than 5 mm. The DVH study with the 2.5 mm gap does not show a considerable variation in the maximum gradient at any gap. It fluctuates between the values of 100 and 150 Gy/cm.

Maximum gradient is low when the target and the OAR overlap and as the width of overlapping area decreases the dose falls more sharply (figure 3.22(a)). Figure 3.22(b) displays the maximum gradient position relative to the edge of the target. A negative value in the Y axis indicates that the maximum gradient occurs inside the target. A positive value indicates that the maximum gradient occurs outside the target and an increase in this value means that the maximum gradient is positioned farther away from the edge of the target. When the target and the OAR overlap, the position of the maximum gradient is outside the target. A reduction in the width of the overlapping area leads to a shift of the maximum gradient toward the edge of the

target. Creating the gap moves the maximum gradient inside the target and it moves further into the target as the gap increases.

Average gradients over 1 cm and 2 cm show an increase as the overlapping area decreases for the gap study. As the gap increases, the average gradient over 1 cm shows a dramatic reduction for the DVH and DVH+2.5 mm gap studies. However the average gradient over 2 cm does not demonstrate a remarkable change as the gap varies (figures 3.22(c) and (d)). The average gradient over 1 cm relative to that over 2 cm is greater for most of the cases in the three studies. This means that the beam profile is not linear from 1 cm inside the target to 1 cm outside the target (over 2 cm). Figure 3.23 illustrates a profile from the DVH study when 2% of the OAR volume was allowed to receive more than 10 Gy.

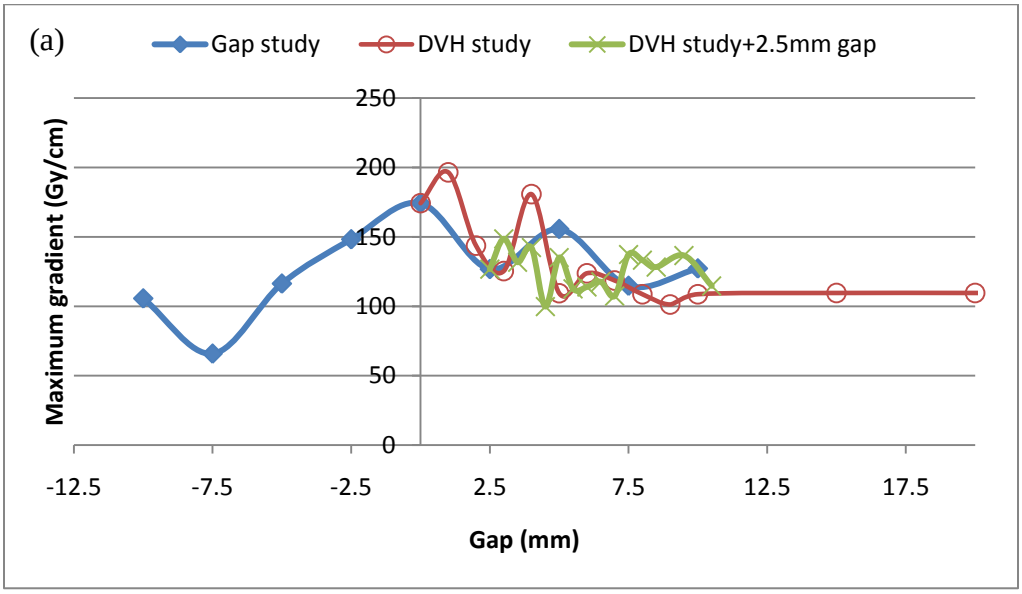

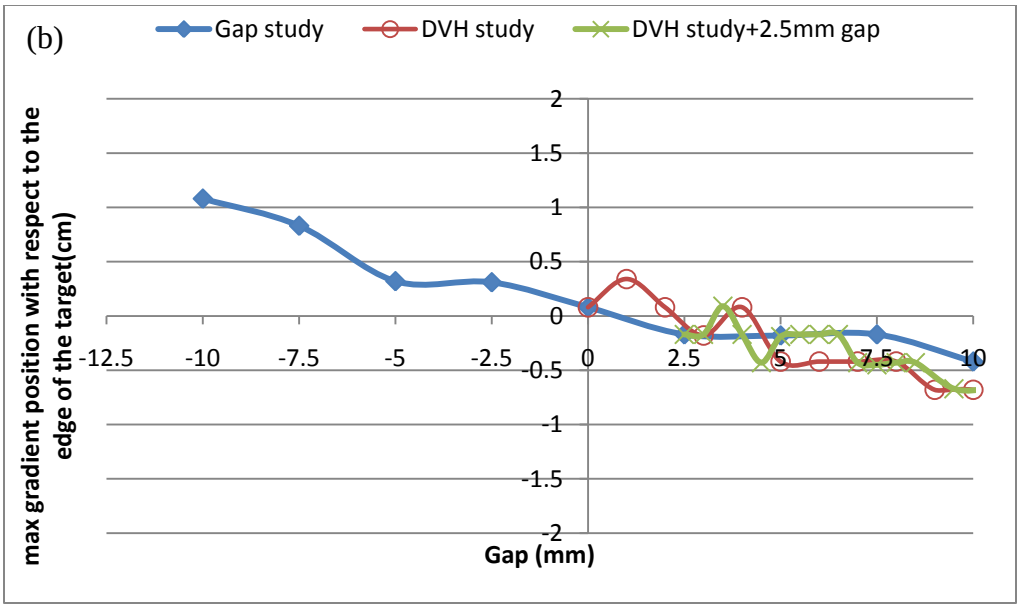
(b)
Gap study
DVH study
DVH study+2.5mm gap
max gradient position with respect to the edge of the target(cm)
2
1.5
1
0.5
0
-0.5
-1
-1.5
-2
-12.5
-10
-7.5
-5
-2.5
0
2.5
5
7.5
10
Gap (mm)

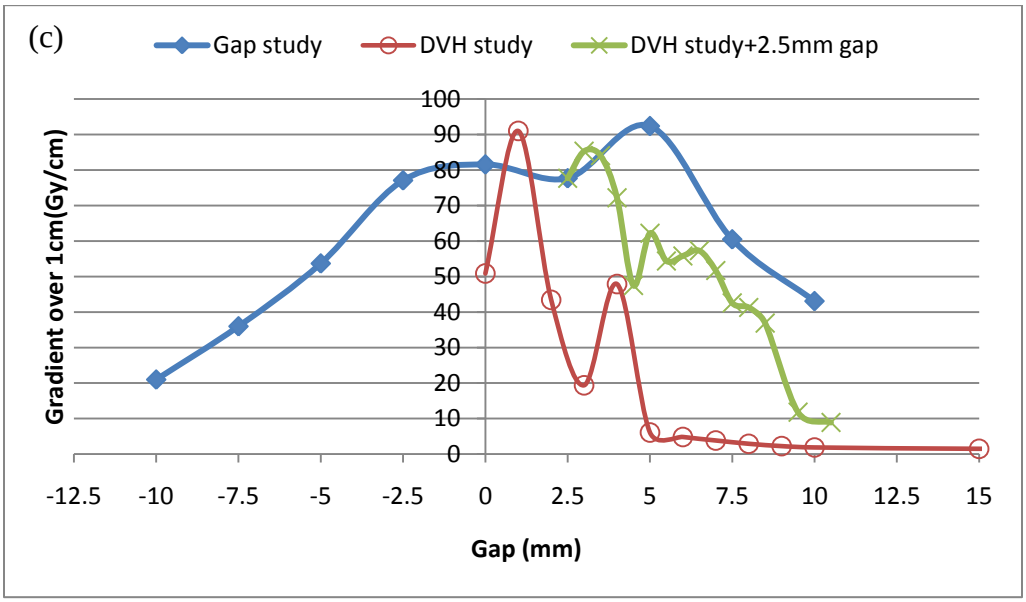
(c)
Gap study
DVH study
DVH study+2.5mm gap
Gradient over 1cm(Gy/cm)
100
90
80
70
60
50
40
30
20
10
0
-12.5
-10
-7.5
-5
-2.5
0
2.5
5
7.5
10
12.5
15
Gap (mm)

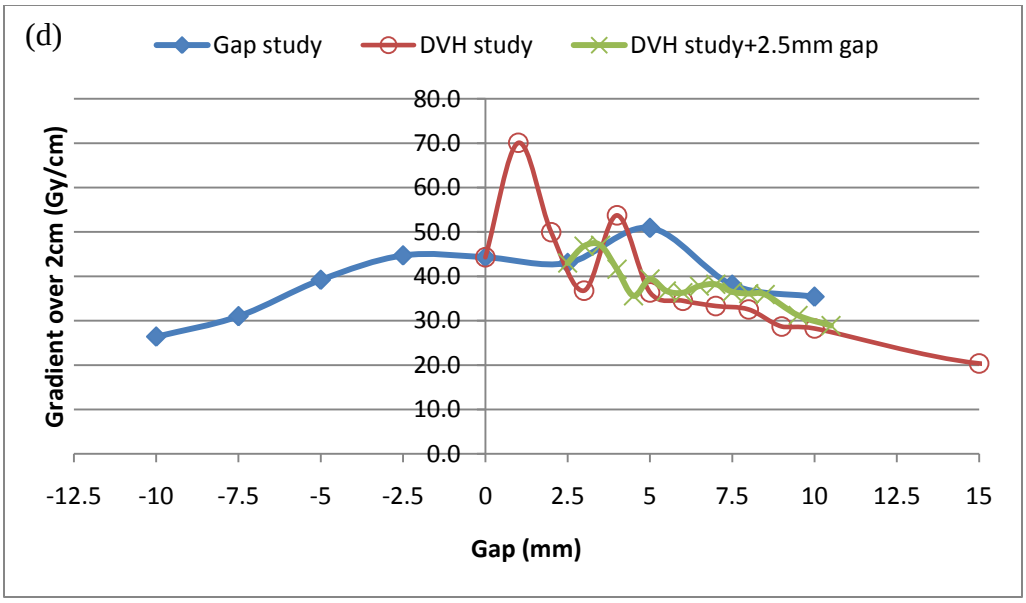

Figure 3.22: Change in the (a) maximum gradient (b) position of the maximum gradient (c) average gradient over 1 cm and (d) average gradient over 2 cm; as gap increases, for three different studies

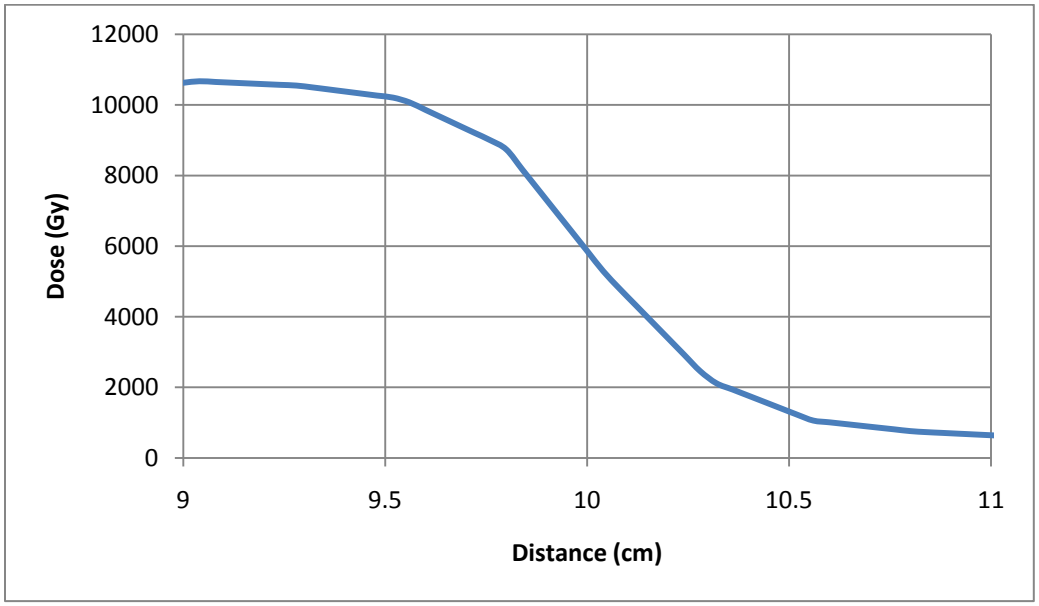

Figure 3.23: Illustration of a profile from 9 cm distance to 11 cm distance for the DVH study when 2% of the OAR volume was allowed to receive more than 10 Gy. It can be seen that the gradient over 2 cm is smaller than the gradient over 1 cm.

R^2 (correlation coefficient squared) values indicated in figure 3.24, demonstrate that the gradients over 1 cm and 2 cm are closely correlated to the maximum gradient for the DVH study and weakly correlated for the gap study. They are not correlated for the DVH+2.5 mm gap study.

Hence a reduction in maximum dose does not mean that the gradient over 1 cm or 2 cm should reduce and vice versa.

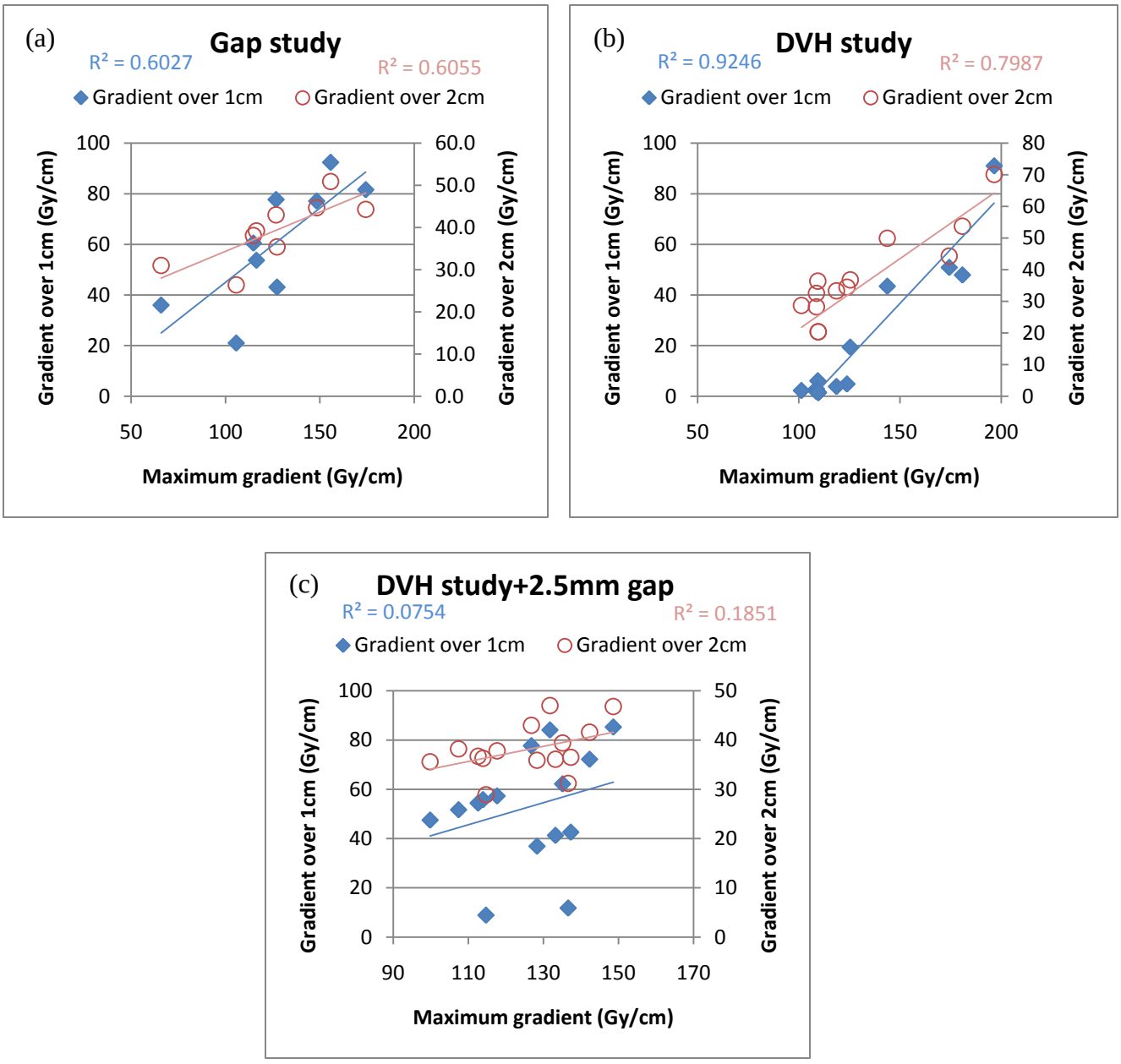

Figure 3.24: Relationship between the maximum gradient and the gradient over 1 cm and 2 cm for (a) Gap study (b) DVH study with zero gap and (c) DVH study with 2.5 mm gap

The gap study in figure 3.25 (a) does not show a significant change in the peak height for gaps between -5 mm and 5 mm. No peaks appear for 7.5 mm wide overlap and for gaps larger

than 5 mm. No peaks appear for equivalent gaps larger than 6 mm and 4.5 mm in DVH studies with zero gap and 2.5 mm gap respectively. Neither peak width and height nor their ratio show a specific trend with respect to the gap.

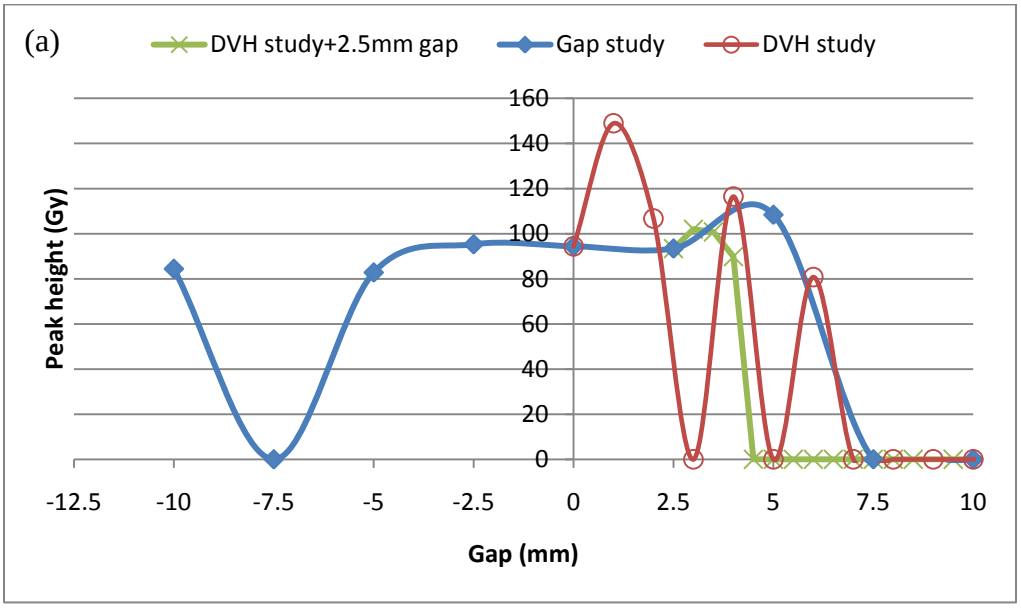

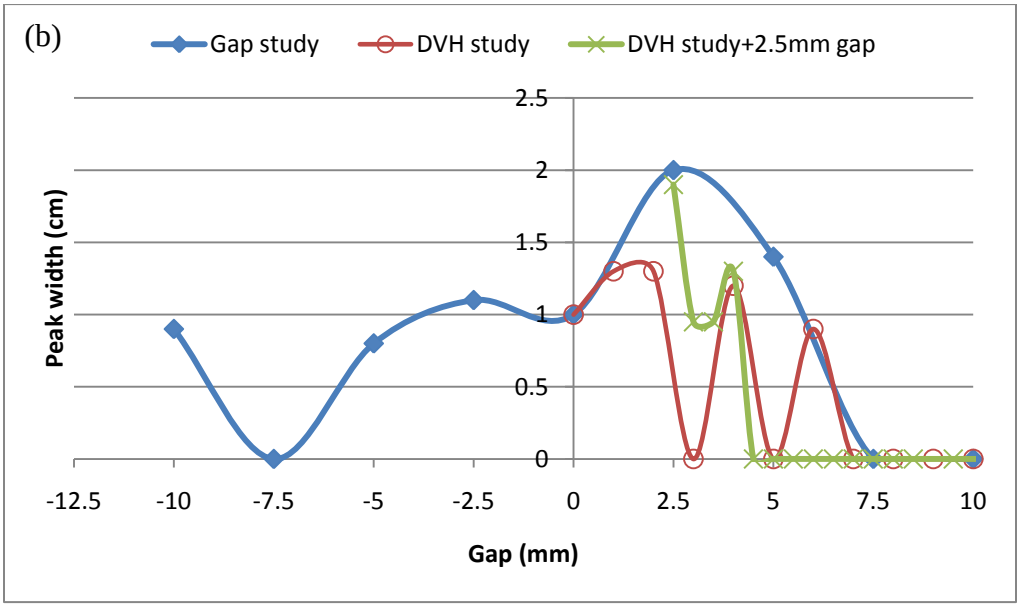

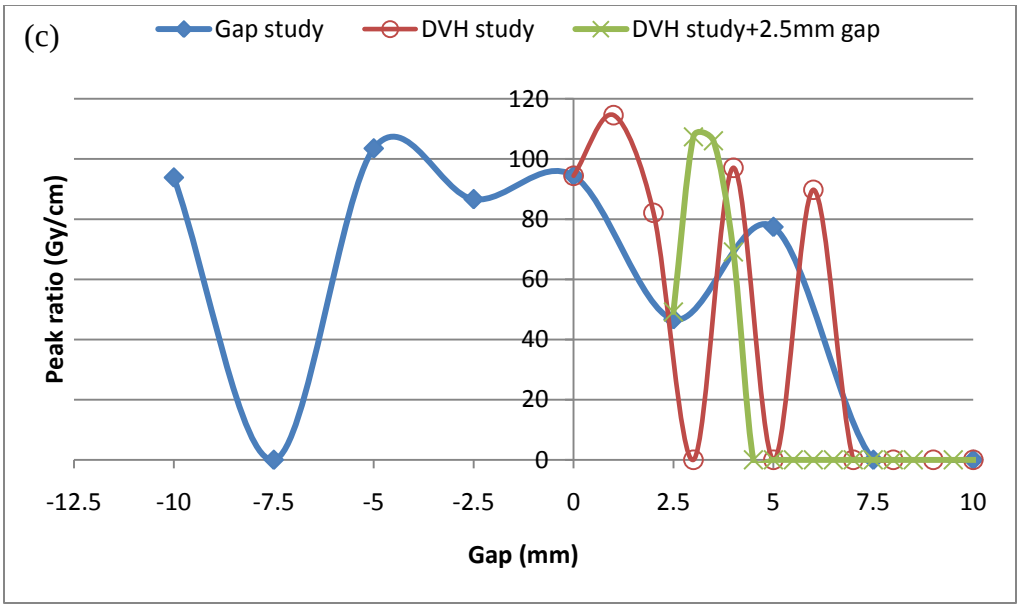

Figure 3.25: (a) Peak height (b) peak width (c) peak ratio; versus gap for three different studies

3.2.3 Consolidation of results

In this section, we investigate relationships among the various parameters introduced previously. Figure 3.26 relates the total number of leaf pairs with 5-8 mm separation to various parameters that characterize the dose distributions. The gap study indicates more than 30 leaf pairs with 5-8 mm separation, whereas the other studies indicate fewer than 15 leaf pairs with 5-8 mm separation. For the gap study we can see that, as the dose outside the target starts to increase above 10 Gy, the total number of leaf pairs with 5-8 mm separation decreases. That happens because with escalating the dose outside the target, the gradient decreases and therefore there is less need for the leaf pairs with very narrow separation (figure 3.26(d)).

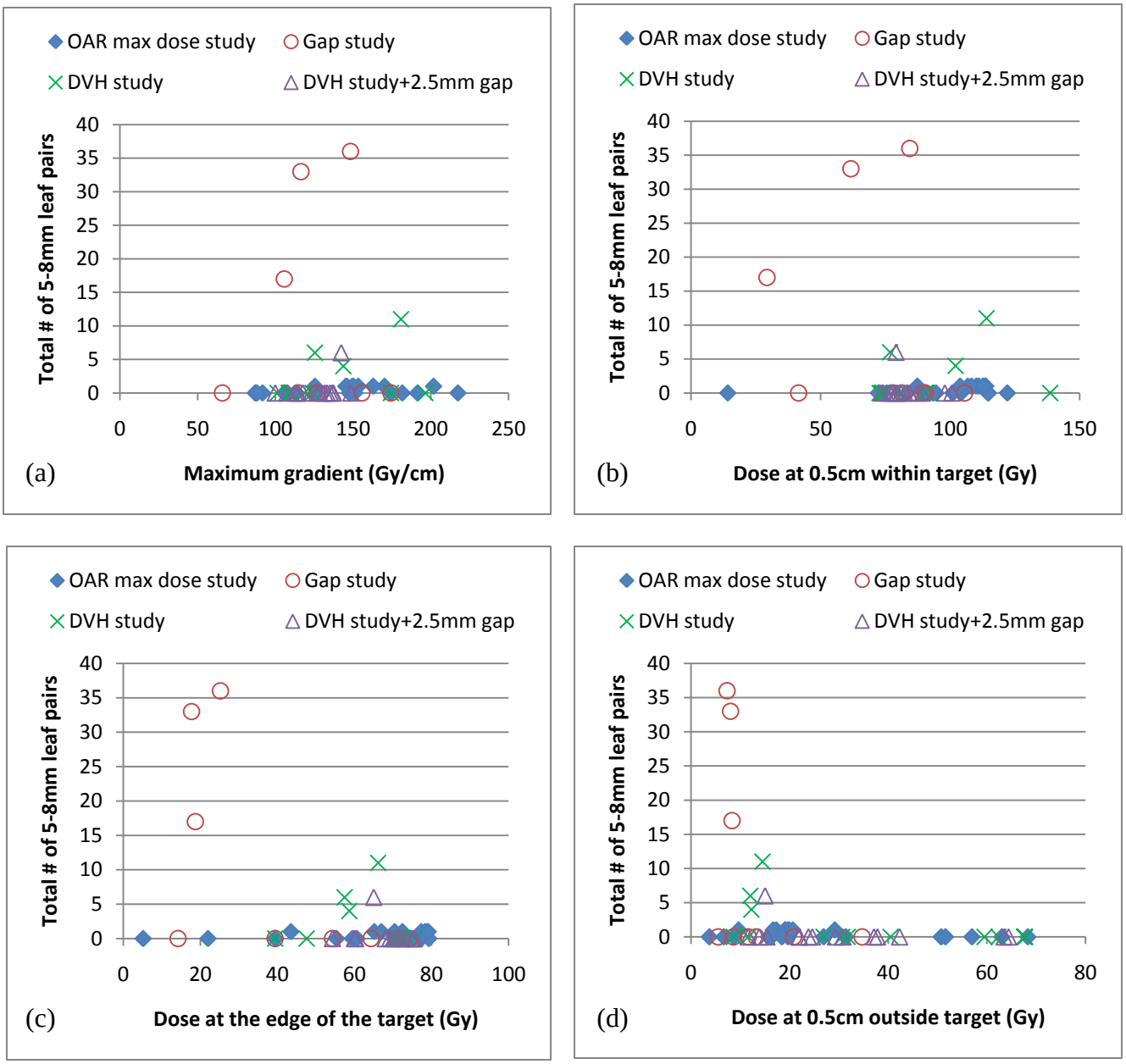

Figure 3.26: Total number of leaf pairs with 5-8 mm separation plotted against (a) maximum gradient (b) point dose at 0.5 within target (c) point dose at interface (d) point dose at 0.5 cm outside the target; for four studies

Figure 3.27 relates the change in the total number of leaf pairs with 8-12 mm separation to the same parameters as in the previous figure. For the doses more than 90 Gy at 0.5 cm within the target and doses below 30 Gy at 0.5 cm outside the target, leaf pairs with 8-12 mm separation arise. They are created to compensate the dose fall-off near the boundary inside the

target and therefore reduce the dose outside the target. Hence they arise when high doses inside the target and low doses outside the target are required to satisfy optimization objectives.

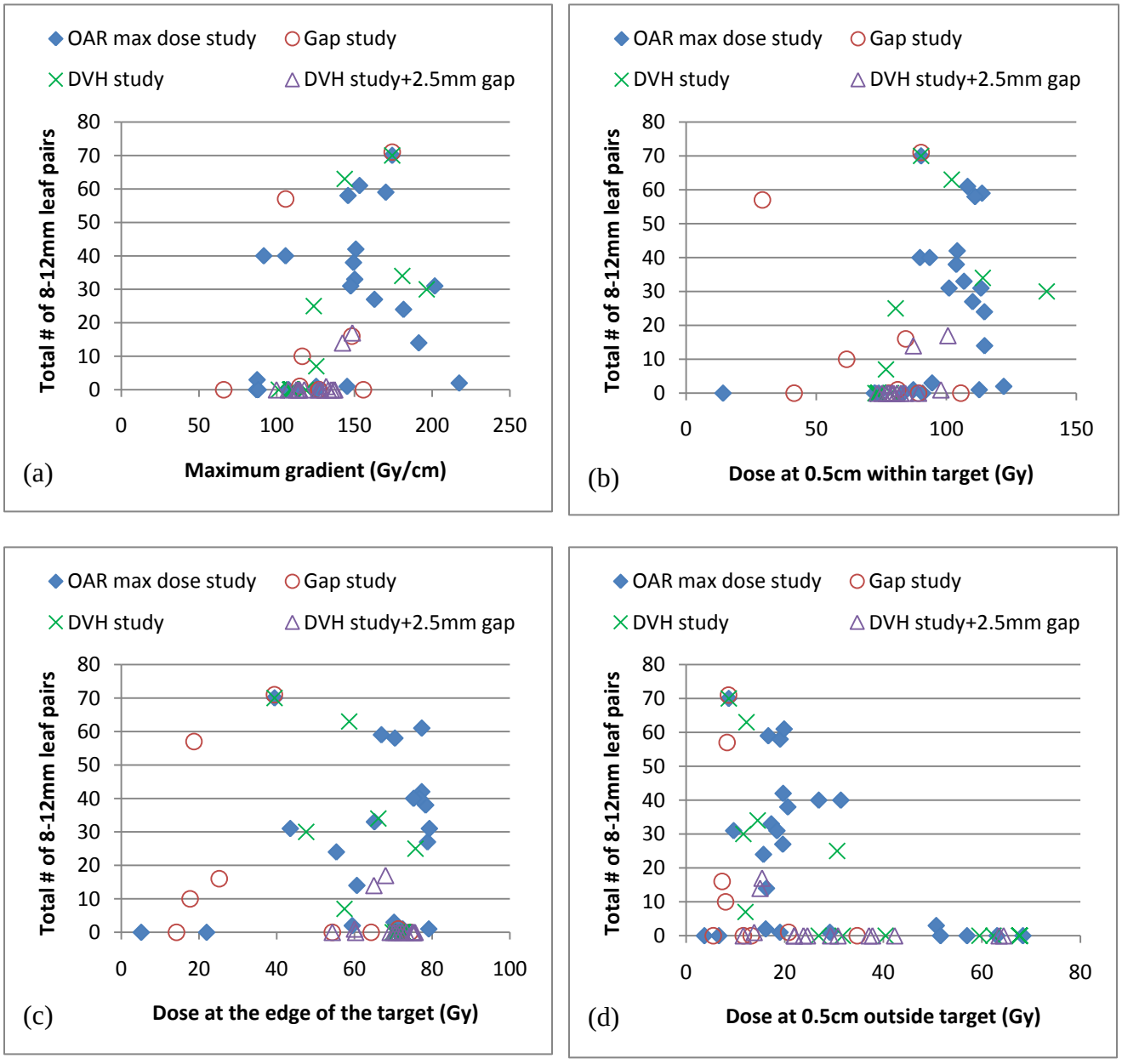

Figure 3.27: Total number of leaf pairs with 8-12 mm separation plotted against (a) maximum gradient (b) point dose at 0.5 within target (c) point dose at interface (d) point dose at 0.5 cm outside the target; for four studies

Leaf pairs with 5-8 mm separation are created for a few cases. Their number is not related to the peak height, peak width or peak ratio (figure 3.28).

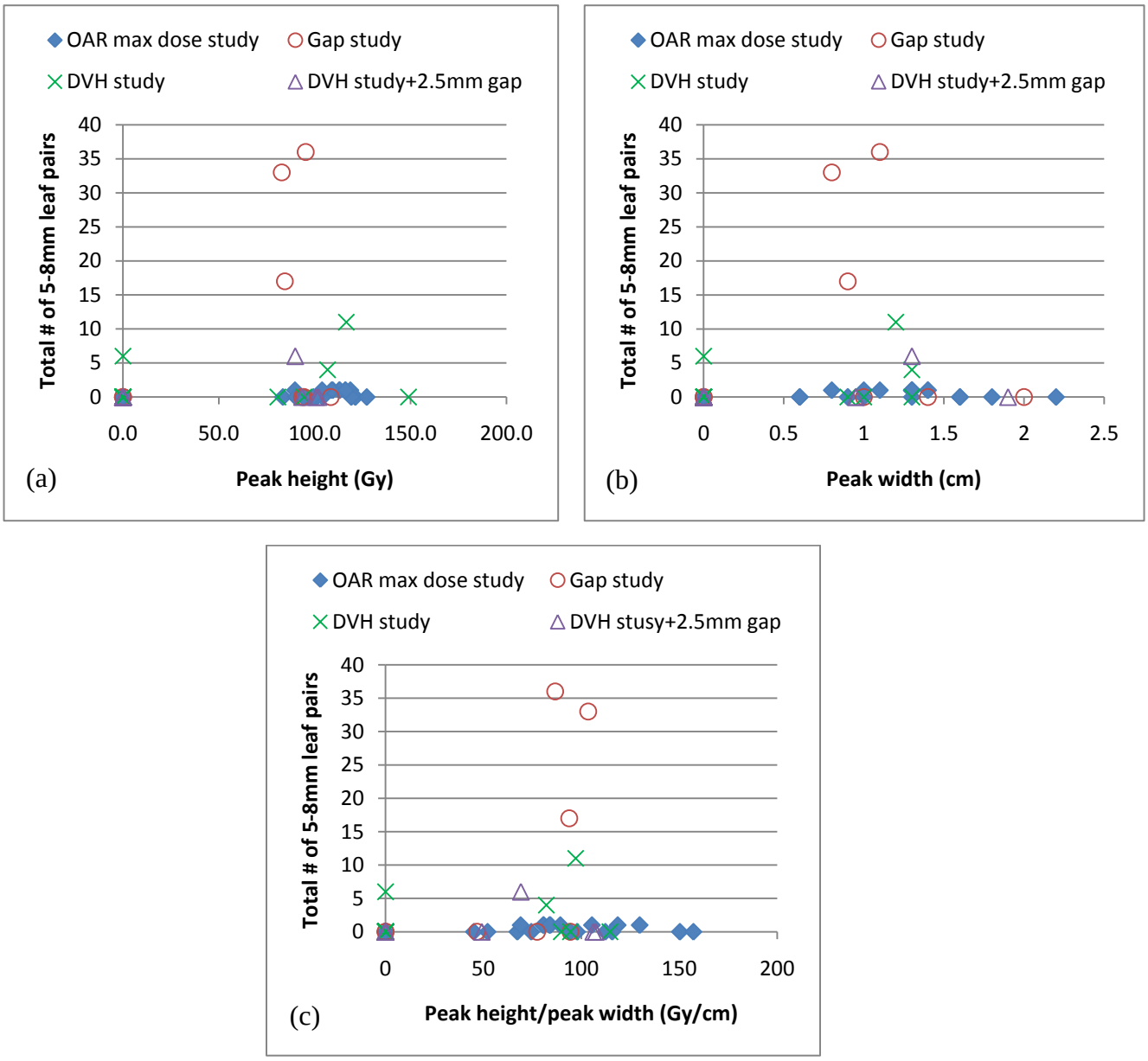

Figure 3.28: Total number of leaf pairs with 5-8 mm separation plotted against (a) peak height (b) peak width and (c) peak ratio; for four studies

Total number of leaf pairs with 8-12 mm separation is also not related to the peak height, peak width or peak ratio (figure 3.29).

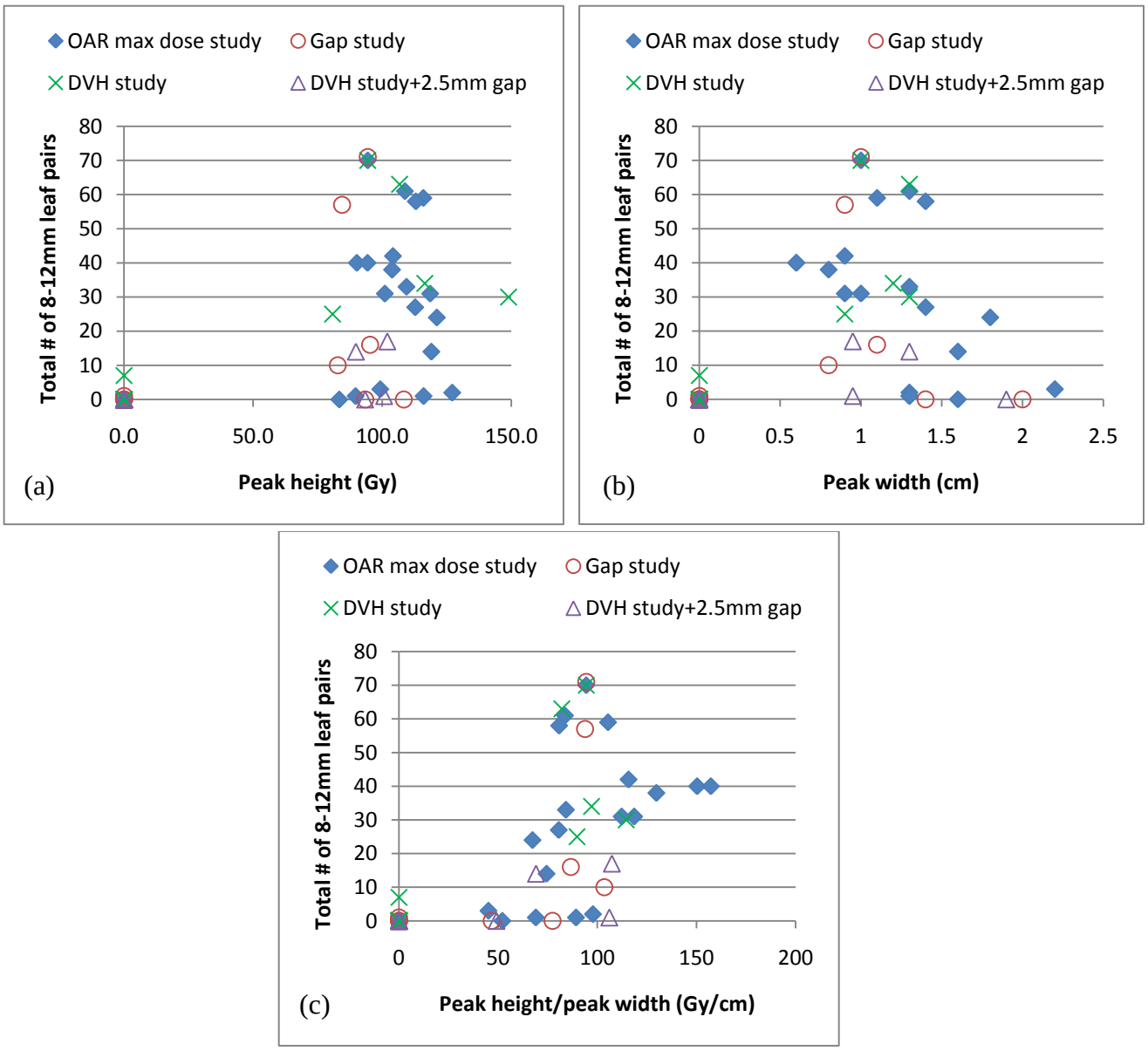

Figure 3.29: Total number of leaf pairs with 8-12 mm separation plotted against (a) peak height (b) peak width and (c) peak ratio; for four studies

From figure 3.30, it can be concluded that there is a general increase in the peak height as the dose gradient increases. The peaks are created to compensate the penumbra and therefore they sharpen the dose gradient with escalating the dose near the boundaries. It is also clear that the peak height increment would lead to an increase in the dose at 0.5 cm within the target since this point is located within the peak. Peak height versus the point dose at the interface and Peak

height versus the dose 0.5 cm outside the target do not display a specific trend, but are not shown in here.

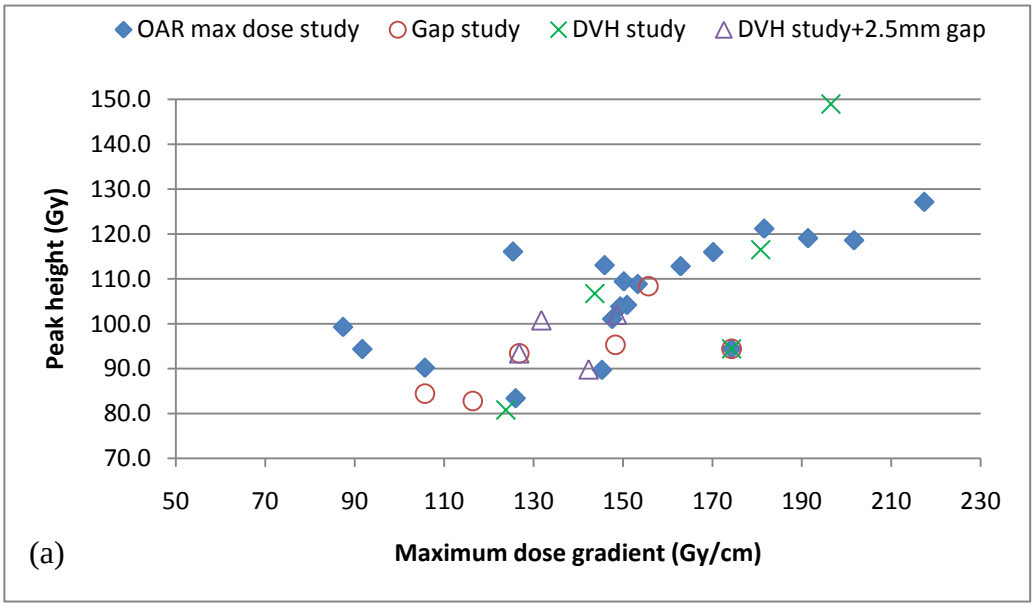

(a)

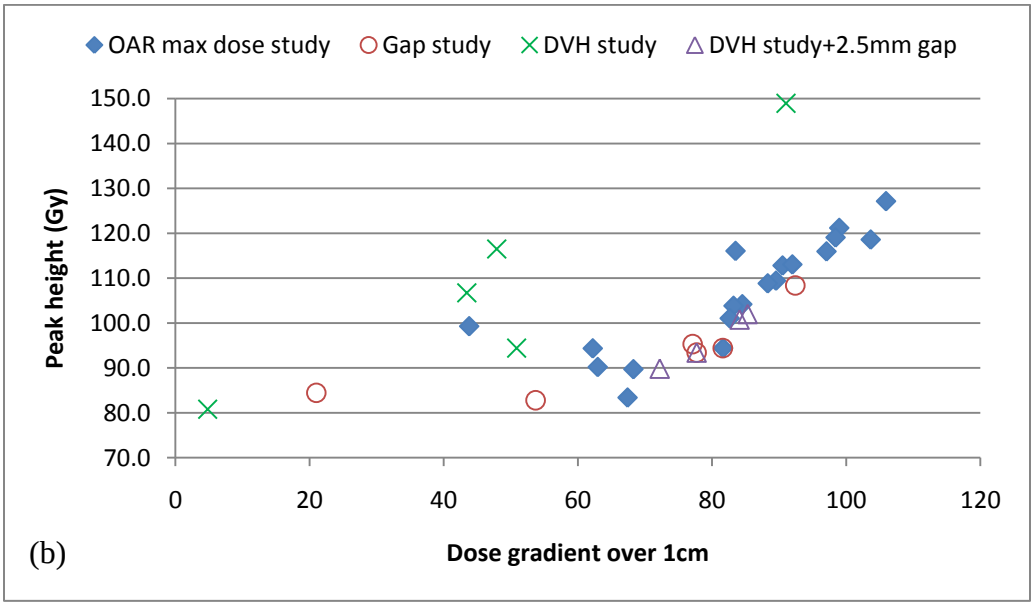

(b)

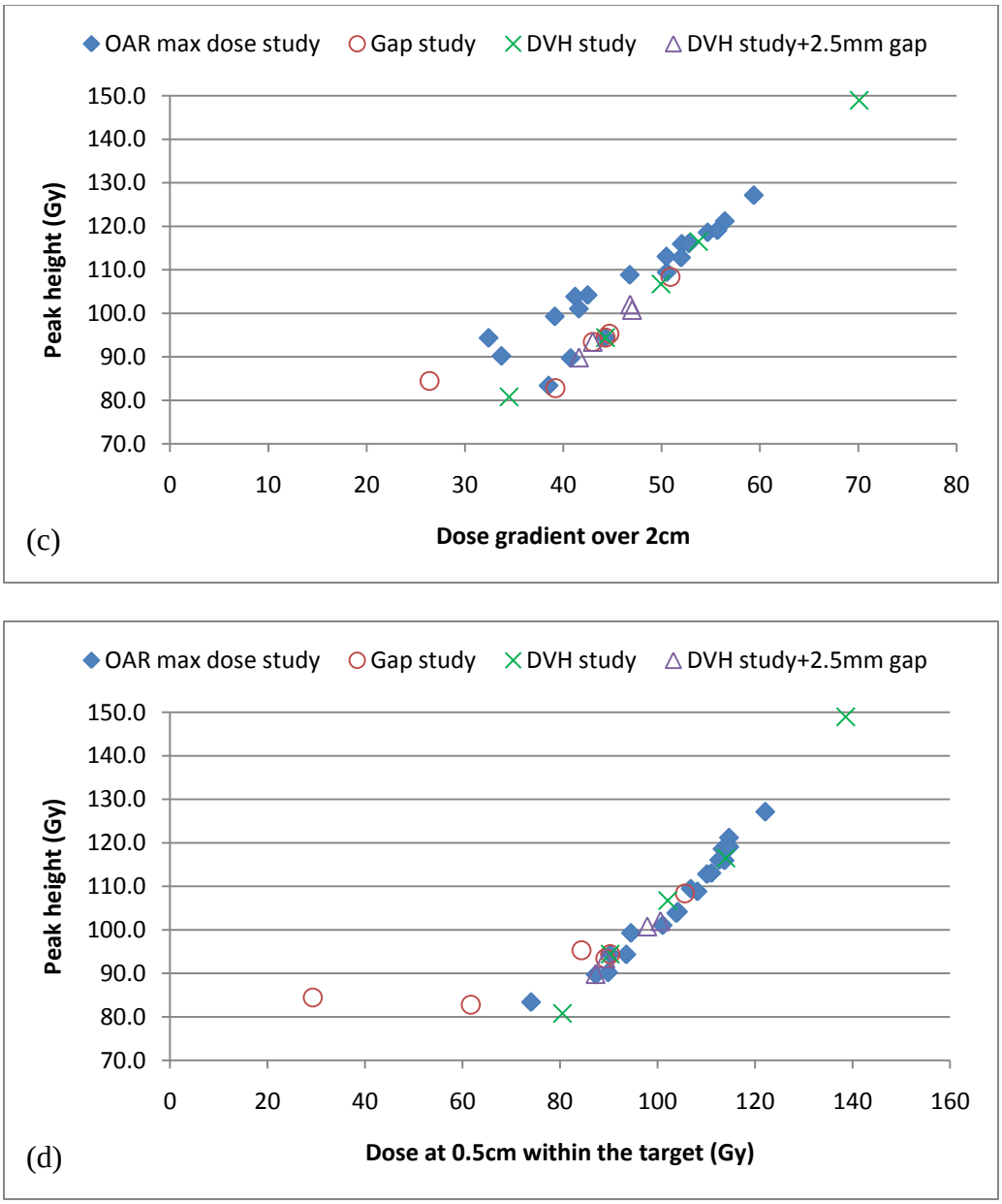

Figure 3.30: Peak height plotted against (a) maximum gradient (b) gradient over 1 cm (c) gradient over 2 cm and (d) dose at 0.5 cm within the target; for four studies

Figure 3.31 presents the peak width plotted against the dose gradient. Peak width changes as the dose gradient and the dose at 0.5 cm within the target changes but not in a predictable fashion. Peak ratio shows scattered data as well. It means that the change in the peak width does not follow a certain rule neither does peak ratio (figure 3.32). That led us to plot the peak height

versus peak width to examine if there was a relationship between them (figure 3.33). We obtain scattered data for all of the studies with the exception of the gap study. The gap study shows an increase in the peak height as the peak width increases up to 1.4 cm. For the peak width of 2 cm the peak height decreases to 93.4 Gy (when 2.5 mm gap is defined between the target and OAR). In general, peaks appear at higher gradients, but at lower gradients they do not necessarily vanish. Most peaks have a width between 0.5 and 1.5 cm.

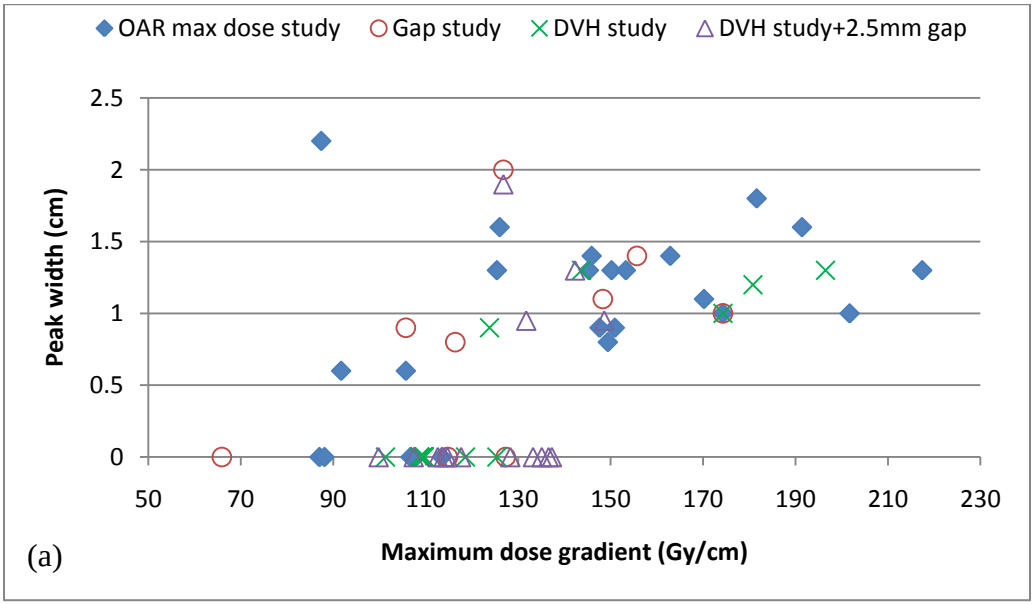

(a)

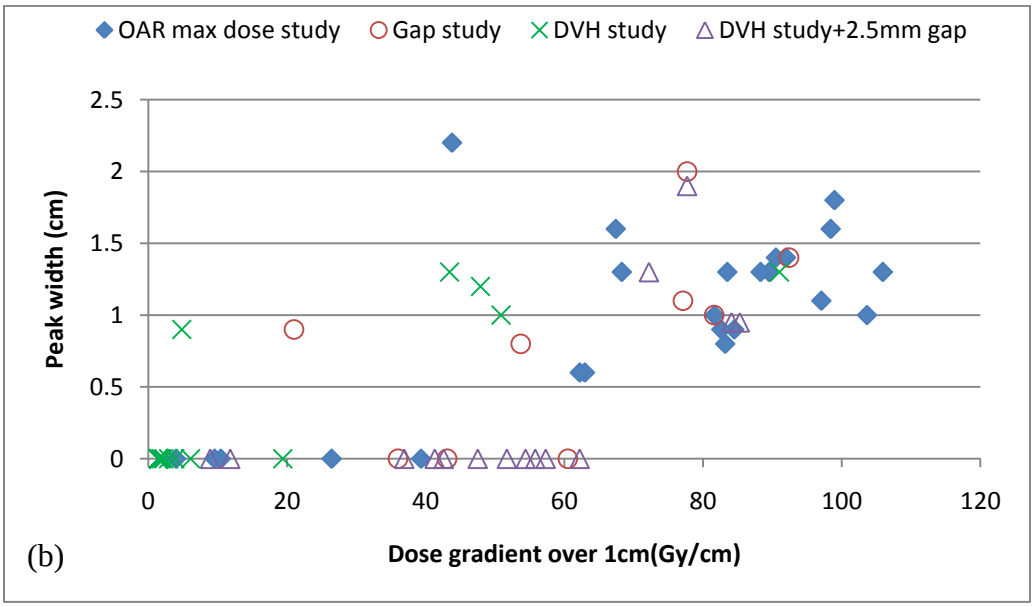

(b)

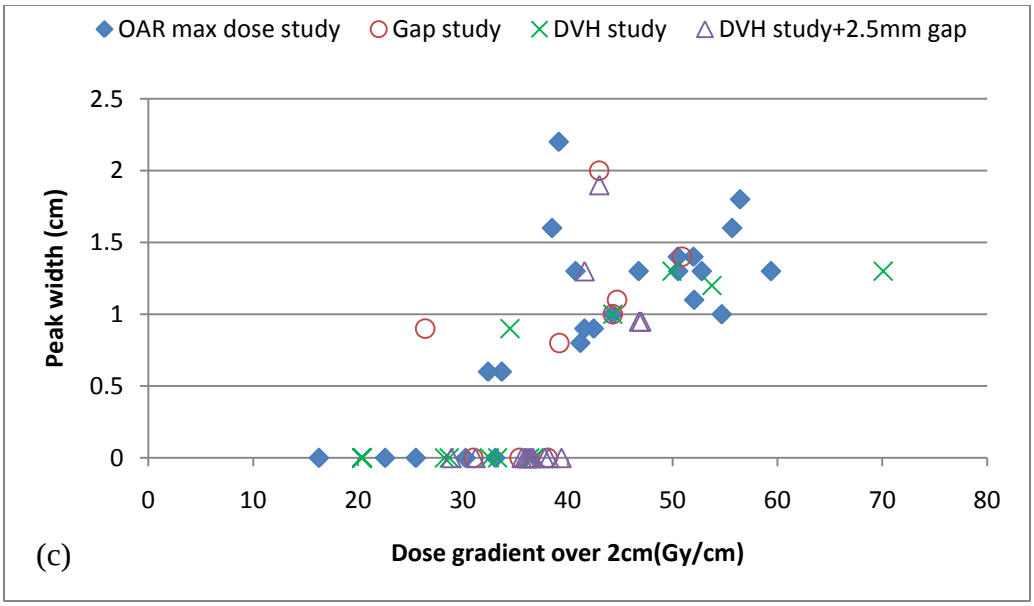

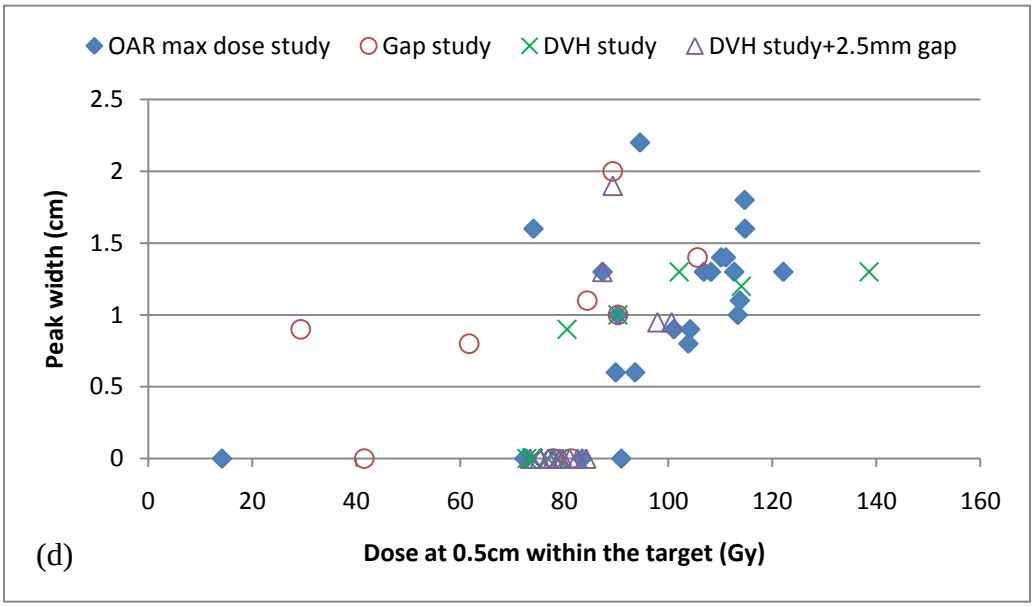

Figure 3.31: Peak width plotted against (a) maximum gradient (b) gradient over 1 cm (c) gradient over 2 cm and (d) dose at 0.5 cm within the target; for four studies

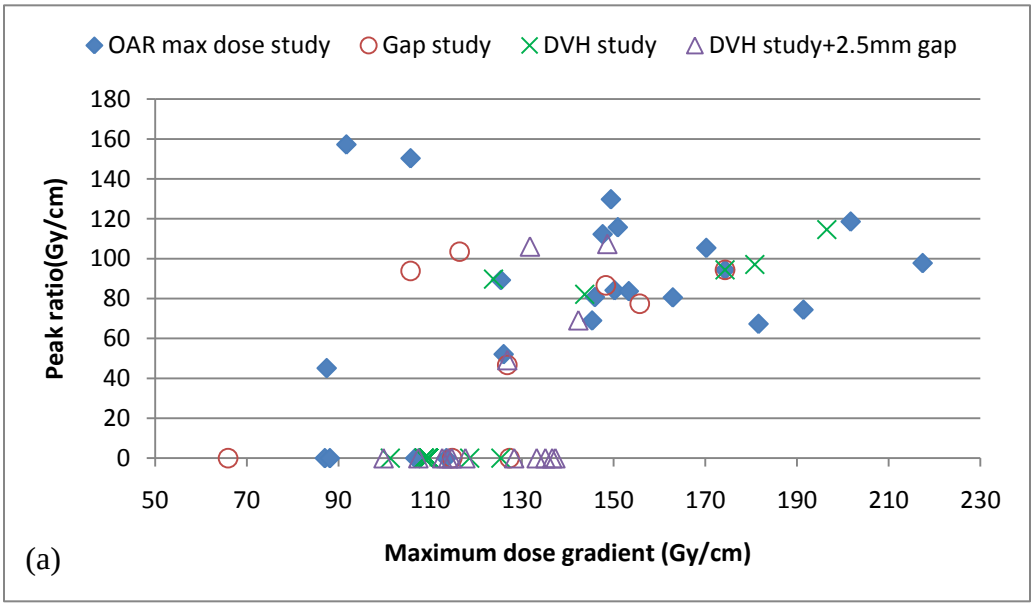
OAR max dose study
Gap study
DVH study
DVH study+2.5mm gap
Peak ratio(Gy/cm)
180
160
140
120
100
80
60
40
20
0
50
70
90
110
130
150
170
190
210
230
Maximum dose gradient (Gy/cm)

(a)

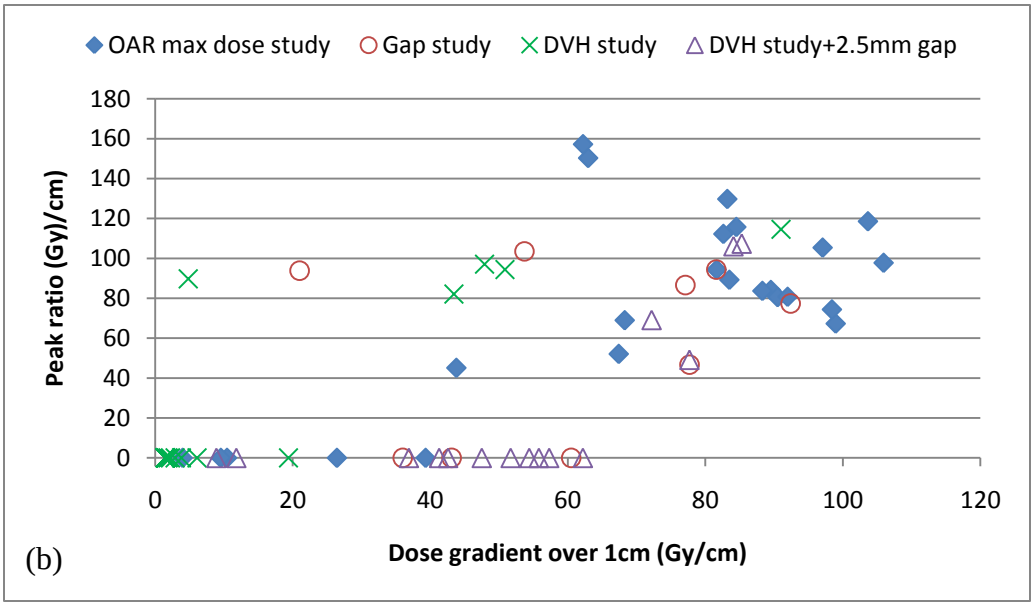
OAR max dose study
Gap study
DVH study
DVH study+2.5mm gap
Peak ratio (Gy)/cm)
180
160
140
120
100
80
60
40
20
0
0
20
40
60
80
100
120
Dose gradient over 1cm (Gy/cm)

(b)

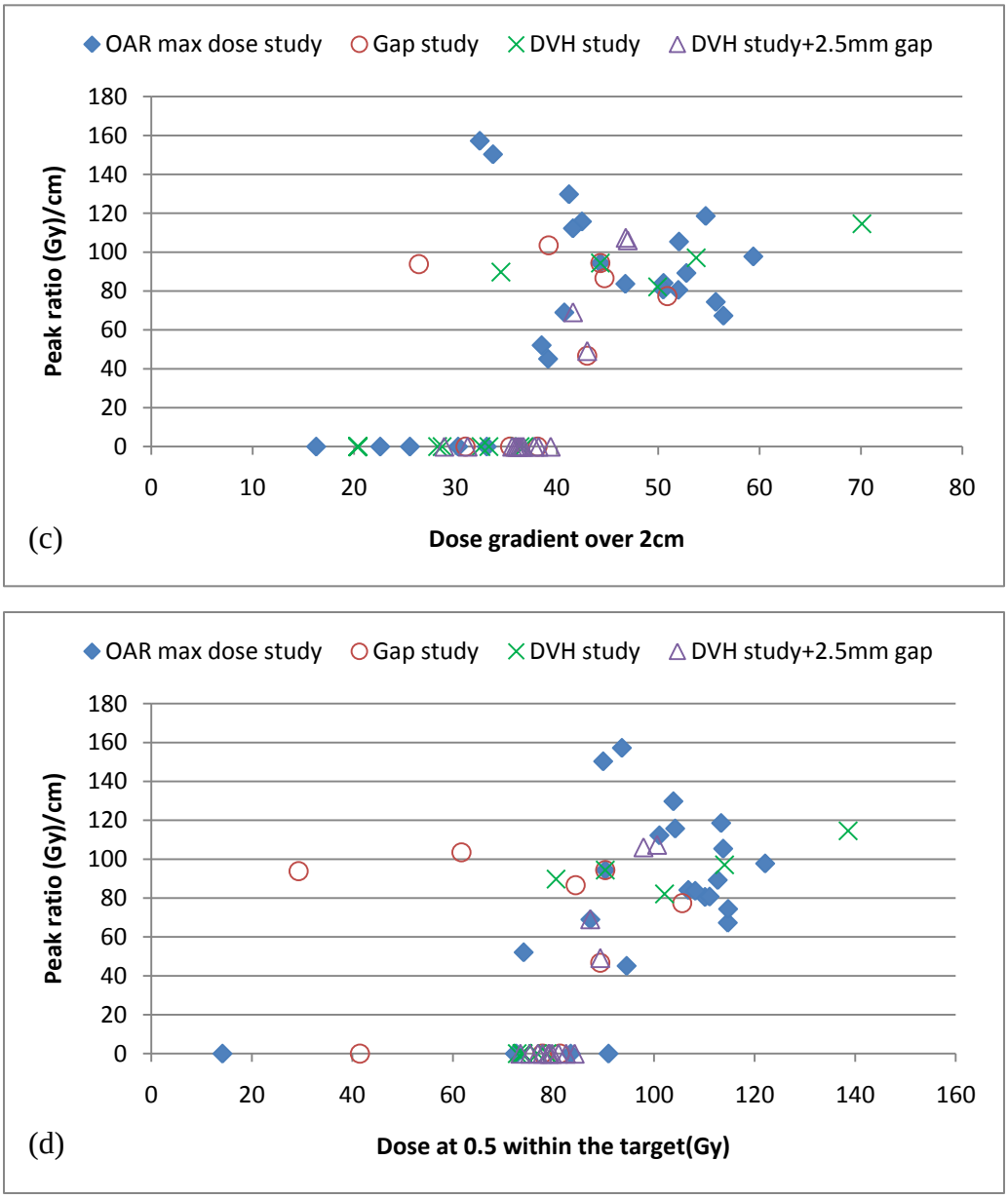

Figure 3.32: Figure 3.28: Peak ratio plotted against (a) maximum gradient (b) gradient over 1 cm (c) gradient over 2 cm and (d) dose at 0.5 cm within the target; for four studies

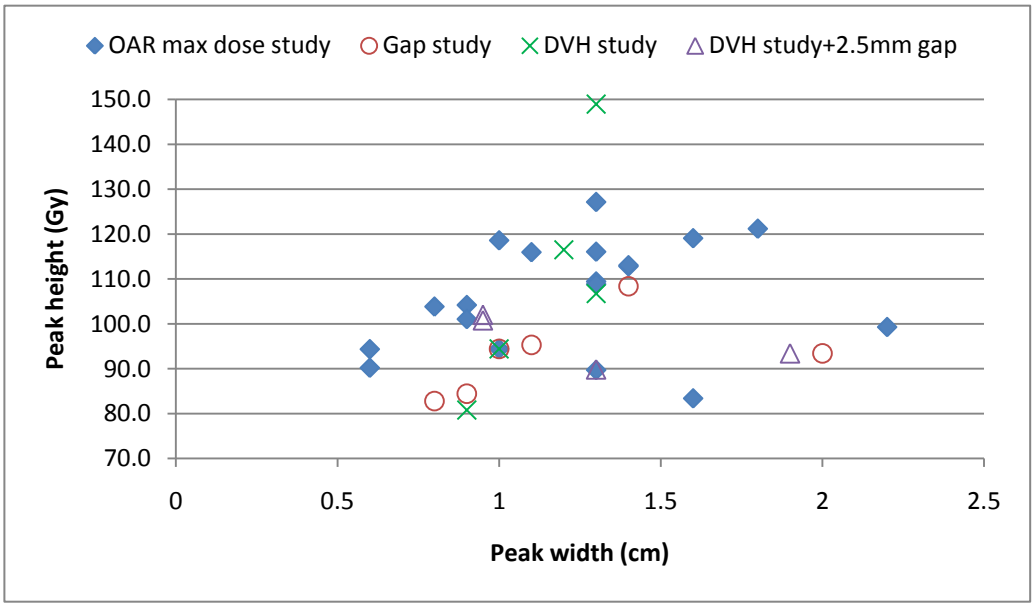

Figure 3.33: Relationship between the peak height and peak width

Chapter 4:
DISCUSSION AND CONCLUSIONS

4.1 Discussion

4.1.1 Thick model

Figure 3.1 displays the relationship between source size and 95-50% penumbra determined for our geometry. For small source sizes (0.01 cm-0.2 cm), the penumbra is dominated by photon scattering and lateral transport of electrons and is therefore relatively constant. For large source sizes, the penumbra is confined by the collimators. The penumbra appears to be proportional to source sizes in the 0.3 cm-1.4 cm range. Although the number of narrow leaf gaps is influenced as the penumbra is varied within this range, there is no clear trend. It is interesting to note that the number of leaf pairs separated by 5-8 mm for beam-1in figure 3.2(a) declines as penumbra increases, while those separated by 8-12 mm initially increase in number and then decrease once the penumbra exceeds 20 mm. This behavior supports the hypothesis that the penumbra determined by the beam model will influence the generation of narrow segments in IMRT optimization.

To investigate the influence of penumbra on the generation of narrow segments over a broad range, other parameters are adjusted. Gaussian height and Gaussian width are used to vary the shoulders of the dose profile and hence the penumbra. As Gaussian height increases, the portion of the Energy fluence from extra-focal radiation (due to scattering from the flattening filter) increases. Hence penumbra increases. Jaw transmission and MLC transmission parameters affect the dose outside of the field. Thus its effect on the penumbra (50% isodose level to the 95% isodose level distance) is negligible.

Beam-2 showed a larger number of leaf pairs with a narrow gap (less than 12 mm) along the periphery of the target. Because a part of the PTV overlaps with the build-up region of beam-1, the optimization algorithm tries to give the other beam (beam-2) higher intensities at that region to compensate this under-dose. Therefore narrow segments are created to escalate the dose (figure 4.1).

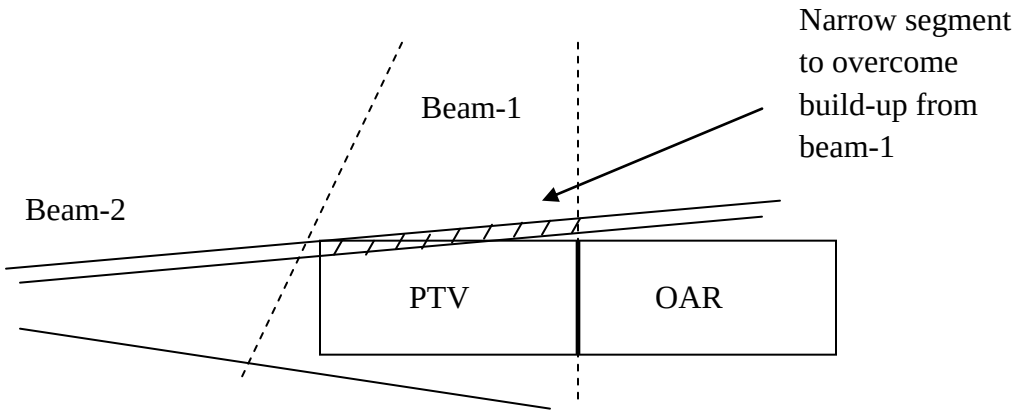

Figure 4.1: Illustration of narrow segments created for beam-2 as a result of overlapping the build-up region of beam-1

A reduction in the density of the material leads to an increase in the lateral distance that secondary electrons travel outside the field edge (Kornelsen *et al.*, 1982), hence the penumbra increases. For our model, the density and penumbra width are not inversely proportional (figure 3.11). Hoban *et al.* studied the effect of density on the penumbra of a 10 MV photon beam. They considered two components for the dose: primary and scattered. When only the primary component of the dose is considered in the Monte Carlo simulations, penumbra is inversely proportional to density. After adding the scattered component to investigate the effect of the total dose, penumbra increases because the scattered particles travel wider than primary particles so the penumbra is no longer inversely proportional to density. Because an increase in density leads

to an increase in the scattered component of the dose, then the penumbra is not inversely proportional to the density for total dose (Hoban *et al.*, 1992).

At this step we were trying to find a relationship between the penumbra and generation of the leaf pairs with a narrow gap (less than 12 mm). The number of narrow separated leaf pairs changes with the change in penumbra but the results from different plans do not show a consistent trend. It can be concluded that with broad range of penumbra variation, the generation of narrow segments cannot necessarily be controlled.

4.1.2 Thin model

For this model, the number of narrowly separated leaf pairs does not display any specific relationship with the examined parameters. The dose outside the target increases with the organ at risk max dose objective as expected, because more dose to the OAR is allowed (figure 3.15). The position of the maximum gradient moves toward the OAR as the difference between the target min dose objective (70 Gy) and OAR max dose objective decreases. It encroaches into the OAR for a dose objective difference of less than 35 Gy (figure 3.16). Therefore letting the OAR receive greater dose, would lead to a high dose gradient inside the OAR.

Figure 3.20 suggests that creating a gap between the target and the OAR removes the narrow segments along the interface but their precision is limited because the dose grid is 2.5 mm and the optimization is repeated for every 2.5 mm gap increment. In the DVH studies, the percent volume that receives the max dose of 10 Gy is related to an equivalent gap. Hence, results are obtained for other values of the gap (between the 2.5 mm gap steps). DVH studies reveal that creating an equivalent gap between the target and the OAR does not necessarily eliminate the narrow segments along the interface. However, the overall number of the leaf pairs

with a narrow separation reduces with equivalent gap, especially when the DVH objective is applied with an initial 2.5 mm gap between the target and OAR. Gap, DVH and DVH+2.5 mm gap studies exhibit an increase in the dose outside the target, as the equivalent gap increases (figure 3.21(a) and (d)). Therefore, creating a gap between the target and the OAR might not be a good way to spare the critical structure, although the position of maximum gradient occurs inside the target as the gap increases (3.22 (b)). There is an overall reduction in the gradients over 1 cm and 2 cm as the gap increases (figure 3.22 (c) and (d)). This is another reason that creating a gap between the target and the OAR can jeopardize the sparing of the critical normal tissue.

Figure 3.29(b) shows that some peaks are narrower than the 8-12 mm leaf pair separation, These peaks must arise from a combination of wider segments that overlap in the area of the peak.

In this thesis we do not investigate the number of narrow segments; we only count the narrowly separated leaf pairs. These leaf pairs may result from either long or short narrow segments. Narrow segments with a short length are least desirable because of rapid loss of lateral electronic equilibrium and occlusion of the extended source model by the collimators (which gives rise to rapid variation of output factors with field size).

Examination of high dose gradients suggests that they are correlated with the peak height near the boundary (figure 3.30). It means that the peaks are generated to compensate the dose fall-off near the edge of the beam. Higher peaks escalate the dose at the dose fall-off region thereby increasing the dose gradient. The peak width does not play a specific role in improving the gradient (figure 3.31).

4.2 Conclusion

Since the generation of narrow segments is a matter of concern in radiotherapy, especially when they are located next to critical structures, at the first stage (thick model) we tried to find a relationship between the penumbra and the generation of narrow segments. The penumbra was varied in different ways but the results for the total number of narrow separated leaf pairs were not consistent. It means that we cannot control the generation of narrow segments by changing the penumbra. These results led us to investigate if there are other parameters that affect the generation of narrow segments and penumbra (Thin model). It seems that creating a gap between the target and the organ at risk reduces the narrowly separated leaf pairs but it jeopardizes the sparing of the OAR by increasing the dose outside the target and the gradient near the edge of the target. DVH studies show an overall decrease in the total number of narrowly separated leaf pairs; however higher dose is delivered to the OAR, as the equivalent gap is increased. Dose profiles appear with a peak near the beam edge. The height of the peaks increases to compensate the dose fall-off, therefore the gradient near the boundary increases with peak height. In some cases, the creation of a narrow peak does not mean that it is produced by a narrowly separated leaf pair.

References:

Arnfield MR, Otto K, Aroumougame VR, Alkins RD. 2005. "The use of film dosimetry of the penumbra region to improve the accuracy of intensity modulated radiotherapy," *Med Phys*. 32(1):12-8

Barish RJ, Fleischman RC, Pipman YM.1987. ''Teletherapy beam characteristics: The first second,'' *Med. Phys*. 14, 657–661

Bayouth J E, Wendt D and Morrill SM. 2003. " MLC quality assurance techniques for IMRT applications," *Med. Phys.* 30 743–50

Bentzen S M. 2005. "Radiation therapy: intensity modulated, image guided, biologically optimized and evidence based". *Radiother. Oncol.* 77 227–30

Bergman AM, Bush K, Milette MP, Popescu IA, Otto K, Duzenli C. 2006. "Direct aperture optimization for IMRT using Monte Carlo generated beamlets," *Med Phys*. 33(10):3666-79

Bjarngard BE, Tsai JS, Rice RK. 1990. ''Doses on the central axes of narrow 6-MV x-ray beams,'' *Med. Phys*. 17, 794–799

Bortfeld T. 2006. "IMRT: a review and preview". *Phys. Med. Biol.* 51 R363–R379

Bortfeld T, Jokivarsi K, Goitein M, Kung J, Jiang SB. 2002. "Effects of intra-fraction motion on IMRT dose delivery: statistical analysis and simulation," *Phys Med Biol*. 47(13):2203-20

Boyer A. 2003. "Static MLC IMRT (step and shoot)". *AAPM Summer School Proceedings*, 2003, pp. 285–317

Brugmans MJ, van der Horst A, Lebesque JV, Mijnheer BJ. 1999. ''Beam intensity modulation to reduce the field sizes for conformal irradiation of lung tumors: A dosimetric study,'' *Int. J. Radiat. Oncol., Biol., Phys*. 43, 893–904

Bucciolini M, Buonamici FB, Casati M. 2004. "Verification of IMRT fields by film dosimetry". *Med Phys*. 31(1):161-8

Cadman P, Sidhu NP. 2000. "Feasibility of penumbra compensating filters for conformal prostate radiotherapy," *Phys Med Biol.* 45(2):295-304

Dawson DJ, Harper JM, Akinradewo AC. 1984. "Analysis of physical parameters associated with the measurement of high-energy x-ray penumbra*," Med. Phys*. 11,491-497

Dirkx ML, Heijmen BJ, Korevaar GA, van Os MJ, Stroom JC, Koper PC, Levendag PC. 1997. ‘‘Field margin reduction using intensity-modulated x-ray beams formed with a multileaf collimator,’’ *Int. J. Radiat. Oncol., Biol*., Phys. 38, 1123–1129

Ekstrand, KE, Barnes WH. 1990. “Pitfalls in the use of high energy x-rays to treat tumors in the lung,” *Int. J. Radiat. Oncol. BioI. Phys*. 18:249-252

Graf R, Boehmer D, Budach V, Wust P. 2010.
“Residual translational and rotational errors after kV X-ray image
“guided correction of prostate location using implanted fiducials” *Strahlenther Onkol.* 186(10):544-50.

Gunilla C. Bentel. “Radiation therapy planning” second edition, copyright © 1996, 1992 by McGraw-Hill companies Inc. P.49

HanleyJ, Lumley MA, Mageras GS, et al. 1997. “ Measurement of patient positioning errors in three-dlmensional conformal radiotherapy of the prostate,” *Int J Radiat Oncol Biol Phys* 37:435-444

Hoban PW, Keal PJ, Round WH. 1992. “The effect of density on the 10MV photon beam penumbra” *Australas Phys Eng Sci Med.* 15(3):113-23

Hunt MA, Desobry GE, Fowble B, Coia LR. 1997. ‘‘Effect of low-density lateral interfaces on soft-tissue doses,’’ *Int. J. Radiat. Oncol., Biol., Phys*. 37, 475–482

International Commision on Radiation Units and Measurements, Maryland, 1994 Report 50, Prescribing, Recording, and Reporting Photon Beam Therapy, Reviewed by Douglas Jones, *Med. Phys*. 21 (6)

Jackson W. 1971. “Surface effects of high-energy X rays at oblique incidence” *British Journal of Radiolo Gy* 44, 109-115

Jaffray DA, Yan D, Wong JW. 1999.‘‘Managing geometric uncertainty in conformal intensity-modulated radiation therapy’’. *Semin. Radiat*. Oncol. 9, 4–19

Jaffray DA, Battista JJ, Fenster A, Munro P. 1993. “X-ray sources of medical linear accelerators: focal and extra-focal radiation” *Med Phys*. 20(5):1417-27

Jiang Z, Earl MA, Zhang GW, Yu CX, Shepard DM. 2005. “An examination of the number of required apertures for step-and-shoot IMRT,” *Phys Med Biol*. 50(23):5653-63. Epub 2005 Nov 23

Jeleń U, Söhn M, Alber M. 2005. “A finite size pencil beam for IMRT dose optimization,” *Phys Med Biol.* 50(8):1747-66. Epub 2005 Apr 6

Jones, AO, Das IJ, Jones FL. 2003. “A Monte Carlo study of IMRT beamlets in inhomogeneous media,” *Med. Phys.* 30296 – 300

Keller-Reichenbecher MA, Bortfeld T, Levegrün S, Stein J, Preiser K, Schlegel W. 1999. “Intensity modulation with the "step and shoot" technique using a commercial MLC: a planning study. Multileaf collimator”. *Int J Radiat Oncol Biol Phys*. 1;45(5):1315-24

Khan Faiz M. “The physics of radiation therapy”, fourth edition, copyright ©2010 Lippincott Williams & Wilkins

Klein EE, Hanley J, Bayouth J, Yin FF, Simon W, Dresser S, Serago C, Aguirre F, Ma L, Arjomandy B. 2009. “Task Group 142 report: quality assurance of medical accelerators,” *Med Phys* 36(9):4197–4212

Kornelsen RO, Young ME. 1982. ‘‘Changes in the dose-profile of a 10 MV x-ray beam within and beyond low density material,’’ *Med. Phys*. 9, 114–116

Kuperman VY, Lam WC. 2006. “Improving delivery of segments with small MU in step-and-shoot IMRT”. *Med Phys*. 33(4):1067-73

Kutcher GJ *et al.*, 1994. ‘‘Comprehensive QA for radiation oncolo Gy: Report of AAPM Radiation Therapy Committee Task Group 40,’’ *Med. Phys*. 21, 581–618

Laub, WU, Wong T. 2003. “The volume effect of detectors in the dosimetry of small fields used in IMRT,” *Med. Phys.* 30:341–7

Lee MT, Purdie TG, Eccles CL, Sharpe MB, Dawson LA. 2010. “Comparison of simple and complex liver intensity modulated radiotherapy,” *Radiat Oncol*. 30;5:115

Lind BK, Kallman P, Sundelin B, Brahme A. 1993. ‘‘Optimal radiation beam profiles considering uncertainties in beam patient alignment,’’ *Acta Oncol*. 32, 331–342

Luan S, Wang C, Chen DZ, Hu XS, Naqvi SA, Yu CX, Lee CL. 2004.“A new MLC segmentation algorithm/software for step-and-shoot IMRT delivery”. *Med. Phys*. 31(4) 695-707

Lydon JM. 2005. “Theoretical and experimental validation of treatment planning for narrow MLC defined photon fields,” *Phys Med Biol*. 50(11):2701-14

Mohan R, Wu Q, Wang X, Stein J. 1996. "Intensity modulation optimization, lateral transport of radiation, and margins". *Med Phys* 23:2011-2021

Mu G, Ludlum E, Xia P. 2008. "Impact of MLC leaf position errors on simple and complex IMRT plans for head and neck cancer," *Phys Med Biol* 53(1):77–88

P[3]IMRT Instructions for Use, *release 8.0,* printed in the United States of America. Document number: 9201-5129A-ENG Rev. A

Pérez-Romasanta LA, Lozano-Martín E, Velasco-Jiménez J, Mendicote-León F, Sanz-Martín M, Torres-Donaire J, Carrascosa-Fernández C, Zapata-Jimínez JC, Arjona-Gutiérrez J, Gil-Agudo A. 2009. "CTV to PTV margins for prostate irradiation. Three-dimensional quantitative assessment of interfraction uncertainties using portal imaging and serial CT scans" *Clin Transl Oncol.* 11(9):615-21

Pnnacle[3] Physics Reference Guide, *release 8.0,* printed in the United States of America. Document number: 9201-5135A-ENG A

Rice RK, Hansen JL, Svensson GK, Siddon RL. 1987. "Measurements of dose distributions in small beams of 6 MV x-rays," *Phys Med Biol*. 32(9):1087-99

Rustgi AK, Samuels MA, Rustgi SN. 1997. ''Influence of air inhomogeneities in radiosurgical beams,'' *Med. Dosim* 22, 95–100

Sharpe MB, Miller BM, Wong JW. 2000[1]. "Compensation of x-ray beam penumbra in conformal radiotherapy". *Med Phys*. 27(8):1739-45

Sharpe MB, Miller BM, Yan D, Wong JW. 2000[2]. "Monitor unit settings for intensity modulated beams delivered using a step-and-shoot approach" *Med Phys*. 27(12):2719-25

Sharpe MB, Jaffray DA, Battista JJ, Munro P. 1995. ''Extrafocal radiation: A unified approach to the prediction of beam penumbra and output factors for megavoltage x-ray beams,'' *Med. Phys.* 22, 2065–2074

Shepard DM, Olivera G, Angelos L, Sauer O, Reckwerdt P, Mackie TR. 1999. "A simple model for examining issues in radiotherapy optimization," *Med. Phys*. 26, 1212–1221

Sixel KE, Podgorsak EB.1993. "Buildup region of highenergy x-ray beams in radiosurgery," *Med. Phys*. 20:761764

Xia P and Verhey L J. 1998. "Multileaf collimator leaf sequencing algorithm for intensity modulated beamswith multiple static segments". *Med. Phys.* 26 1424–34

Yu CX, Symons MJ, Du MN, Martinez AA, Wong JW. 1995. ‘‘A method for implementing dynamic photon beam intensity modulation using independent jaws and a multileaf collimator,’’ *Phys. Med. Biol*. 40, 769–787

Zhang G, Jiang Z, Shepard D, Earl M, Yu C. 2005. “Effect of beamlet step-size on IMRT plan quality,” *Med Phys*. 32(11):3448-54